Band 3 Structure and Function: ^{35}Cl NMR and Topographical Investigations

Thesis by
Katherine J. Kanes

In Partial Fulfillment
of the Requirements for
the Degree of Doctor of Philosophy

California Institute of Technology
Pasadena, California

(1989)
submitted May 10, 1989

Acknowledgements

Caltech has provided me with five and three-quarters of the most eventful years of my life. For that, I would like to thank many colleagues and friends. First, I would like to thank my advisor, Sunney Chan, for letting me go my own way and being especially supportive during the writing of my thesis. Second I would like to thank Tom Gelder and Chloe Webb for a great place to live, moral support, some great clothes and most of the unconventional fun of my stay here.

My scientific maturation was forwarded greatly by John Tomich. I would like to thank him for the use of his peptide sequencer and for many helpful discussions. Towards the end of my stay at Caltech, I monopolized his sequencer. He was always encouraging and optimistic and I am grateful. I also owe Dr. Goddard and Alan Mathiowetz for a great deal of time and the opportunity to use Biograf and the WAGVAX. Many of the sequence comparisons and many of the conventional peptide isolation techniques were attempted in the Hood group, and I am grateful especially to Gary Pipes and the staff in the DNA-Master computer center for their patience and expertise. Some of the HPLC was accomplished in the Richard's group, and I would like to thank them and Dr. Richards for party food and access to their equipment. I would like to thank both Dr. Strausses for AIDS information during the writing of my propositions. I need to give the Baldeschwieler group many thanks for the unlimited use of their Mac's. Warren Kibbe helped with some of the more important gels. Joe Falke was the reason I started with the project. He provided guidance and encouragement. Karl Irikura wrote the amino acid counting program. Dr. Teplow and the staff at the Caltech Microsequencing Facility did much of the initial sequencing and all of the amino acid analysis.

Since I have been constantly financially insolvent, I would like to thank people who kept me from debtor's prison. Dr. Beauchamp gave me a job as a teaching assistant for Chem. 6 for three years, and I was always very happy to have it. Sunney let me take care of the Raman. Dr. Okumura employed me as a slide projectionist.

I would like to thank members of the Chan group for helpful discussions and for putting up with my bad moods. Scott Ross and Mark Li listened to me try to understand transport subtleties. I would like to thank Denise Worthen for help in setting up some of the plotting programs.

My running friends helped keep me sane. They include (in random order), Dave Wheeler, Chris Campo, Sean Moriarty, Tom Gelder, Elliott Andrews, Jessie Clemente and also Richard Dissly. I owe much of my running success to my coaches Carlos Godoy and Chuck Aedo. Margi Pollack was a dependable lifting friend.

My brothers and sister, Matt, Casey, and Karen are anchors in my life. My thanks go to Auden and Lynn Healey for lending Bill to me. Susan Manly helped me understand some things. Jeannie Kanes kept my wardrobe current and kept my father out of my hair.

Most of all, I would like to thank Paula Watnick and Bill Healey, the two people who were always there, and my father, who thinks I'm unbalanced but doesn't mind. I think I'm very fortunate to have the all of them, because I'm not sure that they'll ever get out what they've put in.

Abstract

Band 3 is the anion exchange protein in red blood cells. It is the most abundant protein in the erythrocyte membrane and is the most heavily used ion transport protein in vertebrates. Physiologically, it transports Cl^- into or out of the red blood cell and then transports HCO_3^- in the opposite direction so that electroneutrality is maintained on both sides of the membrane.

The anion exchange mechanism of band 3 is unique among the ion transport proteins. It transports anions by a 'ping-pong' mechanism, meaning it is a gated protein which effects the one-for-one exchange of anions across the membrane. It is also unusual because it transports a wide variety of anions in a very efficient manner (up to 200 sec^{-1}). An arginine has been implicated in the binding and transport of chloride across the red blood cell membrane. The primary goal of this work was to determine the location of that arginine. A second goal was to investigate divalent anion binding to the active site.

^{35}Cl NMR was used to investigate the competition of chloride with divalent anions at the chloride binding site of band 3. These studies were performed to determine if divalent anions compete with chloride for binding at the active site. These investigations indicate that molybdate, sulfate, and sulfate's analogue selenate interfere with chloride's binding to the transport site. Hydrogen phosphate and its analogue hydrogen arsenate also appear to compete with chloride for binding at the transport site. However, it appears that chloride binding is only fractionally inhibited by these two dianions. This is demonstrated by the inability of hydrogen phosphate and hydrogen arsenate to saturate the transport site and completely inhibit transport site linebroadening. pH profiles of chloride competition with divalent anions were also obtained. It appears that these large, inorganic, hydrated, appr-

oximately spherical molecules can reach the transport site in the band 3 channel but not as effectively as chloride.

The goal of the biochemical studies was to determine the location of the band 3 arginine anion binding site. The complete sequence of human band 3 is was not known until very recently, but it has been available for chickens and mice since 1986. On the basis of these sequences, Vogelaar and Chan have modeled transmembrane helices to determine the number of times the protein traverses the membrane[1]. In order to insure that an arginine preferentially labeled by ^{14}C-phenylglyoxal was indeed at a transmembrane peptide and to verify the model, many of the transmembrane sequences have been isolated. This was accomplished by modification of a technique developed to separate hydrophobic synthetic peptides[2]. The band 3 transmembrane helices are tightly associated and very similar in hydrophobicity. Of a probable total of 14 transmembrane helices, the N-termini and/or C-termini have been determined for 6 of them. Because x-ray crystallography has been difficult to achieve for membrane systems (rhodopsin and the reaction center are two that that have been crystallized), this method provides a simple and relatively inexpensive method of studying membrane protein topography.

Finally, ^{14}C-phenylglyoxal has shown the location of at least one arginine in band 3 when labeled by the method of Zaki[3]. (By this method, two to three arginines are labeled per band 3 monomer.) The location of the second arginine has been restricted to two possible other transmembrane peptides (modeled helices 10 and 14). The active site arginine is probably at position R748 in the mouse erythrocyte band 3 sequence.

1. Vogelaar, N.S. (1989) *Doctoral Thesis California* Institute of Technology.

2. Tomich, J.M., Carson, L.W., Kanes, K.J., Vogelaar, N.S., Emerling, M.R., and Richards, J.H. (1988) *Anal. Biochem.* **174**, 197-203.

3. Zaki, L. (1984) *FEBS Lett.* **189**, 234-240.

TABLE OF CONTENTS

Chapter I

Introduction

The exchange of anions across the human red cell membrane is mediated by an integral membrane protein -- called band 3 from its location on a polyacrylamide gel in electrophoresis of the solubilized membrane proteins. It appears to be a large smear in these gels because the protein is heterogeneously glycosylated. Band 3 constitutes almost 30% of the total membrane protein with about 10^6 molecules per cell[1], and accounts for approximately 80% of the integral membrane protein[2] . The other major integral membrane protein is glycophorin A (or PAS-1). Physiologically, band 3 transports chloride in exchange for bicarbonate in order to maintain electroneutrality across the membrane.

Lodish and Kopito have cloned the murine (house mouse, or *mus musculus*) band 3 cDNA[3]. The 929 amino acid mouse erythrocyte band 3 (MEB3) sequence has two distinct structural domains. The N-terminal domain is composed of about 420 amino

acids. This domain is mainly hydrophilic and extends into the cytoplasm where it anchors the spectrin cytoskeleton via interactions with the proteins ankyrin[4] and band 4.1[5]. The N-terminal 420 amino acids have a net negative charge[3]. The remaining part of the protein passes through the membrane several times and contains the molecular machinery responsible for anion transport[3,6]. This domain contains groups of hydrophobic residues which are interrupted with positively charged amino acids. Circular dichroism analysis suggests that about 90% of this domain is α-helical[7]. The C-terminus may also extend into the cytoplasm since 11 of the last 32 amino acids of the protein are negatively charged. Lodish has postulated the edges of 3 transmembrane helices on the basis of helical wheel models[8]. The location of these three helices (and other modeled transmembrane peptides) in the protein's complete primary sequence is shown in Figure 1.1.

The interaction between the anion and the protein takes place in a specialized region called the anion binding site, or transport site. Anion binding to the transport site triggers a protein conformational change between the inner-facing and outer-facing conformations. This change leads to an alternation of the transport site between the inner and outer surface of the membrane. The conformational change gives rise to different reactivities for noncompetitive inhibitors of the transport site at the inner and outer membrane surface. There is some debate about whether it affects the reactivities of inhibitors of the transport site itself[9]. More is known about the outward-facing site than the inward-facing site. From ^{35}Cl NMR studies of the pH dependence of anion binding and chemical modification with phenylglyoxal (an arginine specific inhibitor), the active-site is proposed to contain an arginine.[10] Wieth and Bjerrum suggest that this residue is an outward facing site[11]. Anion transport is regulated by a residue with a pK_a of 11 to 12, which further implicates a functionally essential arginine[12,13]. Proteolytic studies and experiments with radiolabeled inhibitors have led to much of the

Figure 1.1

The location of transmembrane helices 1,3, and 5 as modeled by Lodish[8] is shown in this figure. The helices are labeled L-1, L-3, and L-5 and are marked by blue lines. Transmembrane helices, as modeled by Vogelaar and Chan are labeled VC-# and are marked by red lines. Hydrophobic reggions determined by Jay and Cantley[33] (as adapted from hydropathy plots in Reference 3) are labeled JC and are marked in orange.

BAND 3

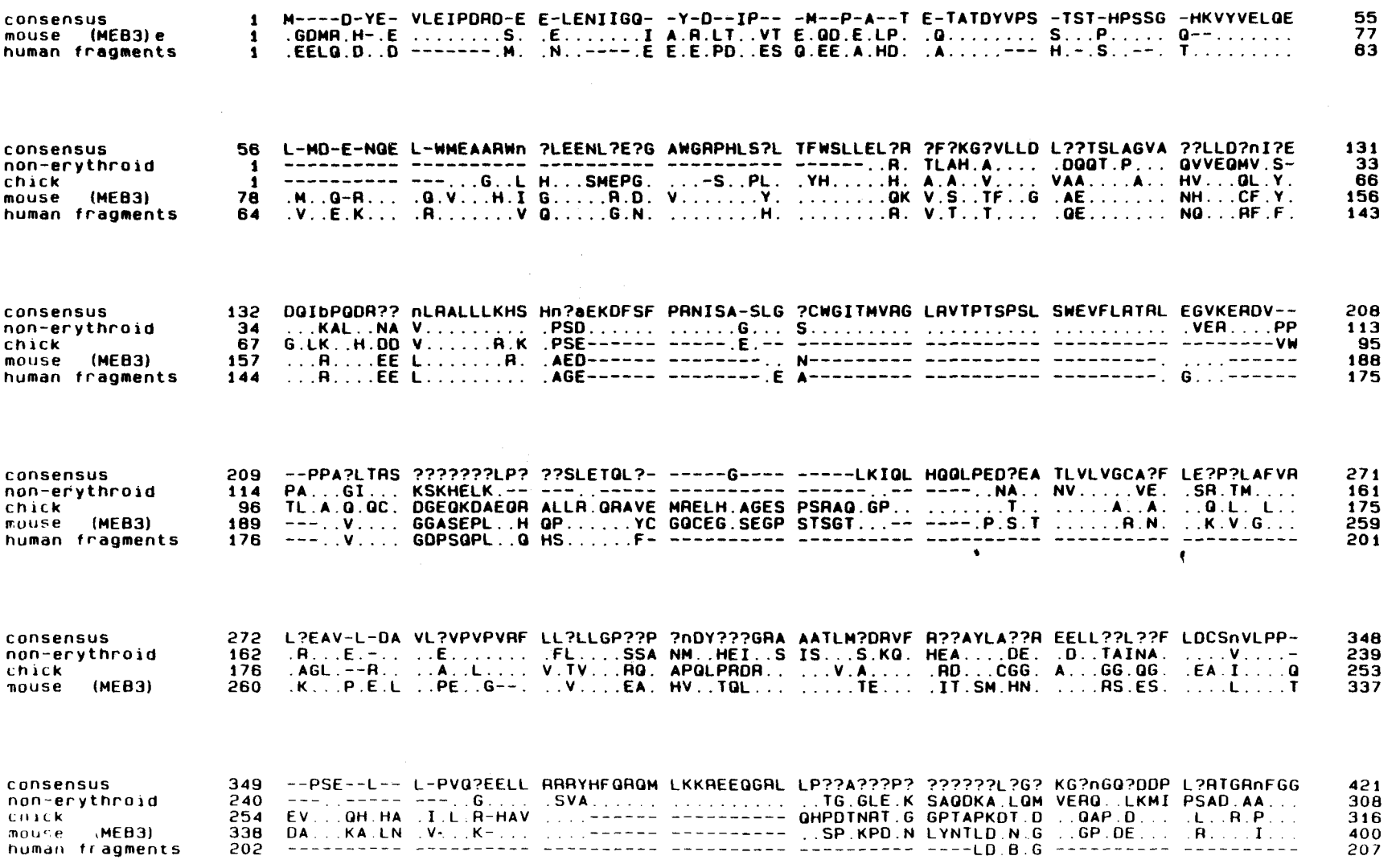
consensus 1 M----D-YE- VLEIPDRD-E E-LENIIGQ- -Y-D--IP-- -M--P-A--T E-TATDYVPS -TST-HPSSG -HKVYVELQE 55
mouse (MEB3) e 1 .GDMR.H-.E ....S. .E.......I A.R.LT..VT E.QD.E.LP. .Q........ S...P..... Q--..... 77
human fragments 1 .EELQ.D..D --------.M. .N..----.E E.E.PD..ES Q.EE.A.HD. .A.....--- H.-.S..--. T..... 63
consensus 56 L-MD-E-NQE L-WMEAARWn ?LEENL?E?G AWGRPHLS?L TFWSLLEL?R ?F?KG?VLLD L??TSLAGVA ??LLD?nI?E 131
non-erythroid 1 ---------- ---------- ---------- ---------- ------..R. TLAH.A.... .DQQT.P... QVVEQMV.S- 33
chick 1 ---------- ---...G..L H...SMEPG. ...-S..PL. .YH.....H. A.A..V.... VAA....A.. HV...QL.Y. 66
mouse (MEB3) 78 .M..Q-R... .Q.V...H.I G.....R.D. V.......Y. ....QK V.S..TF..G .AE..... NH...CF.Y. 156
human fragments 64 .V..E.K... .R.......V Q.....G.N. ....H. ....R. V.T..T.... .QE..... NQ...RF.F. 143
consensus 132 DQIbPQDR?? nLRALLLKHS Hn?aEKDFSF PRNISA-SLG ?CWGITMVRG LRVTPTSPSL SWEVFLATRL EGVKERDV-- 208
non-erythroid 34 ...KAL..NA V......... .PSD...... ......G... S......... .... .VER....PP 113
chick 67 G.LK..H.DD V......R.K .PSE------ -----.E.-- ---------- ---------- ---------- --------VW 95
mouse (MEB3) 157 ...R....EE L.......R. .AED------ --------.. N--------- ---------- ---------- ....------ 188
human fragments 144 ...R....EE L......... .AGE------ --------.E A--------- ---------- ---------- G...------ 175
consensus 209 --PPA?LTRS ???????LP? ??SLETQL?- -----G---- -----LKIQL HQQLPED?EA TLVLVGCA?F LE?P?LAFVR 271
non-erythroid 114 PA...GI... KSKHELK.-- ---.-.----- ---------- ------..-- ----..NA.. NV.....VE. .SR.TM.... 161
chick 96 TL.A.Q.QC. DGEQKDAEQR ALLR.QRAVE MRELH.AGES PSRAQ.GP.. ....T.. .....A..A. ..Q.L..L.. 175
mouse (MEB3) 189 ---..V.... GGASEPL..H QP......YC GQCEG.SEGP STSGT...-- ----.P.S.T ......R.N. ..K.V.G... 259
human fragments 176 ---..V.... GDPSQPL..Q HS......F- ---------- ---------- ---------- ---------- ---------- 201
consensus 272 L?EAV-L-DA VL?VPVPVRF LL?LLGP??P ?nDY???GRA AATLM?DRVF R??AYLA??R EELL??L??F LDCSnVLPP- 348
non-erythroid 162 .R...E.-.. ..E..... .FL....SSA NM..HEI..S IS...S.KQ. HEA....DE. .D..TAINA. ....V....- 239
chick 176 .AGL.--R.. ..A..L.... V.TV...RQ. APQLPRDR.. ...V.A.... .RD...CGG. A...GG.QG. .EA.I....Q 253
mouse (MEB3) 260 .K...P.E.L ..PE..G--. ..V....EA. HV..TQL... .....TE... .IT.SM.HN. ....RS.ES. ....L....T 337
consensus 349 --PSE--L-- L-PVQ?EELL RRRYHFQRQM LKKREEQGRL LP??A???P? ??????L?G? KG?nGQ?DDP L?RTGRnFGG 421
non-erythroid 240 ---.------ ---..G.... .SVA...... ....TG.GLE.K SAQDKA.LQM VERQ..LKMI PSAD.AA... 308
chick 254 EV...QH.HA .I.L.R-HAV ....------ ---------- QHPDTNRT.G GPTAPKDT.D ..QAP.D... .L..R.P... 316
mouse (MEB3) 338 DA...KA.LN .V-...K-... ....------ ---------- ..SP.KPD.N LYNTLD.N.G ..GP.DE... .R....I... 400
human fragments 202 ---------- ---------- ---------- ---------- ---------- ----LD.B.G ---------- ---------- 207

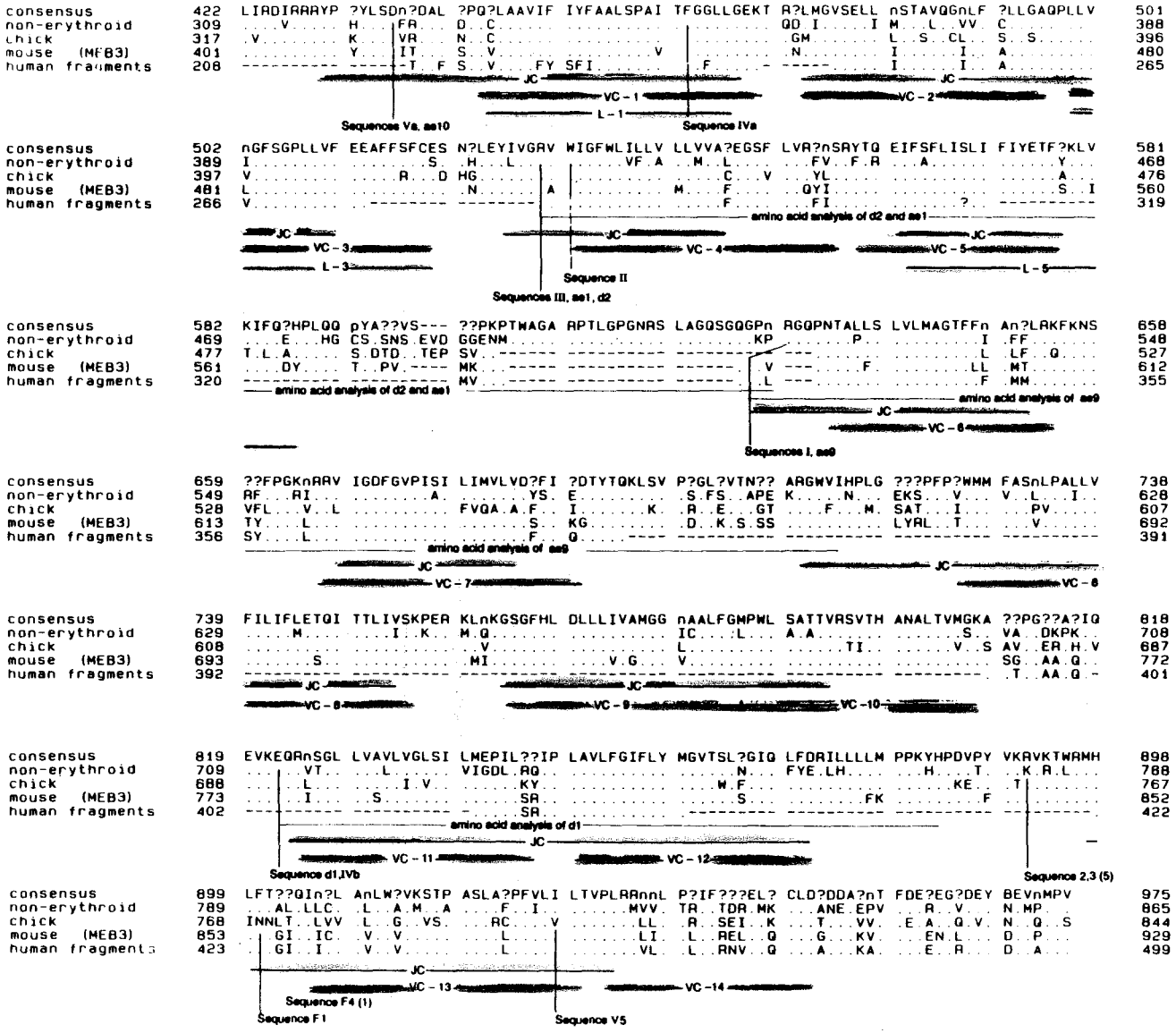
consensus 422 LIADIRRRYP ?YLSDn?DAL ?PQ?LAAVIF IYFAALSPAI TFGGLLGEKT R?LMGVSELL nSTAVQGnLF ?LLGAQPLLV 501
non-erythroid 309 ....V..... H...FR... D..C..... ..... QD.I.....I M...L..VV C..... 388
chick 317 .V..... K...VR... N..C..... ..... GM..... L..S..CL.. S..S..... 396
mouse (MEB3) 401 ..... Y...IT... S..V..... ....V ..... N..... I.....I.. A..... 480
human fragments 208 ---------- ------T..F S..V...FY SFI..... .F..... ----- I.....I.. A..... 265
JC
VC - 1
VC - 2
L - 1
Sequences Va, aa10
Sequence IVa
consensus 502 nGFSGPLLVF EEAFFSFCES N?LEYIVGRV WIGFWLILLV LLVVA?EGSF LVR?nSRYTQ EIFSFLISLI FIYETF?KLV 581
non-erythroid 389 I..... .....S..H...L..... .....VF.A ..M..L..... ...FV..F.R ...A..... .....Y... 468
chick 397 V..... ....R...D HG..... ....C...V ...YL..... ....A... 476
mouse (MEB3) 481 L..... .....N..... .....A ..... M....F..... ...QYI..... ....S..I 560
human fragments 266 V..... .-------- -------- ....F..... ...FI..... .....?.. ---------- 319
amino acid analysis of d2 and ae1
JC
VC - 3
VC - 4
VC - 5
L - 3
L - 5
Sequence II
Sequences III, ae1, d2
consensus 582 KIFQ?HPLQQ pYA??VS--- ??PKPTWAGA RPTLGPGNRS LAGQSGQGPn RGQPNTALLS LVLMAGTFFn An?LRKFKNS 658
non-erythroid 469 ....E...HG CS.SNS.EVD GGENM..... ....KP..... ...P..... .....I..FF..... 548
chick 477 T.L.A..... S.DTD..TEP SV..------ ---------- ---------- ---.....L..LF..Q.... 527
mouse (MEB3) 561 ....DY..... T..PV.---- MK..----- ---------- ---------- ---.....F..... .....LL..MT..... 612
human fragments 320 ---------- ---------- MV..----- ---------- ---------- ---.....F..... .....FF..MM..... 355
amino acid analysis of d2 and ae1
amino acid analysis of ae9
JC
VC - 6
Sequences I, ae9
consensus 659 ??FPGKnRRV IGDFGVPISI LIMVLVD?FI ?DTYTQKLSV P?GL?VTN?? ARGWVIHPLG ???PFP?WMM FASnLPALLV 738
non-erythroid 549 RF...RI..... .....A..... .....YS..E..... .....S.FS...APE K.....N.... EKS...V.... V..L...I.. 628
chick 528 VFL...V..L ..... FVQA.A.F.. I.....K. .R..E...GT ....F...M. SAT...I..... ...PV..... 607
mouse (MEB3) 613 TY....L..... ....S..KG ..... .D..K.S.SS ..... LYRL..T..... ...V..... 692
human fragments 356 SY....L..... ....F..Q. ---------- ---------- ---------- ---------- 391
amino acid analysis of ae9
JC
VC - 7
VC - 8
consensus 739 FILIFLETQI TTLIVSKPER KLnKGSGFHL DLLLIVAMGG nAALFGMPWL SATTVRSVTH ANALTVMGKA ??PG??A?IQ 818
non-erythroid 629 .....M..... ....I..K.. M.Q..... .... IC....L... A.A..... .....S.. VA..DKPK.. 708
chick 608 .... .V..... .... L..... ....TI.. ....V..S AV..ER.H.V 687
mouse (MEB3) 693 .....S..... ..... .MI..... ....V.G.. V..... .... SG..AA.Q.. 772
human fragments 392 ---------- ---------- ---------- ---------- ---------- ---------- ---------- .T..AA.Q.- 401
JC
VC - 8
VC - 9
VC -10
consensus 819 EVKEQRnSGL LVAVLVGLSI LMEPIL??IP LAVLFGIFLY MGVTSL?GIQ LFDRILLLLM PPKYHPDVPY VKAVKTWAMH 898
non-erythroid 709 .....VT..... ...L..... ..... VIGDL.RQ..... ....N... FYE.LH..... ....H....T.. ..K.R.L... 788
chick 688 .....L..... ....I.V... ....KY..... ....W.F... ....KE... .T..... 767
mouse (MEB3) 773 .....I..... ..S..... ....SR..... ....S..... ....FK.. ....F..... 852
human fragments 402 ---------- ---------- ---------- .....SR..... ..... ---------- ---------- ---------- 422
amino acid analysis of d1
JC
VC - 11
VC - 12
Sequence d1,IVb
Sequence 2,3 (5)
consensus 899 LFT??QIn?L AnLW?VKSTP ASLA?PFVLI LTVPLRRnnL P?IF???EL? CLD?DDA?nT FDE?EG?DEY BEVnMPV 975
non-erythroid 789 ...AL.LLC. ..L..A.M..A ....F..I. .....MVV. TR..TDR.MK ...ANE.EPV ...R...V... N.MP... 865
chick 768 INNLT..LVV .L..G..VS. ...RC...V ..... .LL...R..SEI..K ....T...VV. .E.A..Q.V. N..Q..S 844
mouse (MEB3) 853 ...GI..IC. ..V..V..... ....L..... ..... .LI...L..REL..Q ....G...KV. ....EN.L... D..P..... 929
human fragments 423 ...GI..I.. ..V..V..... ....L..... ..... .VL...L..RNV..Q ....A...KA. ....E..R... D..A..... 499
JC
VC - 13
VC -14
Sequence F4 (1)
Sequence F1
Sequence V5

known structural detail. Many of these are summarized in Figure 1.2. Other structural results are described here. Three lysines which are sensitive to chemical modification by 4,4'-diisothiocyanodihydrostilbene-2,2'-disulfonate (H_2DIDS), a potent inhibitor of anion transport, are thought to be K449, K558, and K561 in MEB3[3]. One of three closely spaced lysines (K608, K610, or K618 in MEB3), which is possibly important in the anion transport process, is present in the inner membrane surface[14,15]. Brock *et al.* identified K608 and K610 as the important lysines. As shown in Figure 1.2, a disulfide bond forms near the C terminus, probably between residues C869 and C903 in the MEB3 sequence[16].

Using pyridoxal 5'-phosphate (known to label two integral, chymotryptic domains of band 3) and other transport inhibitors, Salhany *et al.* found possible negative cooperative interactions between nonoverlapping inhibitor binding domains on band 3 monomers. They also suggest two interacting anion binding sites on the outer surface of band 3[17]. ^{35}Cl NMR studies find evidence for a single transport site[13]. Band 3's glycosylation site (which is present on the outside of the red blood cell membrane) has been hypothesized to be at either N612 or N661[3] in MEB3. A band 3 analogue in the cell line HKB3 (referred to as HKB3) apparently has several glycosylation sites which might be located at N483 (which is not conserved in mouse or chicken band 3), N494 or N506 (neither of which is present in mouse or chicken band 3). N661 is not conserved in HKB3, but appears to be the most likely candidate for glycosylation.

Although the band 3 protein seems to exist in the red cell membrane in the form of dimers or even tetramers[18], the monomer appears to be the functional unit. The electrical conductance of the red blood cell membrane is much smaller than the conductance calculated from the rate of anion exchange across the membrane. This indicates that the protein does not operate as an aqueous pore that permits the diffusion

Figure 1.2

The topography and sites of proteolytic cleavage are indicated in this diagram. Well defined sites of chemical alignment have also been included. The actual topography of the cytoplasmic domain has not been represented. Numbers in parenthesis refer to the alignment in mouse erythrocyte band 3. Abbreviations used are: C, C-terminus; Ch, chymotryptic cleavage site; CHO, glycosylation site; H_2DIDS, 4,4'-diisothiocyano-dihydrostilbene-2,2'-disulfonate; LI, site of lactoperoxidase catalyzed radioiodination; N, N-terminus; P, pepsin cleavage site; Pa, papain cleavage site; RM, site of reductive methylation; SH, cysteine; Tr, trypsin cleavage site. (Taken from Reference 32.)

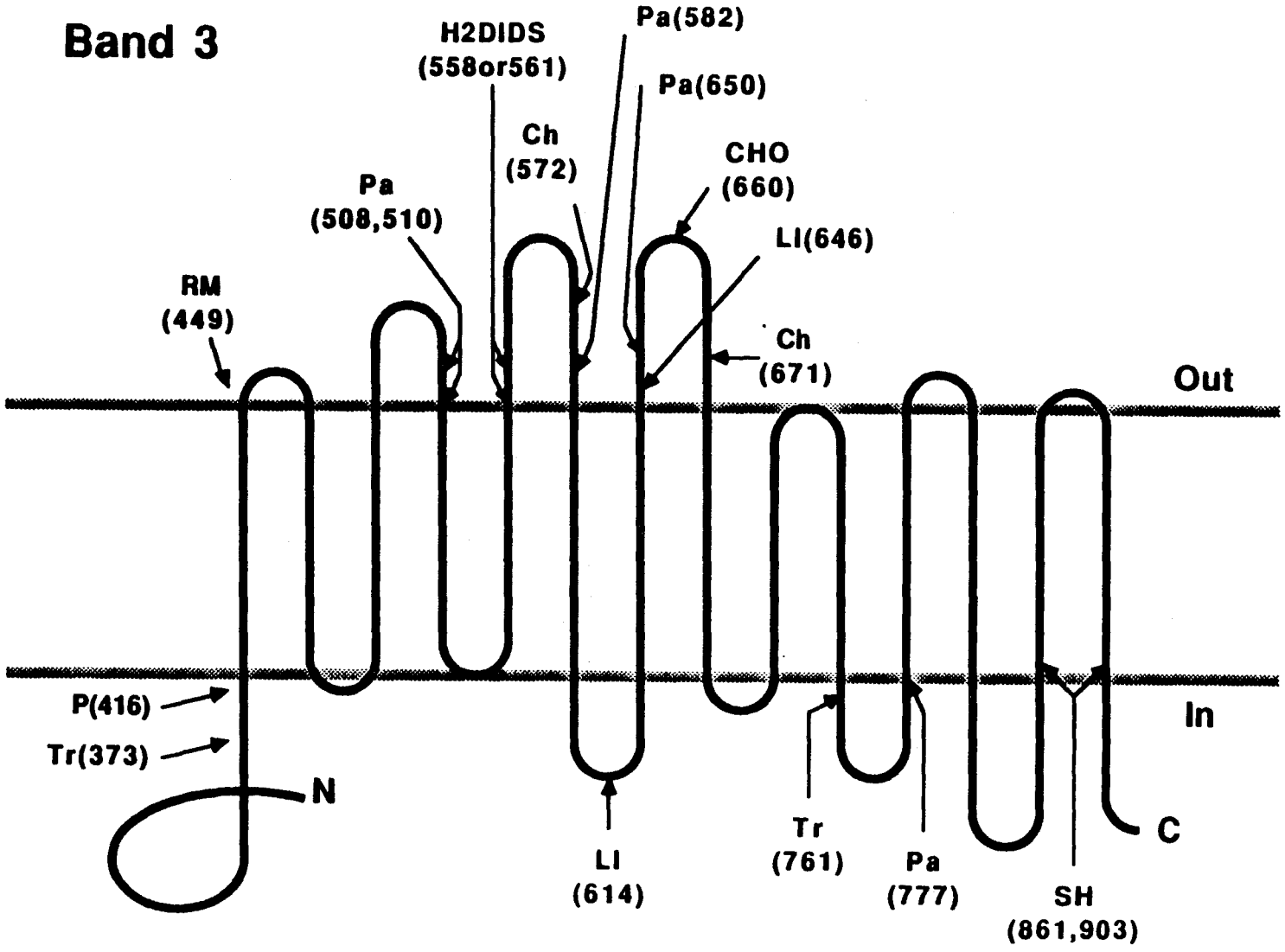
Band 3
H2DIDS
(558or561)
Pa(582)
Pa(650)
Ch
(572)
CHO
(660)
Pa
(508,510)
LI(646)
RM
(449)
Ch
(671)
Out
In
P(416)
Tr(373)
N
C
LI
(614)
Tr
(761)
Pa
(777)
SH
(861,903)

of the free anion. Anion binding to band 3 seems to be a prerequisite for anion exchange. A conformational change upon binding appears to lead to the translocation of the bound anion across the membrane[9].

Band 3 exhibits several interesting characteristics which must be considered when postulating models for the protein. First, it catalyzes the transport of anions extremely efficiently. The half time for chloride exchange as measured by $^{36}Cl^-$ flux experiments is only 52 msec at 38°C[19]. The turnover rate of the transport cycle is 2-5 X 10^4 sec^{-1} for Cl^- at 37°C and 400 sec^{-1} at 0°C[20]. Second, band 3 effects the rapid one-for-one exchange by the so called ping-pong mechanism, i.e., the transport site is alternately exposed to one side of the membrane and then to the other[13,21,22]. There is general agreement that slippage (a change in conformation of the unloaded carrier) is a rare phenomenon because of the electroneutral nature of the anion transport[9]. Third, the protein lacks specificity for the anions transported. It will transport monovalent anions more readily than divalent anions, yet it transports all halides and various organic anions such as formate[23]. Fourth, substrate transport is self-inhibited at high anion concentrations as evidenced by a maximum in chloride self exchange flux at 150 mM followed by a decrease in the flux. This self-inhibition is thought to be caused by saturation at a 'modifier site'[21,22]. Fifth, translocation of bound chloride across the membrane (rather than dissociation of chloride at the transport site) appears to be the rate limiting step in the transport cycle, so that the dissociation constant can be defined by the equation $K_D = k_{off}/k_{on}$[24] and can be determined for each face of the membrane[25].

^{35}Cl NMR has also provided evidence against a 'modifier site' if it is defined as a low affinity site for chloride binding within the transport machinery. ^{35}Cl NMR experiments show that even at high chloride concentrations, the outward facing transport site behaves like a simple anion binding site, indicating that the 'modifier site'

has no effect on chloride binding to the tranport site[27]. Tanford has described the effect of access channels leading to the transport site on the flux at high substrate concentrations and has shown that self-inhibition at high concentrations can occur because the bound anion can only be released when the access channel is empty[26].

In addition to the band 3 cloned from mice, chicken erythrocyte band 3 has also been cloned[28]. There are also a variety of polypeptides which are immunologically related to the erythrocyte band 3 protein in non-erythroid cells[8,29]. These polypeptides will also bind to band 3 inhibitors[30]. A cDNA clone, called pHKB3, has been obtained for a non-erythroid anion transport band 3-like protein from the house mouse (*mus musculus*). It encodes 919 amino acids in which the cytoplasmic domain has only 35% homology and in which the membrane-bound domain (amino acids 421-929 in MEB3) has 71% homology to mouse erythrocyte band 3[31]. This protein has proven useful in searches of conserved residues that may be important for function.

Vogelaar and Chan have modeled band 3 as having 14 transmembrane helices[32]. Lodish has also proposed that there are 14 membrane-spanning helices (although two do not completely span the membrane)[8]. Using experimental evidence, including that already described, Vogelaar and Chan have modeled the band 3 protein's helical arrangement in the membrane as is shown in Figure 1.3. They propose that the anion transport channel is composed of helices VC-4, VC-5, VC-7, VC-10, VC-13, and VC-14. The arginine residues which are most likely to be involved in high-affinity binding from the external solution are MEB3 residues R748 on helix 10 or R888 on helix 14. Of these, MEB3 residue R748 is more buried in the membrane and is a more likely candidate. Vogelaar and Chan argue that a histidine residue, H752 in the MEB3 sequence, may provide the functional group which can be titrated by a proton to enable the protein to transport divalent anions. This histidine is about one turn of an α-helix from the arginine and is therefore aligned properly to aid in translocation of a divalent

Figure 1.3

The helical arrangement proposed by Vogelaar and Chan for a band 3 dimer is shown in this figure. Numbers correspond to the transmembrane helices marked VC-# in Figure 1.2. The view is from the cytoplasm. (Taken from Reference 32.)

Helix Arrangement for Band 3

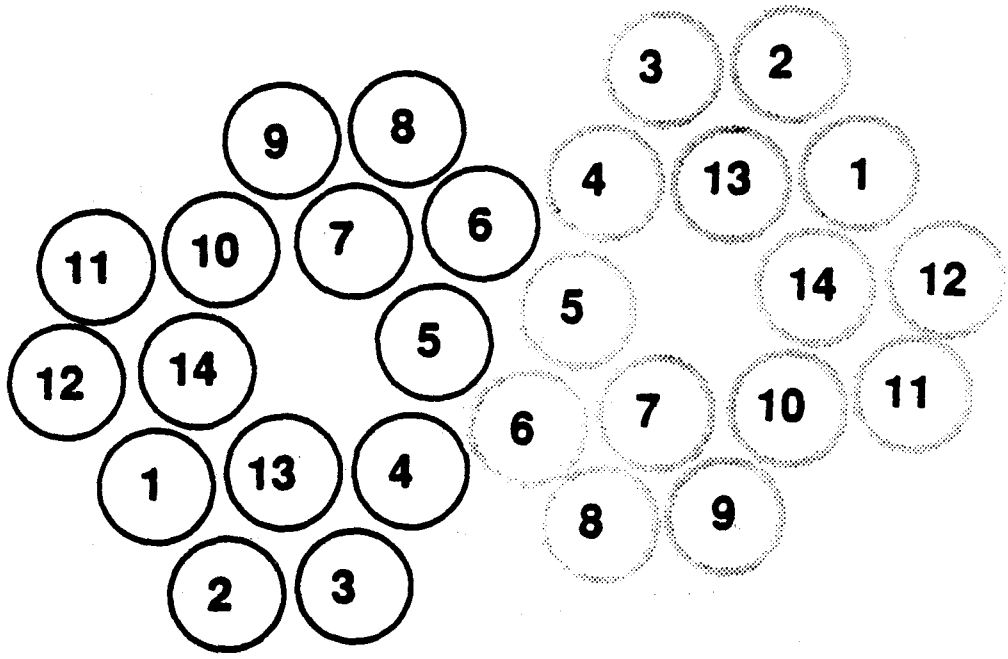

anion. Vogelaar and Chan suggest that the most buried portion of the band 3 anion channel (as opposed to the ends of the channel) is composed of mainly hydrophobic residues. These form a hydrophobic barrier to movement of charged residues which have not been neutralized by a counterion. In their model the arginine side chain, neutralized by the monovalent anion, merely rotates across the barrier. When the anion is released, the positively-charged arginine side chain may not cross the barrier until it has bound another anion in order to translocate it. In the case of divalent anions, two positively charged amino acid side chains, R748 and H752, can effect the same translocation. Therefore, the histidine must by titrated with a proton for effective divalent exchange. Both mechanisms are consistent with experiments elucidating monovalent and divalent anion transport. Vogelaar and Chan have also modeled band 3 inhibition by pyridoxal phosphate, 4,4'-diisothiocyanodihydrostilbene-2,2'-disulfonate (H_2DIDS) and 4,4'-dinitrostilbene-2,2'-disulfonate (DNDS). These inhibitors react with band 3 only from the exofacial medium because they react initially with the positively charged residues which lead into the anion transport channnel. Once again, this model can account for the outward-facing and inward-facing aspects of the protein having different reactivities to these inhibitors[32].

While some of the results in this thesis provided proteolysis information for the Vogelaar and Chan model, the goals of this thesis were to experimentally determine the location of the essential arginine in the transport site of the band 3 protein and to obtain as much topographical information about its organization in the membrane. In order to identify the functionally essential arginine, the protein was labeled using arginine-specific radioactive chemical modification with ^{14}C-phenylglyoxal. The protein was then proteolyzed into smaller membrane-spanning fragments prior to sequencing. The postition in the protein of the proteolytic fragment containing the active site was restricted. Many experiments in this thesis were performed on ghosts, which are red

blood cells which have been lysed by osmotic shock to yield a partial biconcave disk with an open end. The purpose of using ghosts is to expose as much of the membrane protein as possible to chemical modification and proteolysis. In addition to determining the probable location of this essential arginine, topograghical information was also obtained for the protein by sequencing other proteolytic fragments which had been isolated using a new HPLC method. This method consists of continual detergent saturation of the HPLC column in order to separate hydrophobic peptides of similar size. The non-membrane spanning parts of the protein, or loops, were modeled using the Biograf computer graphics program to supplement the Vogelaar-Chan model and provide a complete picture of the protein in the membrane. ^{35}Cl NMR was performed to obtain dissociation constants for a variety of inorganic divalent anions using experiments based on competition for chloride's binding site. Using the same methods, pH profiles were obtained for chloride competition with divalent anions for active site binding in the pH range of 5.5 to 8. These NMR experiments were used to provide evidence for or against the Vogelaar and Chan model for divalent anion transport.

REFERENCES

1. Wieth, J.O., Andersen, O.S., Brahm, J., Bjerrum, PJ., and Borders, C.L., Jr. (1982) *Phil. Trans. Royal Soc.(London)* **299**, 383-399.
2. Knauf, P.A. (1986) **Physiology of Membrane Disorders** (T.E. Andreoli, J.F.Hoffman, D.D. Fanestil and S.G. Schultz, eds.) Plenum Medical, New York, 191-220.
3. Kopito, R.R., and Lodish, H.F. (1985) *Nature* **316**, 234-238.
4. Bennet, V. and Stenbruck, P.J., (1980) *J. Biol. Chem.* **255**, 6424-6432.
5. Pasternack, G.R., Andersen, R.A., Leto, T.L., and Marchesi, V.T. (1985) *J. Biol. Chem.* **260**, 3676-3683.
6. Kopito, R.R., Andersson, M., and Lodish, H.F., (1987) *J. Biol. Chem.* **262**, 8035-8040.
7. Oikawa, K., Lieberman, D.M. and Reithmeier, R.A.F., (1985) *Biochem.* **24**, 2843-2848.
8. Lodish, H.F. (1988)*The Harvey Lectures* **Series 82**, 19-46.
9. Passow, H. (1986) *Rev. Phys. Biochem. Pharmacol.* **103**, 61-223.
10. Falke, J.J. and Chan, S.I. (1986) *Biochem.* **25**, 7888-7894.
11. Zaki, L., (1984) *FEBS Lett.* **169**, 234-240.
12. Wieth J.O., and Bjerrum P.J. (1982) *J. Gen. Physiol.* **79**, 253-282.
13 Falke, J.J., and Chan, S.I. (1985) *J. Biol. Chem.* **260**, 9537-9544.
14. Brock, C.J.,Tanner, M.J.A., and Kempf, C. (1983) *Biochem. J.* **213**, 577-586.
15. Kempf, C., Brock, C.J., Tanner, M.J.A. and Zahler, P. (1981) *Biochim. Biophys. Acta* **641**, 88-98.
16. Rao, A. (1979) *J. Biol. Chem.* **254**, 3503-3511.
17. Salhany J.M., Rauenbuehler, P.B. and Sloan R.L. (1987) *Biochem. Biophys. Res. Commun.* **143**, 959-964.

18. Steck, T.L. (1972) *J. Mol. Biol.* **66**, 295-305.

19. Brahm, J. (1977) *J. Gen. Physiol* .**70**, 283-306.

20. Frolich O., and Gunn, R.B. (1981) **Advances in Physiological Sciences, v.6** (S.R. Holland, G. Gardos, and B. Sarkadi, eds.), 275-280.

21. Gunn, R.B. and Frolich O. (1979) *J. Gen. Physiol.* **74**, 351-374.

22. Knauf, P.A. and Mann, N. (1984) *Biophys J.* **45**, 18a.

22. Cass, A. and Dalmark (1973) *Nature New Biol.* **244**, 47-49.

23. Barzilay, M., Ship,S., and Cabantchik, Z.I. (1979) *Membr. Biochem.* **2**, 227-254.

24. Falke, J.J., Kanes, K.J., and Chan, S.I. (1985) *J. Biol. Chem.* **260**, 9545-9551.

25. Falke, J.J., Pace, R.J., and Chan, S.I. (1984) *J. Biol. Chem.* **259**, 6481-6491.

26. Tanford, C. (1985) *Biophys. J.* **47**, 15-20.

27. Falke, J.J. and Chan S.I. (1985) *J. Biol. Chem.* **260**, 9537-9545.

28. Cox, J.V. and Lazarides, E. (1988) *Mol. Cell. Biol.* **8**, 1327-1335.

29. Drenckhahn, D., Zinke, K., Schaur, U. Appell, K., and Low, P. (1984) *Eur. J. Biochem.* **34**, 144-150.

30. Cheng, S. and Levy, D., (1980) *J. Biol. Chem.* **255**, 11337-11344.

31. Demuth, D.R., Showe, L.C., Ballantine, M., Palumbo, A., Fraser, P.J., Cioe, L.,Rovera, G., and Curtis, P.J. (1986) *EMBO J.* **5**, 1205-1214.

32. Vogelaar, N.S. (1989) *Doctoral Thesis*, California Institute of Technology.

33. Jay, D., and Cantley, L. (1986) *Ann. Rev. Biochem.* **55**, 511-538.

Chapter II

^{35}Cl NMR Studies of Divalent Anions

Binding to the Transport Site

INTRODUCTION

In addition to monovalent anion transport, there is a great deal of experimental evidence for the transport of divalent anions by band 3[1]. Flux experiments have shown that divalent anion transport and monovalent anion transport are very similar in some ways but notably different in others. Many of the results described below are derived from equilibrium exchange flux experiments. In these experiments, intact red blood cells or resealed vesicles are allowed to come to equilibrium with substrate present at equal concentrations on both sides of the membrane. After equilibrium is reached, a radioactively labeleled substrate is added to one face of the membrane in low concentrations such that the substrate concentration is essentially unchanged. The rate of flow of labeled substrate is then measured[2]. The labeled substrates commonly used are $^{36}Cl^-$, $^{35}SO_4^{2-}$, and $H^{32}PO_4^{2-}$. Chloride and sulfate have been the anions most commonly used to monitor and model monovalent and divalent exchange[3].

As reviewed separately by Knauf[3] and Passow[4], the following observations indicate that band 3 transports both monovalents and divalents similarly. Sulfate fluxes, like chloride fluxes, reach maxima and are inhibited at high substrate concentrations. This suggests self-inhibition at high substrate concentrations. The activation enthalpies for both anions have the same large values. Monovalent anions are competitive inhibitors of divalent anions, and vice versa. A large number of band 3 inhibitors produce the same fractional inhibition of chloride and sulfate transport. Notable differences in monovalent and divalent anion exchange are also reviewed in references 3 and 4. The rate of transport for divalent anions is about 10^4 times slower than for monovalent anions[5,6]. Most important, monovalent and divalent anion transport fluxes are affected in very different ways by changes in pH, as shown in Figure 2.1. One observation is that lowering the extracellular pH strongly accelerates sulfate flux into chloride-loaded cells[7, 8]. Falke and Chan have provided convincing evidence for a band 3 transport mechanism involving a single transport site.

The unique features of the different responses by monovalent and divalent anions to changes in pH can be explained by the 'titratable carrier model'. This model, in its present form, basically states that there is an interconversion of the band 3 protein from a carrier for a monovalent anion into a carrier for a divalent anion[4]. The earlier and more detailed titratable carrier model postulated three states for the carrier[9]. When the transporter is unprotonated at a certain site, it can complex with small monovalent anions and rapidly transport them. After a single titration reaction at this site, the protonated transporter can complex and slowly transport divalent anions. A titration reaction at a second site inhibits all transport by band 3. In this model, the band 3 transport apparatus requires one more proton to transport divalents than to transport monovalent anions.

Early data on pH effects on sulfate fluxes indicated that a proton activated the sulfate flux. The influx of each sulfate to Cl^- loaded cells (at pH<7) is accompanied by the influx of 0.8 protons for each chloride that exits, while the external solution becomes more alkaline[10]. Later data suggested that a proton which both alters the selectivity of the transporter and activates the sulfate flux may also be the transported proton[11]. One additional experiment extends this titratable carrier model: The dependence of a pK_a of proton activation on the sulfate concentration indicates that the proton and sulfate bind in random order[11].

Figure 2.1 shows that as pH values increase from 6 to 8, the chloride flux increases[12]. Above pH 8, the chloride flux across resealed red cell ghost membranes plateaus[13]. Initial experiments showed that at values around 6 to 6.5, sulfate flux is maximized[14,15]. More recent experiments by Milanick and Gunn have shown that external protons activate sulfate influx 100-fold at a single site with a pK_a of 5.9 at 22° C and 5.5 at 0° C. They postulate that sulfate influx at 22° C between pH 3 and 10 is the sum of sulfate transport without an accompanying proton and a proton/sulfate cotransport step--both mediated by band 3. The proton-dependent cotransport influx is activated by the binding (and transport) of a single proton to a site with an effective pK_a of 5.9. These results indicate that there is some titratable amino acid residue which accelerates the transport rate of divalent anions when protonated[8].

As described below, this protonated amino acid could be either histidine, aspartate or glutamate. The fact that a low pK_a of the proton binding stimulates sulfate influx and inhibits monovalent anion transport has been used to suggest that an important carboxylate group is being protonated. The existence of a titratable carboxylate in band 3 has not yet been proven[4]. Wieth *et al.* maintain that anion binding and translocation depend on the integrity and degree of protonation of two sets of exofacial groups with apparent pK_a values of 12 and 5, respectively. These authors suggest that, from the

Figure 2.1

Comparison of the effect of pH on the equilibrium flux of chloride, sulfate, and phosphate. The flux units are shown in a logarithmic scale. The anion concentrations were 150 mM in the chloride experiment, 1 mM phosphate in the phosphate experiment, and 5 mM sulfate in the sulfate experiment. The slopes of the dashed lines through the transport values were approximately 2/pH unit. The pH of the intersection points between the horizontal dashed lines and vertical lines was approximately 6. (This figure was taken from Reference 48a and references therein.)

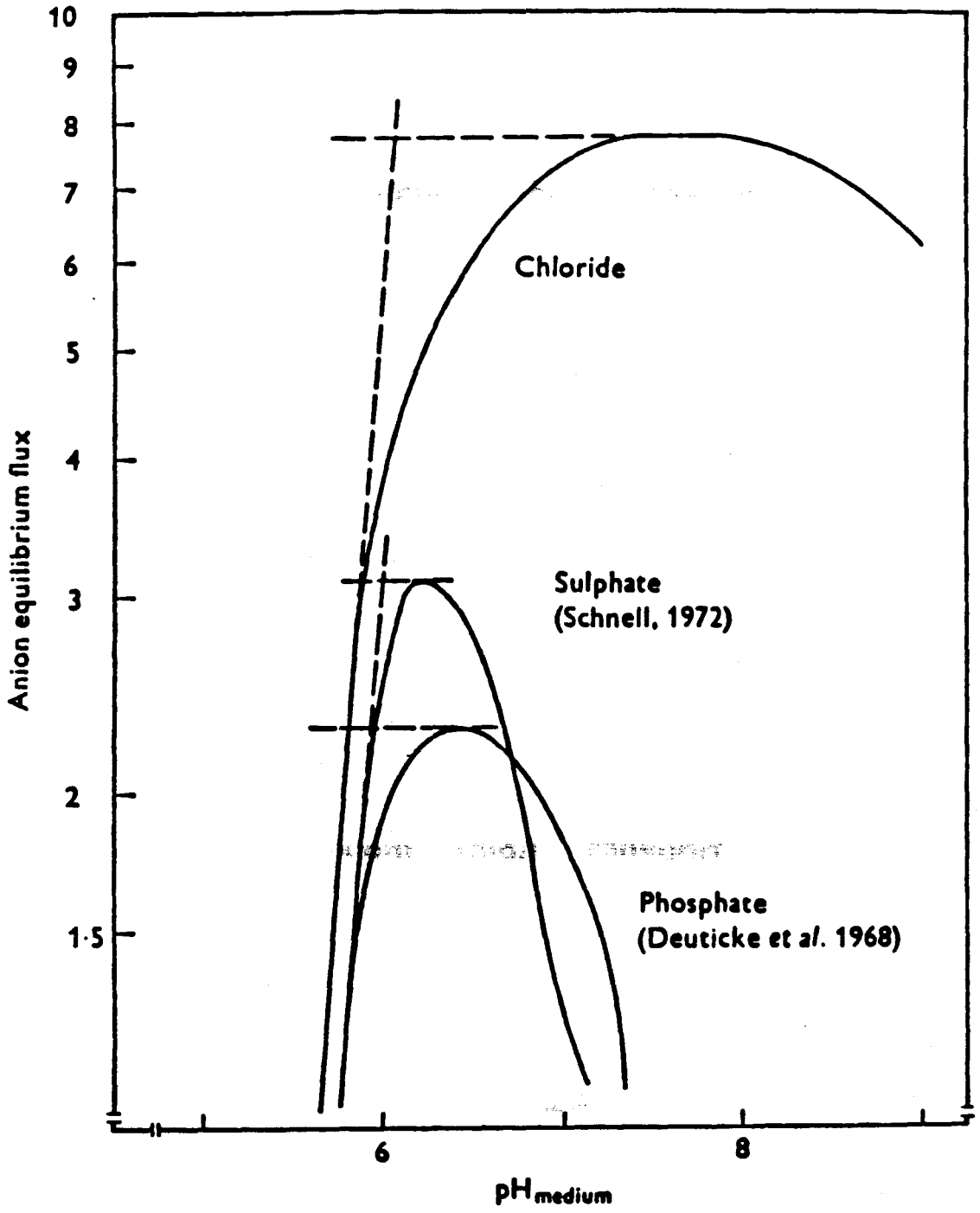
10
9
8
7
6
5
4
3
2
1·5
Anion equilibrium flux
Chloride
Sulphate
(Schnell, 1972)
Phosphate
(Deuticke et al. 1968)
6
8
pH medium

reactivities of phenylglyoxal and other α-dicarbonyls for the transport site, the group whose $pK_a = 12$ is the quanidino group of arginine, while the group whose $pK_a = 5$ is likely to be the carboxylate of glutamate or aspartate. They choose a carboxylate instead of an imidizole group (as the pH 5 titratable group) because the pK_a of this titratable group has a low temperature dependence[16]. In addition, Werner and Reithmeier propose that the inhibition of anion exchange by 1-ethyl-3-[3-(trimethylammonio)propyl]carbodiimide (ETC) in the absence of citrate appears to involve the modification of a protein carboxyl residue(s), either directly by ETC or by subsequent displacement of the carbodiimide by a hydrophilic nucleophile. Their results point to a reversible inhibition of a carboxyl by ETC when stabilized by the addition of certain nucleophiles[17]. Recent evidence has indicated that two glutamate (not aspartate) residues lie near the stilbenedisulfonate binding site. The basis for this conclusion is that acid hydrolysates of band 3 which has been inhibited by carboxylate reagents contain modified glutamates[18]. Many of these carboxylate inhibition studies are difficult to interpret, though, since the rate of anion transport inhibition appears to be greatly influenced by the ionic composition and pH of the media inside and outside the cells[16,19,20].

Alternatively, there is strong evidence for the involvement of a histidine residue in red cell anion exchange of divalents. Matsuyama *et al.* show that, in the absence of a pH gradient across the membrane in resealed ghosts, the curve representing phosphate flux reaches a maximum at pH 6.8. They propose participation of a histidine residue in the transport of both inorganic phosphate and phosphoenolpyruvate[21]. There is other evidence from Chiba *et al.* that a histidine residue is present in the active site. In their experiment, the amino acid residues of the band 3 protein taking part in the ionic interaction with an anion transport inhibitor--eosin 5-isothiocyanate (EITC)--were determined by pH titration. Absorbance measurements reveal that EITC is probably

interacting with histidine and arginine residues. Furthermore, the intensity of the induced circular dichroism (CD) band at 530 nm of the EITC molecule bound to ghosts was decreased by pre-incubation with arginine-specific reagents, phenylglyoxal and 1,2 cyclohexanedione, and histidine specific reagents, diethylpyrocarbonate (DEPC) and *p*-diazobenzene sulfonate. Additionally, it was found that DEPC effectively inhibited the sulfate efflux from intact erythrocytes. These results were taken by the authors to mean that the histidine residues participate in the anion transport system of human red cells. pH titration of the EITC-ghost system shows an intensity change for the pH-equilibrium profile with a pK value at 6.4. The authors implicate a histidine (with a free amino acid pK_a of 6.0) as the residue responsible for the interaction of EITC in the anion recognition site[22].

As mentioned above, other laboratories have discounted the imidazole group of histidine because it has a rather large enthalpy of ionization[3,23,24,25]. Such a large enthalpy is inconsistent with the observation that the apparent pK_a of the transport regulatory groups changes very little between 0° C and 38° C. According to the study of Barzilay *et al.*, histidine should have a smaller enthalpy of ionizaion if the microenvironment of substrate recognition site bears a positive multipolar character and possesses functionally essential groups with electron donor capacity embedded in a hydrophobic area. They pointed out that imidazole groups can be implicated as strong electron donors (as can NH_2 or SH groups) and, if there is an arginine (or lysine) anion recognition site in a hydrophobic area, the positive charge condition is met. Barzilay *et al.* base their model on inhibitor studies with reversible and irreversible inhibitors with large hydrophobic moieties and negatively charged functional groups such as substituted stilbene disulfonates[26]. Their results strongly support the Chiba *et al.* investigation mentioned above. Thus, a histidine may be responsible for the protonation step in the cotransport of a proton with sulfate.

Sulfate has been the most extensively studied divalent anion since any results with hydrogen phosphate (the other major physiological divalent anion) are complicated by the monovalent to divalent pK_a of 7.2. Runyon and Gunn have reported that the transport of divalent phosphate is negligible in comparison to the monovalent species[27]. It should be noted that, while both phosphate and arsenate are transported by band 3, a fraction of the flux (up to 20%) of both anions may occur via some other pathways (possibly via a sodium-dependent cotransport system)[28].

Aubert and Motais demonstrated that the intercharge distance of carboxylates in organic dianions transported across the red blood cell membrane must not exceed that of maleic acid (3.7Å)[29]. Although Aubert and Motais never showed conclusively that band 3 was the protein responsible for transporting these organic dianions, Hajjawi and Hider showed that malonate (an organic anion) is transported by band 3[30]. The distance of 3.7 Å is consistent with the hypothesis of Vogelaar and Chan that residues arginine 748 and histidine 752 (in the mouse erythrocyte band 3 sequence) are responsible for transporting divalents across the hydrophobic layer in the middle of the band 3 channel[31]. In their model, seen in Figure 2.2, the proton's ability to increase divalent binding is not an allosteric effect, but results from the protonation of a histidine proximal to the arginine responsible for monovalent binding and transport. In an α-helix, about 3.5 amino acids form a complete turn, so residues R856 and H860 are positioned to allow cooperation in dianion transport.

The purpose of this chapter's experiments is to address the question of whether divalent anions were indeed transported across the membrane by band 3 by binding the same amino acid residue(s) as chloride and thus, presumably, by the same mechanism. Flux studies are of limited use in this respect because they can only show gross transport phenomena. ^{35}Cl NMR experiments allow study of the binding characteristics of chloride within the transport channel, since divalents were transported

Figure 2.2

The mechanism proposed by Vogelaar and Chan is illustrated schematically in this figure. The stationary hydrophobic barrier is represented by a shaded horizontal band. Mechanisms for the transport of both monovalent and divalent anions have been drawn. (Taken from Reference 31.)

Stationary Barrier / Swinging Arm Mechanism

Monovalent Anion Transport

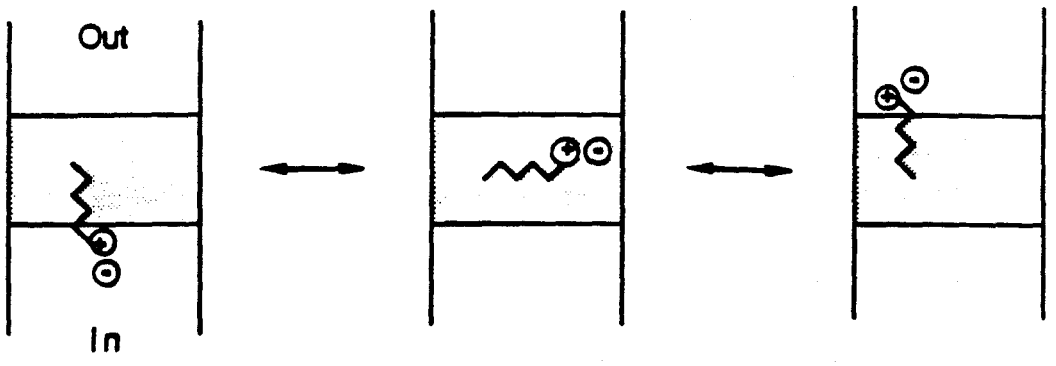

Divalent Anion Transport

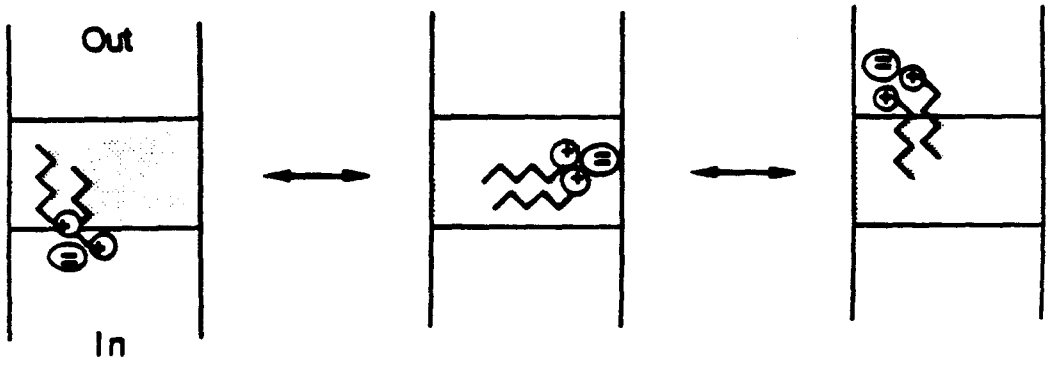

down the channel and interacted with the same residues as the chloride. ^{35}Cl NMR transport site linebroadening studies showed that all dianions tested (sulfate and hydrogen phosphate, their analogues selenate and hydrogen arsenate, and molybdate) can reduce $^{35}Cl^-$'s DNDS-sensitive NMR linecbroadening. This is demonstrated by the calculation of apparent K_D's from best-fit curves using an equation describing K_D's for a homogeneous set of binding sites. However, no divalent anion was completely able to prevent chloride from binding to the active site within the range of concentrations used. This was demonstrated by the dianions' inability to abolish the chloride DNDS-sensitive linebroadening. Hydrogen phosphate and hydrogen arsenate, in particular, had unexpectedly low K_D's. Additionally, plots of activity versus DNDS-sensitive linebroadening for these two anions unexpectedly level off. It is possible that only a fraction of the hydrogen phosphate are interacting with chloride at the transport site. This possibility, in conjunction with the increasingly smaller activity coefficients at high concentrations, precludes saturating the transport site. Falke and Chan have described a mechanisms of inhibition of transport-site linebroadening. The divalent anions show behavior consistent with prevention of exchange at the transport site or with competition at the transport site[54].

^{35}Cl NMR was also used to observe the characteristics of chloride binding to the transport site in the presence of divalent anions over a range of pH's. It appears that pH has very little effect on divalent anion binding to the chloride transport site. Monovalent oxyanions seem to compete somewhat more effectively than divalents for the chloride binding site, but the effect is within experimental error. Selenate and hydrogen arsenate seem to bind the chloride binding site more effectively than their smaller, more hydrated, and more electronegative analogues, sulfate and hydrogen phosphate.

BACKGROUND

^{35}Cl NMR.

^{35}Cl has a nuclear spin of S=3/2 and an electric quadrupole moment. Accordingly, there are 4 nuclear energy levels and there are three possible $\Delta m = \pm 1$ transitions in the presence of an applied magnetic field. The shape of the spectrum is determined by quadrupolar effects. When the electron cloud surrounding the nucleus is unperturbed so that the cloud has spherical symmetry (in the case of a chloride ion in a vacuum), the three transitions have the same resonance frequency and linewidth. In this case, a single Lorentzian line is observed in the NMR spectrum for the 3 transitions. However, in a crystal the three transitions do not have identical resonance frequencies due to the electric quadrupole interaction. In that case, all three transitions are visible in the spectrum. The middle transition (m_I = 1/2 --> -1/2) occurs at about the same frequency as the single line for the chloride ion in solution, but the flanking transitions (m_I = 3/2 --> 1/2 and -1/2 --> -3/2) are separate from the central transition. The central resonance contains 40% of the integrated intensity and the other 2 transitions contain 30% each of the integrated intensity.

For chloride in solution, rapid tumbling of the electric field gradient relative to the static magnetic field averages the quadrupolar interaction (and thus the quadrupolar splitting) to zero and a single Lorentzian line is seen, as it is in the case of a chloride ion in a vacuum. The tumbling of hydrated chloride ions in water is unrestricted, essentially isotropic and rapid. The tumbling is rapid enough to average the quadrupolar perturbation to zero. When $\omega\tau_c << 1$ (where ω is the NMR frequency and τ_c is the correlation time for the isotropic reorientation of the field gradient), the collapsed resonance widths of the three transitions are the same as are the nuclear spin relaxation rates, $1/T_1$ and $1/T_2$. The fluctuation of the energy levels from the tumbling enhances

the observed relaxation rate so that the observed resonance is about 10 times broader than in the vacuum case where there is no quadrupolar interaction[32].

When chloride is bound to the membrane-associated protein binding sites, it slows the tumbling sufficiently so that the chloride oriented in the binding site should give a spectrum similar to that in an oriented crystal. This is because a large quadrupolar interaction occurs when chloride binds to an asymmetric binding site on a protein. The powder pattern is not observed. Because in the rapid exchange conditions that exist for chloride associating and dissociating for the transport site, the binding events that the chloride ion experiences have random orientations. This reduces the observed quadrupolar splitting because the ion experiences an average environment[32].

For all samples in these experiments, the concentration of chloride in solution is over 1000 times larger than the concentration of the bound chloride. The Lorentzian shape of the solution chloride resonance therefore dominates the spectrum. However, when chloride binds sites on the protein, it can cause broadening of the observed spectrum. This results from frequent sampling of the protein binding site by the solution chloride ions and the large difference between the spectral widths of solution and bound chloride. The linewidth of solution chloride is about 10 Hz. The linewidth of chloride bound to a site on a protein in solution has a spectral width of 10^4 to 10^6 Hz.

In the rapid exchange case, each chloride ion visits many binding sites before magnetization in the x-y plane dephases. The quadrupolar splitting must be averaged to zero due to sampling of different binding site orientations. The observed resonance frequency in the rapid exchange limit is similar to the resonance frequency of the solution chloride. In the slow exchange case, complete dephasing occurs during a single visit to the binding site. If the on-rate for binding is sufficiently large then the

observed line width will be larger that the pure solution[32]. The theoretical treatments of this subject are available elsewhere[33]. The experimental justification for the $^{35}Cl^-$ linebroadening assay is that, at constant concentrations of chloride, ^{35}Cl NMR linebroadening is directly proportional to the concentration of chloride binding sites on leaky ghost membranes[33].

DNDS-Sensitive Linebroadening.

It has been shown by Falke *et al.* that 4,4'-dinitrostilbene-2,2'-disulfonate or dinitrostilbenedisulfonate (DNDS) is a competitive inhibitor of chloride binding to band 3 transport sites. As a reversible inhibitor of anion transport by band 3, DNDS has a high affinity for the chloride binding site in band 3. This is evidenced by its low apparent dissociation constant, or K_D, of 6.4 ± 0.5 μM. Thus, linebroadening which occurs in the presence of DNDS can be subtracted from total linebroadening of a given sample to generate the DNDS-sensitive linebroadening, or transport site linebroadening[33].

Expressions for K_D and K_I.

The K_D curves are the nonlinear least-squares best-fit plots ($y = A - Bx / (x + K_D)$) for a homogeneous set of binding sites where K_D is the apparent dissociation constant, A is a constant describing the maximum linebroadening possible (when there is no inhibitor present), and B is a constant characteristic of the band 3 transport site which represents the inhibitor-sensitive linebroadening (usually having values of between 1 and 2). These curves are calculated assuming that the DNDS-sensitive sites represent a class of identical sites. This is a reasonable assumption based on the shape of the curves. The relationship between K_D, the apparent dissociation constant, and K_I, the actual dissociation constant, is found by the equation, $K_D = K_I (1 + [Cl^-] / K_{I'})$. $[Cl^-]$ is 150 mM in these experiments, and $K_{I'}$ is 67 mM, the actual dissociation constant for

chloride at the transport site. The apparent K_D's of the DNDS-sensitive sites are larger than the acual K_I values because the former are obtained in the presence of competing chloride. This apparent dissociation constant increases linearly as a function of chloride concentration. The derivation of these equations has been described by Falke *et al.*. The value in obtaining K_I lies in the fact that it is a measure of the affinitiy of a substrate for a binding site. In particular, $K_I = k_{off} / k_{on}$, where k_{off} is the dissociation rate, and k_{on} is the association rate[34].

MATERIALS AND METHODS

Materials

Chemicals: Reagents and their sources are: sodium phosphate and sodium chloride (Malinckrodt); sodium selenate and sodium arsenate (Aldrich); sodium sulfate, sodium citrate and sodium chloride (J.T. Baker Chemical Co.); 0.22 μm filters (Nalgene).

Methods

NMR Sample Preparation for K_D Experiments.

Buffers used in the NMR experiments containing 2 x concentration were prepared. The final concentration of chloride was 150 mM for all experiments. All buffers were filtered before use. Buffers and membranes were kept on ice at all times to maintain the temperature at 4° C. The ionic strengths were kept constant at 1.35 and pH 8 using sodium citrate. Three ml of 2 x concentrated NMR buffer were added to 3 ml of ghost membranes in test tubes on ice. For some of the initial experiments, the test tube suspension was sonicated for 3 to 4 minutes on ice, using a Heat Systems-Ultrasonics Model W33SR sonicator at an output setting of 7 with a 50% duty cycle. Nitrogen was blown into the sample tubes to reduce oxidation of lipids. Sonication does not result in a significant change in the ^{35}Cl transport site linebroadening[32]; it merely fragments the membrane to prevent protein aggregation or vesiculation[35]. Phase contrast microscopy showed that ghosts did not reseal after adding NMR buffer, performing the NMR experiment and allowing to sit overnight at 4° C. They retained their normal shape even in the presence of high ionic strength buffers.

DNDS (the band 3 active site inhibitor) stock solution (40 mM) was prepared in water. 100 μl of DNDS was added to every other NMR tube. 100 μl of water was

added to the other half of the tubes. The final concentration of DNDS was 1 mM when the ghost suspension was added to the samples.

NMR Sample Preparation for pH Experiments.

One hundred ml of 2 X concentration NMR buffer was prepared. After the ghosts had been added, the final concentration of buffer components was 0.15 M NaCl, 20% D_2O (v/v) and 50 mM divalent anion. This solution had an initial pH of 5.5 which was attained by adding citric acid. The pH was raised in 0.25 pH unit increments by adding concentrated NaOH while stirring the ghost/NMR buffer suspension. Concentrated NaOH was added to minimize volume changes which affect protein concentrations and therefore the amount of linebroadening. After reaching the desired pH, 3 ml aliquots were added to NMR tubes containing DNDS or water, as above.

^{35}Cl NMR Spectroscopy.

Except for one selenate K_D experiment, ^{35}Cl NMR spectra were obtained using a JEOL FX-90 NMR spectrometer. The ^{35}Cl resonance frequency on this instrument is 8.8 MHz. The spectral width was 1000 Hz, containing 256 data points and centered on the solution chloride peak in the ^{35}Cl NMR spectrum. A window of 10.0 Hz linebroadening was added to the samples to improve the signal to noise ratio. The central 500 Hz of the spectrum were plotted and the ^{35}Cl peak line width at half-height was measured by hand. Ten mm NMR tubes were used without spinning. The temperature was maintained at 4° C and 400 to 800 scans were obtained for each sample.

In one selenate K_D experiment, ^{35}Cl NMR spectra were obtained on a Varian XL200 spectrometer at the ^{35}Cl resonance frequency of 19.6 MHz. The width at half height was measured directly by the spectrometer.

NMR Sample Analysis.

Samples were stored on ice at 4° C prior to analysis. Modified[36] Lowry assays[37] were performed to determine protein concentration so that linebroadening could be normalized.

Microscopy.

NMR samples were examined using a Zeiss Model D7082 phaase-contrast microscope. Photographs were taken using Kodak Pan 400 film.

Curve Fitting.

Up to 12 data points were obtained for each point on the sulfate K_D curve. These were averaged to obtain the final value for the point. Up to 10 data points were obtained for each point on the hydrogen phosphate K_D curve. Up to 4 points were obtained for each point on the molybdate curve. Because of the low sum of squares value for the hydrogen arsenate experiment, only one data set was obtained. The curves were fit to the equation $y = A - Bx / (x + K_D)$ in the Background section using two different curve fitting programs.

The average value of each point in the sulfate pH curve in was taken from the average of values at that pH for 4 data sets. Two data sets were obtained for the hydrogen phosphate pH curve. These had different two concentrations of hydrogen phosphate.

RESULTS and DISCUSSION

Divalent Anions May Compete with Cl^- for its Band 3 Anion Binding Site:

In an effort to clarify the question of whether the divalent anions are being transported via the same mechanism as monovalent anions in band 3, ^{35}Cl NMR competition experiments were performed on a variety of divalent anions. Falke *et al.* have shown that the DNDS-sensitive sites are transport sites[33]. If an anion competes with chloride for binding to an anion binding site, the ^{35}Cl NMR assay can be used to study the anion's binding. In such an experiment, the concentration of chloride is held constant, while the anion's concentration is varied[33]. Figures 2.3-2.5 show the plots of transport site linebroadening versus $[A^{2-}]$ for the divalent anions HPO_4^{2-}, SO_4^{2-}, $HAsO_4^{2-}$, SeO_4^{2-}, and MoO_4^{2-}. Table 1 summarizes the K_I's for these anions. This series was chosen for two reasons. Sulfate and hydrogen phosphate are physiological band 3 substrates. In addition, the greatest amount of information on divalent anions interaction has been gathered in experiments using sulfate and, to a lesser extent, phosphate. The plots in Figures 2.3-2.5 seem to show that hydrogen phosphate and sulfate compete with chloride for binding at the band 3 transport site. Their analogues, SeO_4^{2-} and $HAsO_4^{2-}$, also decrease the DNDS sensitive, or transport site linebroadening . The large size of the hydrated dianions and their larger analogues does not prevent them from reducing the DNDS sensitive linebroadening. The radii of these ions is found in Table 2. If only the crystal radius or the hydrated radius of the ions is important for binding at the transport site, molybdate and sulfate should have similar K_I's. The K_I of molybdate was measured since molybdate and sulfate are approximately the same radii and are completely divalent at pH 8.0 . They did, in fact, have similar K_I's. Yet there is no obvious correlation between hydrated

Figures 2.3 to 2.5

Apparent dissociation constant ($K_{D(apparent)}$, or K_D) curves for different divalent anions are shown in these figures. The curves are calculated using a least-squares best-fit program using the equation $y = A - Bx / (x + K_D)$. A is a constant describing the maximum linebroadening possible with no inhibitor present. B is a constant characteristic of the homogeneous class of band 3 transport sites which lead to inhibitor sensitive linebroadening. K_I (the actual dissociation constant) is found from the equation $K_D = K_I (1 + [Cl^-] / K_{I'})$. $[Cl^-]$ is 150 mM, the constant concentration of chloride used in these experiments. $K_{I'}$ is the actual dissociation constant for chloride at the transport site. In Figure 2.3, (A) shows the curve for hydrogen phosphate and (B) for hydrogen arsenate. In Figure 2.4, the curve for molybdate is shown. In 2.5, (A) shows the curve for sulfate and (B) for selenate.

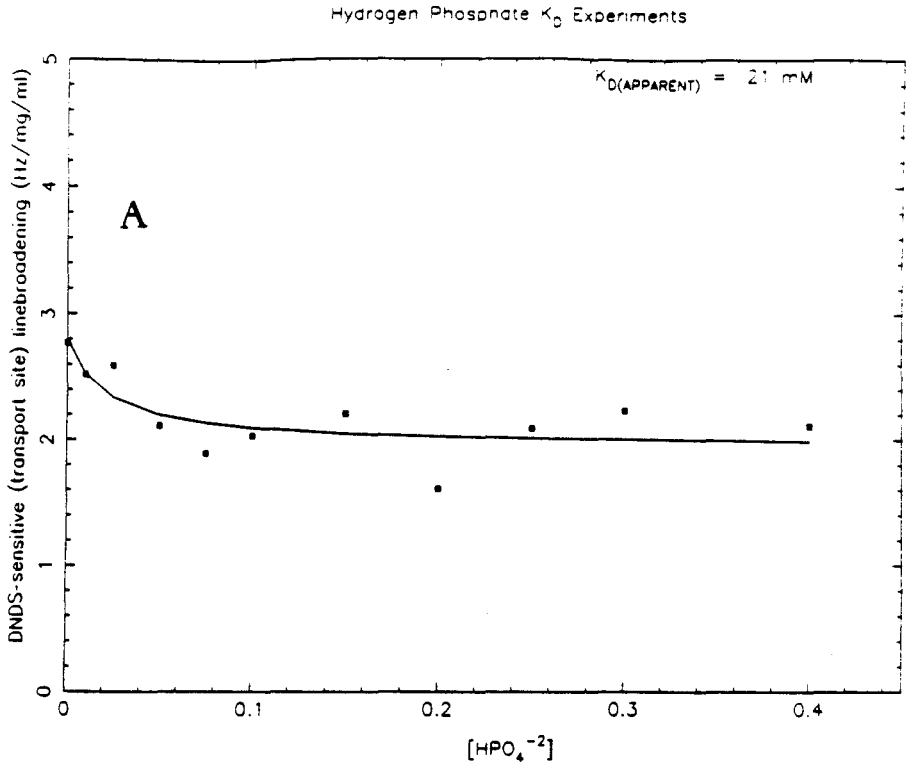
Hydrogen Phosphate K_D Experiments
$K_{D(APPARENT)}$ = 21 mM
A
DNDS-sensitive (transport site) linebroadening (Hz/mg/ml)
0
1
2
3
4
5
0
0.1
0.2
0.3
0.4
$[HPO_4^{-2}]$

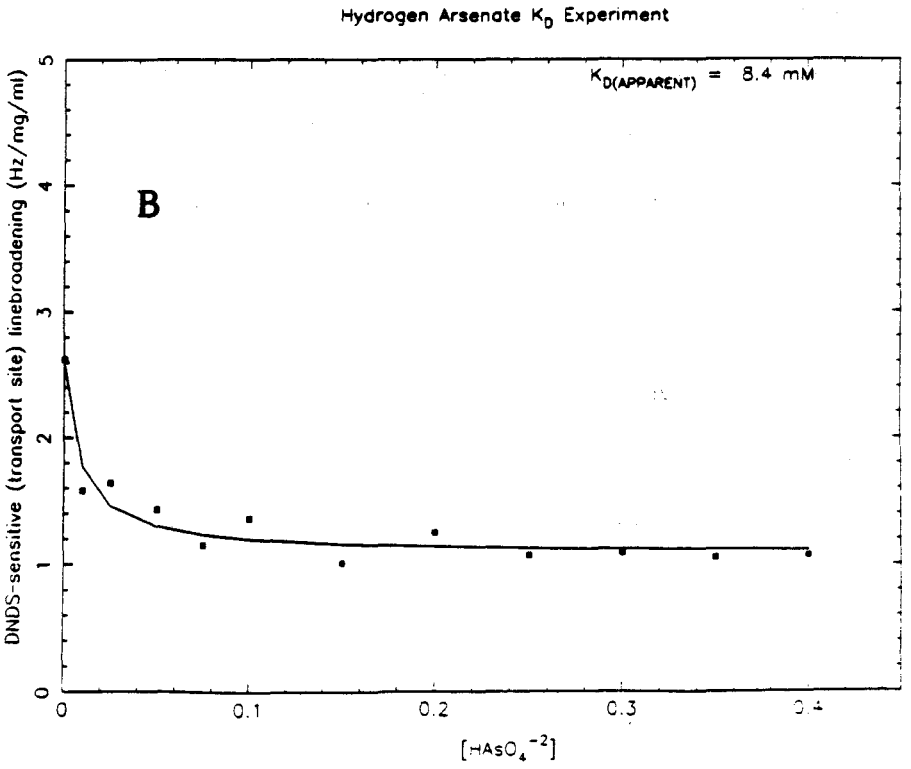
Hydrogen Arsenate K_D Experiment
$K_{D(APPARENT)}$ = 8.4 mM
B
DNDS-sensitive (transport site) linebroadening (Hz/mg/ml)
0
1
2
3
4
5
0
0.1
0.2
0.3
$[HAsO_4^{-2}]$

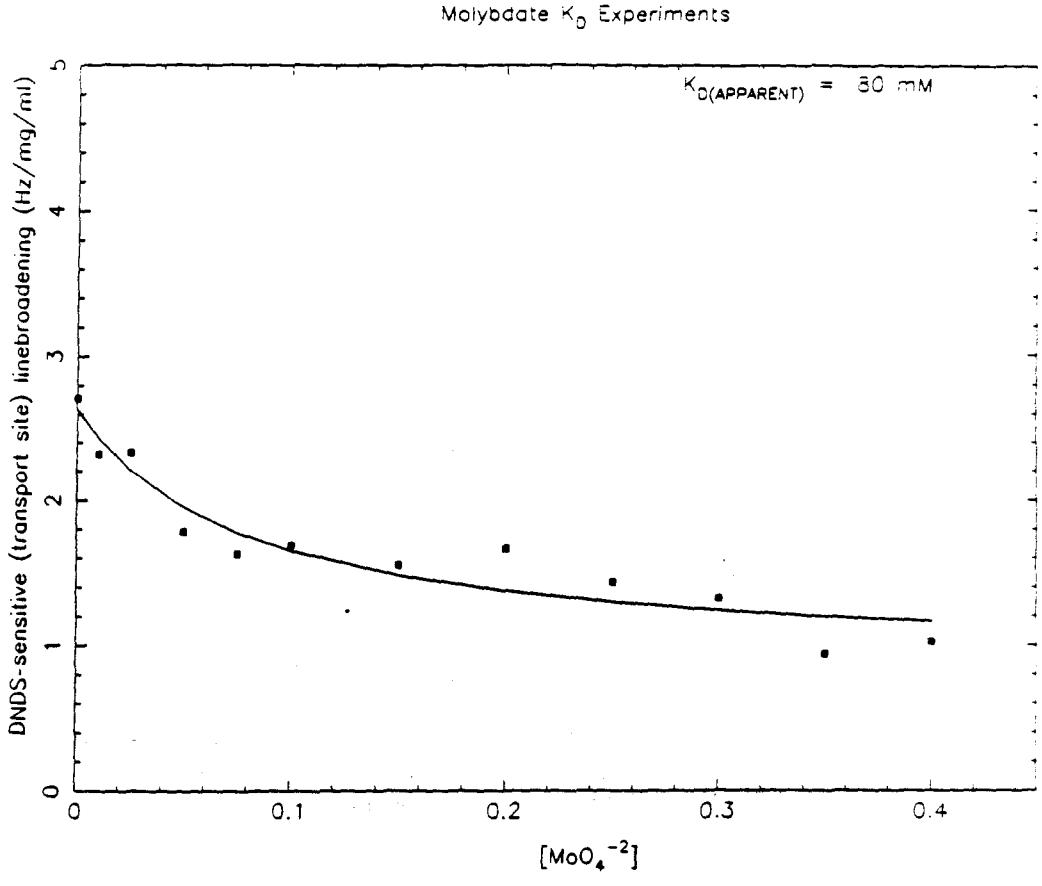
Molybdate K_D Experiments
$K_{D(APPARENT)}$ = 80 mM
DNDS-sensitive (transport site) linebroadening (Hz/mg/ml)
0
1
2
3
4
5
0
0.1
0.2
0.3
0.4
$[MoO_4^{-2}]$

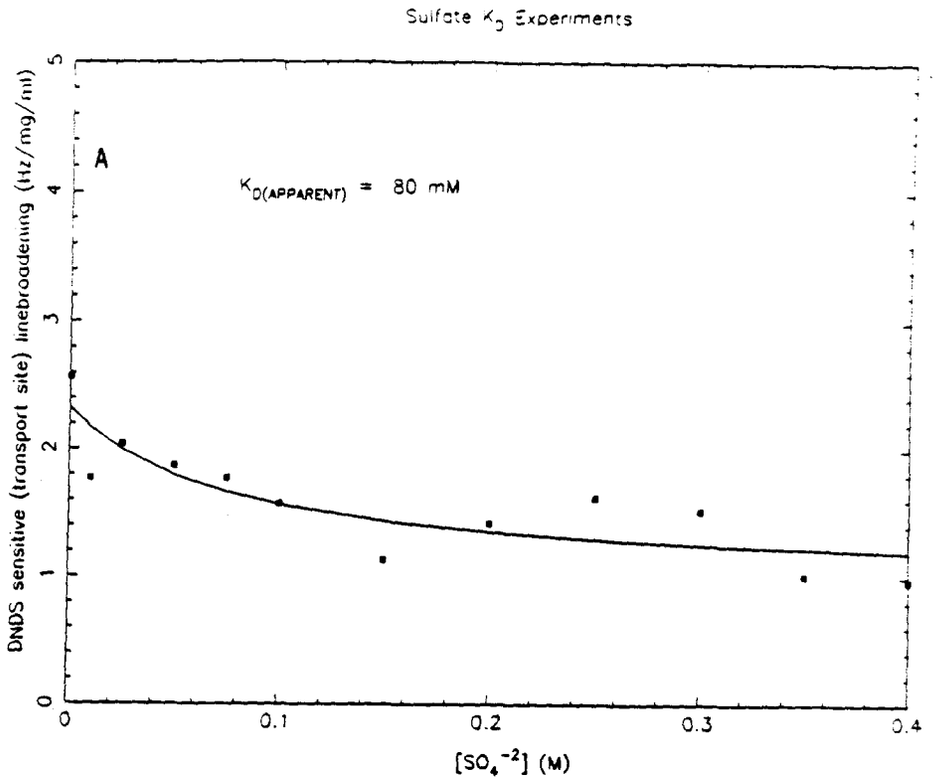
Sulfate K_D Experiments
A
$K_{D(APPARENT)}$ = 80 mM
DNDS sensitive (transport site) linebroadening (Hz/mg/ml)
0
1
2
3
4
5
0
0.1
0.2
0.3
0.4
$[SO_4^{-2}]$ (M)

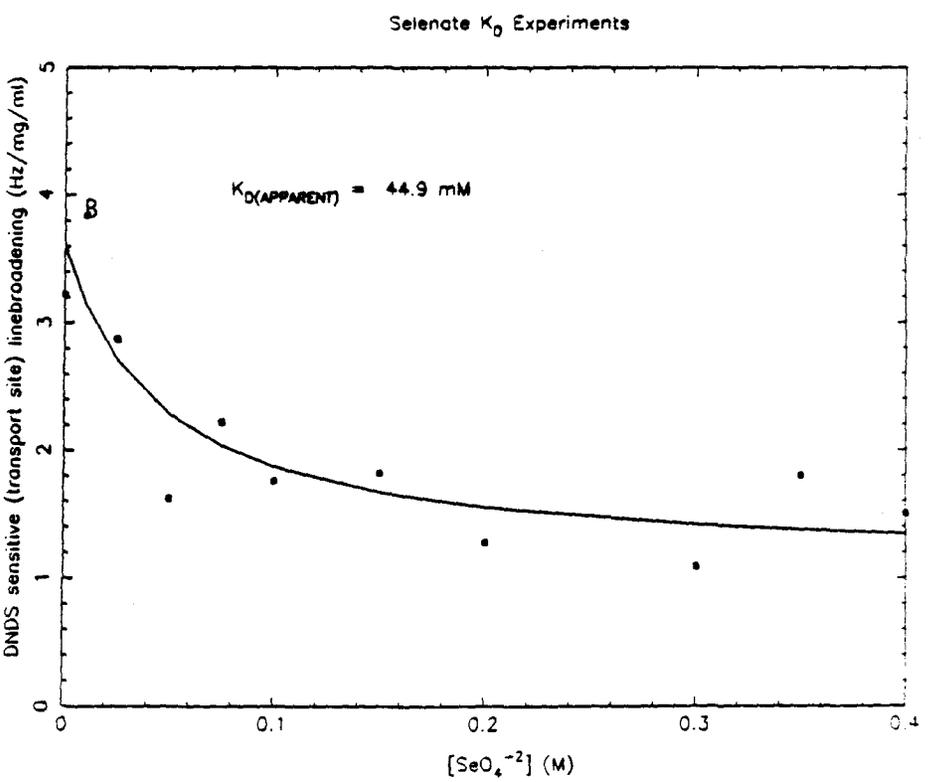
Selenate K_D Experiments
B
$K_{D(APPARENT)}$ = 44.9 mM
DNDS sensitive (transport site) linebroadening (Hz/mg/ml)
0
1
2
3
4
5
0
0.1
0.2
0.3
0.4
$[SeO_4^{-2}]$ (M)

Table 1. A comparison of apparent dissociation constants (heretofore called K_D or $K_{D(apparent)}$) measured by ^{35}Cl NMR at a constant [Cl^-] of 150 mM at 4°C), actual dissociation constants (K_I) and the literature values for the dissociation constants of a variety of anions transported anions. K_D's were fit from the nonlinear least-squares best-fit curve of $y = A - Bx / (x + K_D)$, where A is the maximal transport site linebroadening and B is a constant characteristic of the homogeneous class of DNDS sensitive binding sites. K_I's were calculated from the experimentally obtained K_D's using the relation $K_D=K_I(1+[Cl^-]/K_{I'})$.

Anion	K_D (mM)	K_I (actual) (mM)	K_I (literature)(mM)
F^-	290 ± 30[a]	88[a]	88[b]
Cl^-	190[a]	67[a]	65 ± 5[c]
Br^-	90 ± 10[d]	36 ± 4[d]	32[b]
I^-	34 ± 3[a]	10[a]	10[b]
HCO_3^-	55 ± 4[a]	16[a]	16[b]
MoO_4^{2-}	80[e]	24 ± 11[e]	--
SO_4^{2-}	77[e]	23 ± 11[e]	30[f], 41 ± 14[g]
SeO_4^{2-}	45[e]	14 ± 10[e]	--
HPO_4^{2-}	21[e]	6.3 ± 6[e]	53 - 70[h], 80[i]
$HAsO_4^{2-}$	8.4[e]	2.5 ± 1[e]	--

[a] Measured as in Reference 33 by competing the anion with 100 mM Cl^- at 4° C.
[b] From Reference 48 at 0° C.
[c] From Reference 49 at 0° C.
[d] From Reference 32 at 4° C.
[e] Measured as described in text by competing the anion with 150 mM Cl^- at 4°, pH 8.
[f] From Reference 15 at 0° C.
[g] As reviewed in Reference 3 at 0° C.
[h] From Reference 40 at 25°C. Values were taken from the half-maximal flux since the dependence of phosphate flux was found to be sigmoid in Reference 41
[i] From Reference 41 at 25° C.

Table 2. Different radii for monovalent and divalent anions discussed in this chapter or experimentally determined to be transported by band 3.

anion	ionic radius (crystalline)	ionic radius (hydrated)	number of waters of primary shell hydration
	r_i (Å)	r_h (Å)	n
F^-	1.36[a]	3.52[a]	4 ± 1[b]
Cl^-	1.81[a]	3.32[a]	1 ± 1[b]
Br^-	1.95[a]	3.30[a]	1 ± 1[b]
I^-	2.16[a]	3.31[a]	1 ± 1[b]
HCO_3^-	2.66[c]		
MoO_4^{2-}	3.23[c]	3.85[d]	
SO_4^{2-}	2.90[c]	3.79[d]	
SeO_4^{2-}	3.05[c]	3.84[d]	
HPO_4^{2-}	2.95[c]	4[e]	
$HAsO_4^{2-}$	3.15[c]		
$H_2PO_4^-$	2.95[c]	4-4.5[e]	
$H_2AsO_4^-$	3.15[c]		

[a] p. 73 in Reference 51.
[b] p. 597 in Reference 51.
[c] p. 483 in Reference 51.
[d] Reference 52.
[e] Reference 53.

ionic radius and K_I since fluoride, with a large hydrated radius, has a very different K_I than iodide.

In theory, the DNDS-sensitive linebroadening should go to zero as the concentration of dianion increases and saturates the transport site. Two possible scenarios can explain why this did not occur. First, the activity coefficient of the divalent anions continues to decrease to the point where much of the increase in dianion concentration is offset by the decrease in the activity coefficient for that anion. For example, at 25° C Na_2SO_4 has an activity coefficient of about 1 at infinitely dilute concentrations, 0.452 at 0.1 molal and 0.294 at 0.4 molal[38]. The effect of the decrease in activity on the K_D curves for several divalent anions is illustrated in Figures 2.6-2.7. In Figure 2.6, the sulfate's activity is plotted against transport site linebroadening. The activity, a, is obtained from the equation of $a = \gamma \times m$, where γ is the activity coefficient and m is the molality of the solution at 25° C.The divalent competition experiments were actually performed at concentrations measured in molarity. Because citrate is present in the solution, there are negligible changes in solvent volume. (This is because citrate, used to buffer and maintain ionic strength, occupies enough mass to compensate for differing amounts of solute.) However, the conversion from molarity to molality introduces an approximately constant conversion factor when the solute is not too heavily hydrated or has too high a molecular weight. For sulfate, a conversion factor of 0.937 was needed because Na_2SO_4 (anhydrous) was used. For hydrogen phosphate, a constant conversion factor of 0.889 molal/molar was used. However, hydrogen arsenate is heavily hydrated and has a large molecular weight (not compensated by citrate) so conversion factors were calculated for each concentration. They ranged from 0.933 at dilute concentrations to 0.873 at high concentraions. Since the dissociation constant, K_D, was so low, it was divided by 0.933 to convert from molal to molar. Further, we have assumed that the change in activity coefficient (based on activity coefficients for

Figures 2.6 and 2.7

Plots of activity versus DNDS-sensitive linebroadening are shown in these figures. The dissociation constants (K_D) are calculated using the equation $y = A - (Bx/(x+K_D))$. Activities are used instead of molar concentrations as the values for x above. The resulting K_D is given in molal. In the case of sulfate and phosphate, molal is directly converted to molar by dividing by constants (0.937 and 0.889, respectively). Molality is converted to molarity for arsenate using a concentration dependent conversion factor (0.933). Selenate's activity coefficients were not found.

Hydrogen Phosphate K_D Experiment

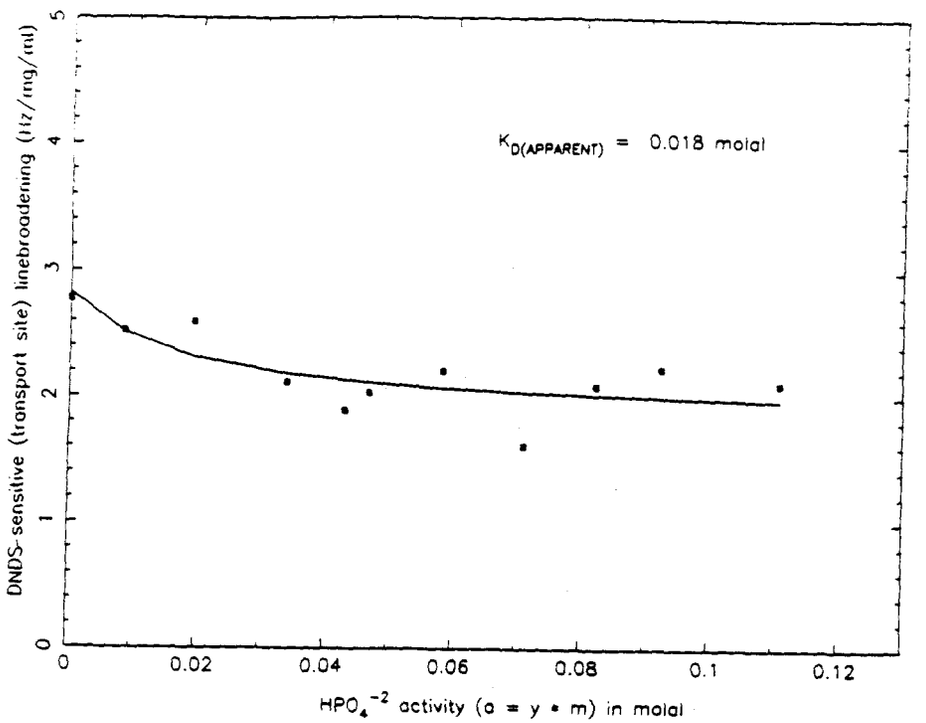

Hydrogen Arsenate K_D Experiment

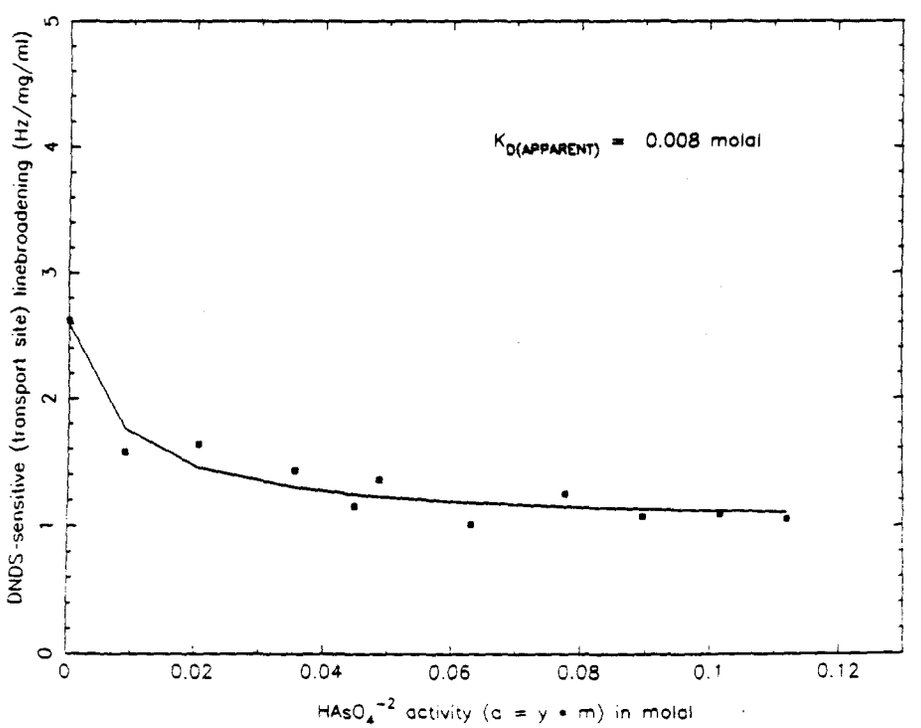

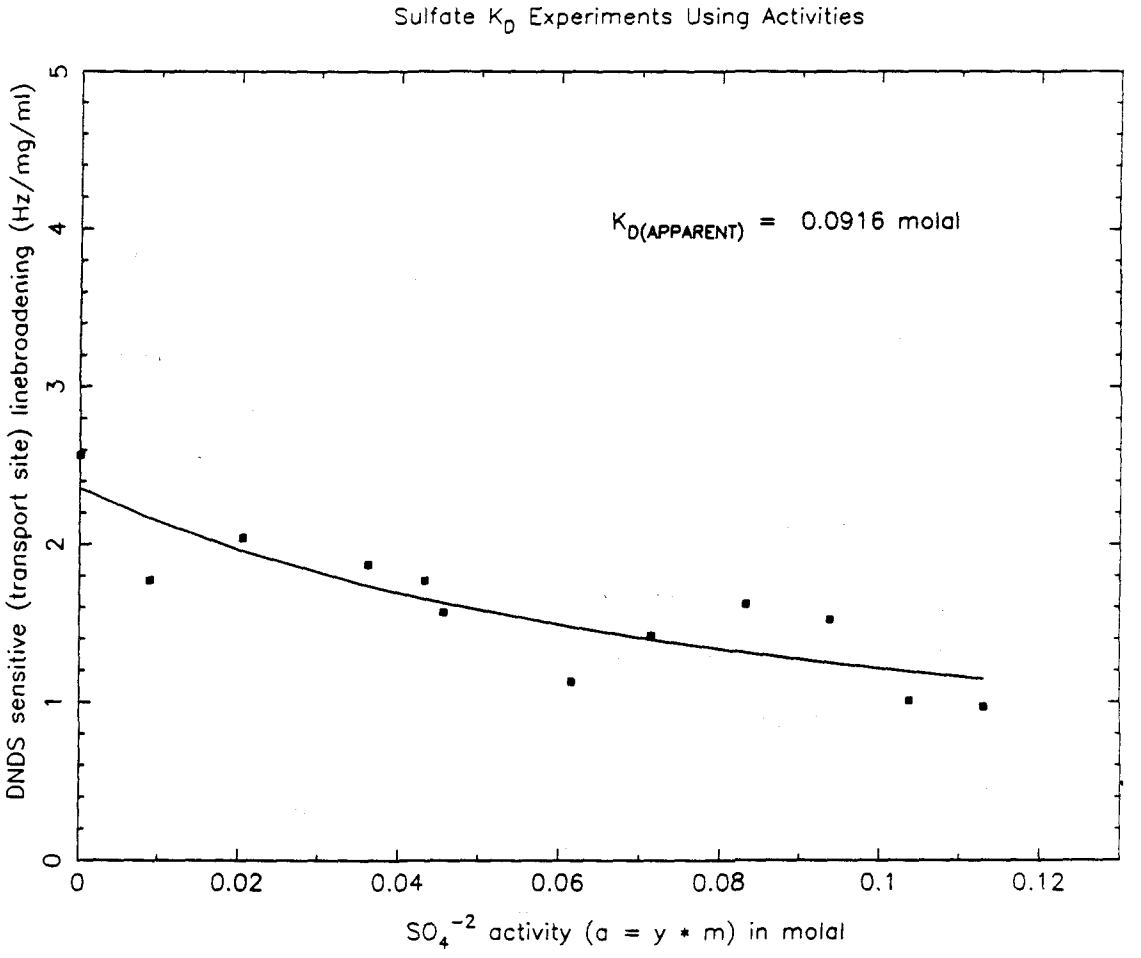
Sulfate K_D Experiments Using Activities
$K_{D(APPARENT)}$ = 0.0916 molal
DNDS sensitive (transport site) linebroadening (Hz/mg/ml)
0
1
2
3
4
5
0
0.02
0.04
0.06
0.08
0.1
0.12
SO_4^{-2} activity (a = y * m) in molal

H_2SO_4 at dilute concentations and more general characteristics of Na_2SO_4 activity coefficient curves[39]) is linear in the region of 0.0 molal to 0.1 molal. The same asssumption between 0.1 molal and 0.2 molal because the change is relatively small (0.452 to 0.371). Finally, the density of water changes from .9999 to .9971 from 5° C to 25° C while the activity coefficients change less than 10% in all listed (monovalent) cases in the same temperature range[38]. Because the errors are already large, the assumptions made are valid. When the K_D curve for sulfate was plotted using the activities, the apparent K_D was calculated to be 0.916 molal, which converts to 97.7 mM. An apparent K_D of 97.7 mM gives an actual K_I of 29.4 mM, which is somewhat closer to the literature value than the value obtained using concentrations.

The second problem lies in the fact that DNDS is much less soluble at high concentrations of inorganic oxyanions than it is in citrate, as evidenced by salting out phenomena at high dianion concentrations in samples with DNDS. This is presumably due to the fact that the number grams of solute increases slightly between 0.0 M dianion and 0.4 M dianion. These experiments were performed at the limit of DNDS solubility, so if there were contaminants in the buffers, they caused precipitation of the DNDS. Any samples with obvious salting out were rejected. Thus, the DNDS-sensitive linebroadening cannot go to zero even at high concentrations of these inorganic oxyanions. The cumulative result is to diminish the magnitude of the effect of the dianions on DNDS-sensitive linebroadening and to lower the values for the apparent K_D's obtained by this method.

Sulfate seems to compete with chloride for the transport site as demonstrated by the fact that the DNDS-sensitive linebroadening is decreased and can be fit by the least-squares best-fit to the curve $y = A - (Bx / (x + K_D))$. It is also observed that, when K_D curves are found for a plot of activity versus DNDS-sensitive linebroadening, the sulfate's curve slopes downward towards zero. This is not true with hydrogen

phosphate. Although the plot of concentration of hydrogen phosphate versus DNDS-sensitive linebroadening can yield a K_D, the curve levels off very quickly. Thus, hydogen phosphate's curve does not demonstrate an ability to saturate the transport site. Saturation is a necessary condition of competitive inhibition. A possible conclusion from the hydrogen phosphate K_D experiment is that not all divalent hydrogen phosphate is competing directly with chloride for the transport site.

The literature values for the K_I's of the above oxyanions are shown in Table 1. Within experimental error, the value found by ^{35}Cl NMR chloride competition experiments for sulfate agrees with the value for sulfate found in the literature. The value for hydrogen phosphate is extremely low. However, the literature value is actually a half-saturation constant obtained at 25° C. Measurements made at room temperature should lead to a higher value for K_D than those taken at 4° C because of band 3's high activation energy. (The apparent activation enthalpies lie in the range of 30 to 35 kcal/mol for slowly penetrating anion species such as sulfate, as reviewed in Reference 4.) Within experimental error, using our value for phosphate's K_D at 4° C and Schnell's value of 80 mM[41], the ΔH^o value for the phosphate transport has been calculated to be about 20 kcal/mole. K_D values for selenate and hydrogen arsenate have not previously been determined. However, based on hydrogen arsenate's 25% inhibition of the hydrogen phosphate flux in band 3[28], it is reasonable to assume that hydrogen arsenate binds more tightly to the transport site and has a lower K_D than hydrogen phosphate. SO_4^{2-} appears to be a competitive inhibitor of chloride *transport* by band 3 (as reviewed in References 3 and 39). The results found by ^{35}Cl NMR show that sulfate can inhibit DNDS-sensitive linebroadening.

Hydrogen phosphate transport data are more ambiguous. Kenney and Kaplan have reported that about 20% of the inorganic phosphate which is transported across the red blood cell membrane is transported via a sodium-dependent cotransport system.

Furthermore they found that the addition of arsenate (10 to 20 mM) resulted in a 25% inhibition of the band 3 phosphate flux[28]. In other experiments performed at pH 7.2, Dixon plots exhibit a linear relation between the inverse phosphate flux and the concentration of inhibiting anions (either sulfate or chloride), but the straight lines intersected below the abscissa[40]. The unidirectional phosphate flux across the red blood cell membrane exhibits saturation kinetics with a sigmoidal increase of the flux at low phosphate concentrations and self-inhibition at high phosphate concentration[41,42].

Interpretations of the data for hydrogen phosphate experiments are complicated by several features: 1) As seen in Table 3, one of the pK_a's for phosphate is 7.2. Many experiments which have been performed at pH's near 7 contain a mixture of monovalent and divalent phosphate; this is problematic because it has been reported that the divalent anion is transported at a lower rate than the monovalent[27]. It has also been found that only the monoanionic form of phosphate appears to inhibit chloride exchange[43]. 2) The concentration of unidirectional phosphate flux and the behavior of the Dixon plots point to an inhibition which is partly competitve and partly noncompetitive[39]. 3) As mentioned above, another protein can presumably transport inorganic phosphate across the red blood cell membrane. 4) Other anions present in solution presumably can compete more favorably than phosphate for transport since phosphate is transported at a rate 10^6 slower than chloride and about 10 times slower than even sulfate[3]. 5) The ionic media and pH conditions under which phosphate studies are performed affect the results[41]. In an effort to demonstrate that the K_D's obtained in this report are not pH dependent, pH profiles of divalent anion binding to the transport site were generated. The ^{35}Cl results obtained for hydrogen phosphate and hydrogen arsenate are consistent with a model in which both anions inhibit chloride binding to the transport site both noncompetitively and competitively. Thus, plots can be generated which will be fit to a K_D curve, but the these two oxyanions will not

Table 3. Acid dissociation constants at 25°C for the anions of interest.

Acid	Formula	K_1	K_2	K_3
Arsenic	H_3AsO_4	6×10^{-3}	1.05×10^{-7}	3.0×10^{-12}
Phosphoric	H_3PO_4	7.11×10^{-3}	6.34×10^{-8}	4.2×10^{-13}
Selenic	H_2SeO_4	strong	1.2×10^{-2}	
Sulfuric	H_2SO_4	strong	1.2×10^{-2}	

saturate the chloride binding site. This behavior suggests that a more complicated situation exists where only a fraction of the phosphate interferes with chloride binding to the transport site even at high concentrations.

pH Profiles of Divalent Anion Binding to the Transport Site

In order to determine whether dianion binding to the transport site had any pH dependence between pH 5.5 to 8.0, the pH profiles of phosphate, sulfate, selenate and arsenate in this region were examined. There is little effect of pH on the transport site linebroadening for chloride between pH's 5.5 and 8, shown in Figure 2.8. Band 3 pH profiles for *transport* of chloride, phosphate and sulfate were shown in Figure 2.1. pH experiments were not performed on molybdate since it undergoes polymerization reactions at pH's below 6.0. (For example, an abundant species from pH 4.5 to 6 is $H_3Mo_3O_{11}^{4-}$[44].)

Figure 2.8 showed that there is no titration event for chloride binding to the DNDS-sensitive site in the pH range of 5.5 to 8.0. Figures 2.9-2.10 show that, for dianion binding to the transport site, there is no obvious titration event in the same pH range. Results with sulfate, in particular, are accurately fit to a line with slope of 0. One data set was acquired for selenate, but it also gave a horizontal line. When fit to lines, hydrogen phosphate and hydrogen arsenate results gave positive slopes. Both have monovalent to divalent ($H_2PO_4^-$ <-- > HPO_4^{2-}) K_a's in this region. The fact that both are able to prevent more chloride binding at low pH's is consistent with experimental evidence suggesting that monovalent phosphate is transported much more efficiently than divalent phosphate[27,45]. This would also be consistent with the ^{31}P NMR results of Labotka and Omachi, who report that $H_2PO_4^-$ has an influx rate of 170 while HPO_4^{2-} has an influx rate of 1[46]. However, because of large errors at the individual points, it cannot be stated conclusively that the monovalent

Figure 2.8

The effect of pH on the transport site linebroadening. This figure shows no observable titration event in the pH range of 5.5 to 8.0. (Taken from J.J. Falke, unpublished results.)

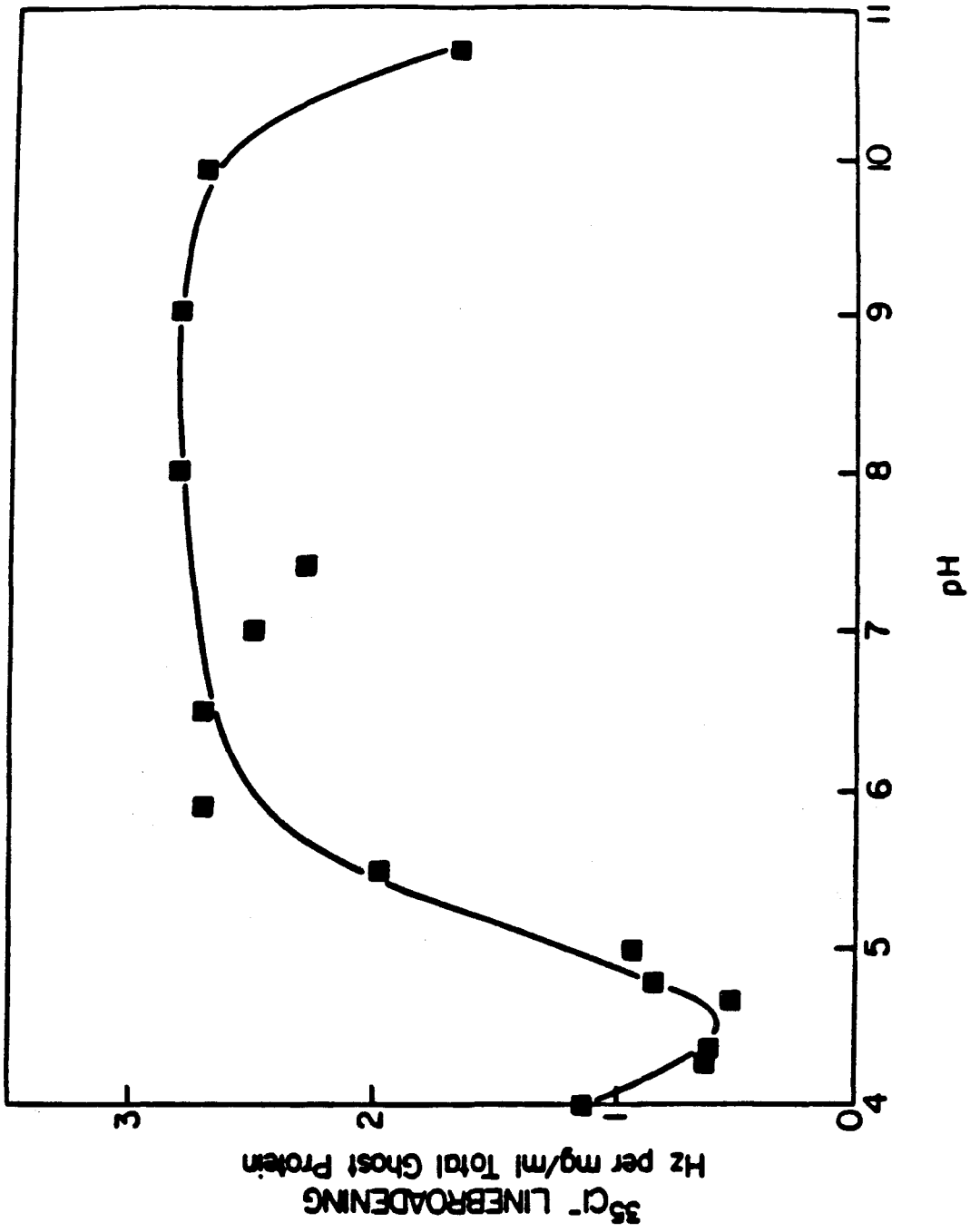
35Cl- LINEBROADENING
H2 per mg/ml Total Ghost Protein
pH
0
1
2
3
4
5
6
7
8
9
10
11

Figures 2.9 and 2.10

Figures 2.9 and 2.10 show the effect of titrating on DNDS-sensitive ^{35}Cl NMR linebroadening between pH's 5.5 and 8 in the presence of different divalent anions. The line for sulfate is obtained from points averaged from four data sets. Phosphate's lines were obtained from two data sets at different concentrations. The plots for selenate and arsenate each contain 1 data set.

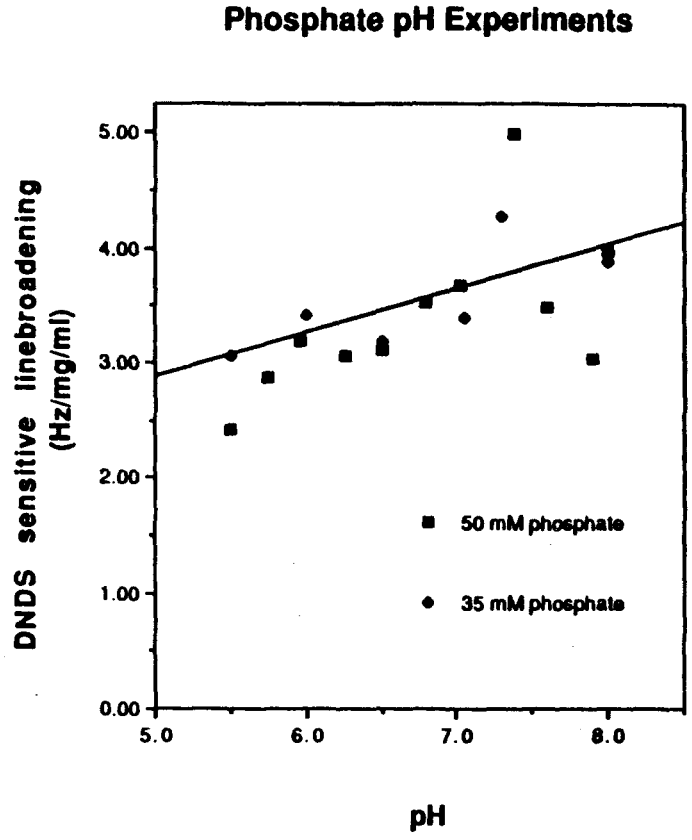
Phosphate pH Experiments
DNDS sensitive linebroadening (Hz/mg/ml)
5.00
4.00
3.00
2.00
1.00
0.00
5.0
6.0
7.0
8.0
pH
50 mM phosphate
35 mM phosphate

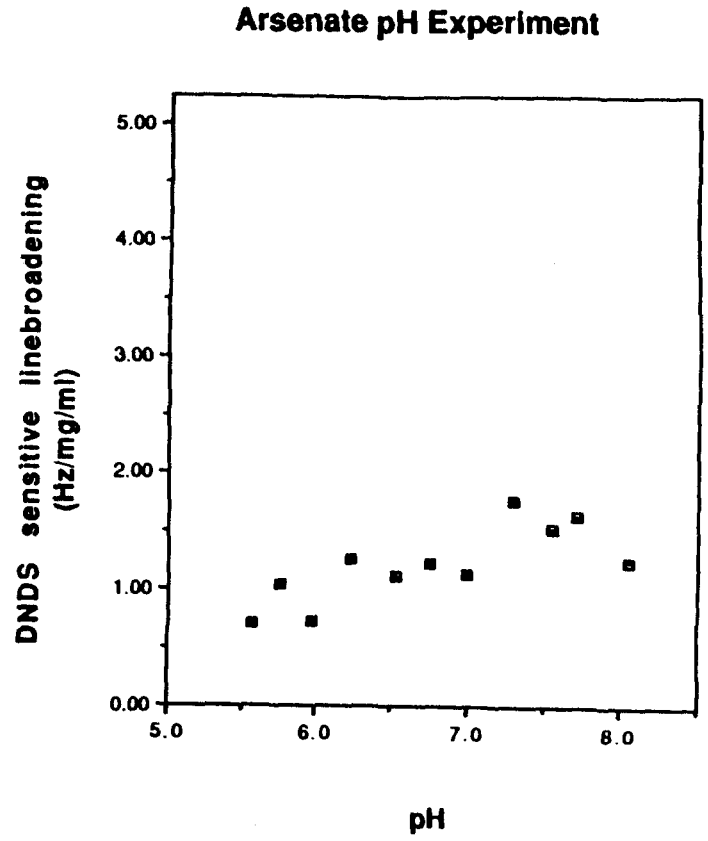
Arsenate pH Experiment
DNDS sensitive linebroadening (Hz/mg/ml)
5.00
4.00
3.00
2.00
1.00
0.00
5.0
6.0
7.0
8.0
pH

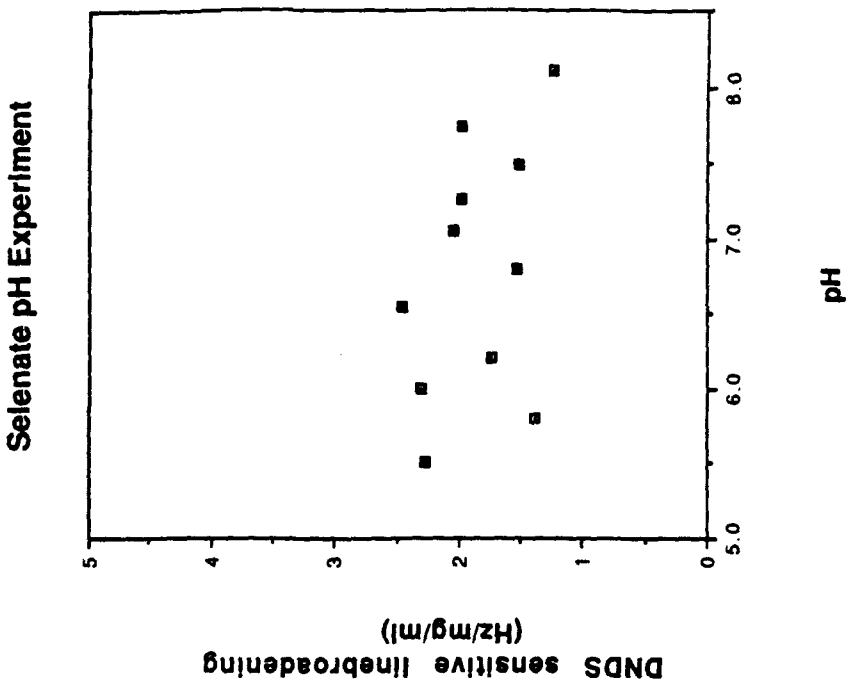
Selenate pH Experiment
DNDS sensitive linebroadening
(Hz/mg/ml)
0
1
2
3
4
5
5.0
6.0
7.0
8.0
pH

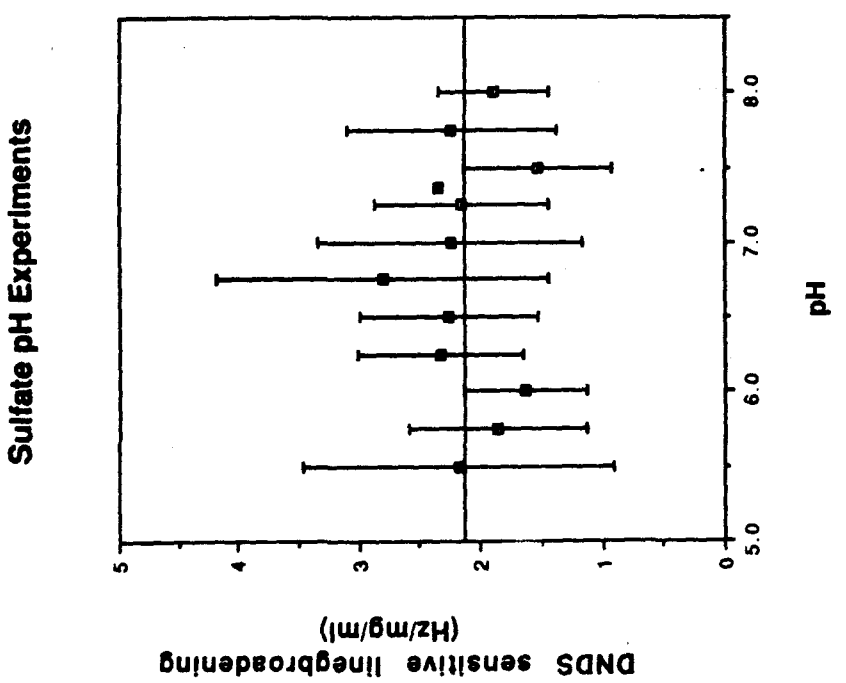
Sulfate pH Experiments
DNDS sensitive linebroadening
(Hz/mg/ml)
0
1
2
3
4
5
5.0
6.0
7.0
8.0
pH

form competes more effectively than the divalent for the DNDS-sensitive transport site. If only a fraction of the phosphate is binding to the transport site, then the upward slope would be significant. Brauer *et al.* have used ^{35}Cl and ^{31}P NMR to monitor chloride binding to band 3, internal and external pH's, and phosphate influx and efflux from red blood cells. Their results are consistent with either the model of transport of $H_2PO_4^-$ or cotransport of H^+ and HPO_4^{2-}, although they report that more than 80% of the net phosphate influx was due to transport of its monoanionic form[47]. The plots of the pH experiments using our experimental protocol show that the K_D's obtained at pH 8 should be relatively characteristic of the K_D over the pH range of 5.5 to 8.

CONCLUSIONS

All divalent oxyanions tested seemed with chloride for the DNDS-sensitive band 3 active site since all could be fit to curves to obtain K_D's. However, since the K_D curves hydrogen arsenate and hydrogen phosphate do not saturate the transport site even at high concentrations, there appears to be some mechanism different from that of chloride for their transport. The values obtained for the dissociation constants of this series of divalent oxyanions were reduced from, but within experimental error of, the values of the half-saturation constant obtained by flux experiments. They were low because of the low activities encountered at the high ionic strengths used. Another explanation is that the low K_D's at the chloride binding site may in fact reflect tighter binding at this site (for example, prior to some cooperative interaction with another amino acid residue). This is the model of Vogelaar and Chan as shown in Figure 2.2. Vogelaar and Chan have proposed that a histidine residue, working in concert with the active-site arginine, could allow translocation by providing a positive charge to ion pair with the extra negative charge of divalent anions. This histidine stabilizes the dianion's interaction with the active site.

Sulfate and selenate may competitively inhibit chloride binding at the transport site. This is especially evident in the plots of acitivity versus ^{35}Cl NMR DNDS-sensitive linebroadening, where the curves resemble classical competitive inhibitors. However, Falke and Chan have shown that if exchange is prevented (by whatever mechanism), an inhibitor will exhibit a curve which can be least squares best-fit to obtain a K_D. This was evident for the inhibitor dipyrimidole, although it acts to prevent chloride binding to the transport site by blocking the band 3 transport channel. The large size and extra charge of both hydrated selenate and hydrated sulfate make it important to demonstrate that they are being transported by the same mechanism as chloride and can competitively inhibit chloride binding to the transport site. These experiments do not prove conclusively show competitive inhibition. They do show that sulfate and selenate can interfere with chloride's binding to the transport site. Only a fraction of hydrogen phosphate and hydrogen arsenate appear to be competitive inhibitors of chloride binding to the transport site, but their inablility to saturate the transport site precludes stating that they are transported by the same mechanism as other anions.

Although there exists a great deal of experimental evidence leading to the 'titratable carrier model' for divalent anion transport by band 3, the ^{35}Cl NMR pH experiments did not show any definite titration event. If the mechanism for transport is similar to that of Vogelaar and Chan, a pH titration event might be visible using ^{35}Cl NMR. The fact that a titration event is not seen could be due to two reasons. First, these experiments may be too insensitive to the environment around the chloride binding active site residue to observe other binding events which involve the divalent anions. Second, because ^{35}Cl NMR experiments probe only chloride binding to the transport sites, and since translocation is an event separate from binding, ^{35}Cl NMR will not assay any titration event which occurs during the translocation process (as distinct from the binding process). Thus, the only unambiguous conclusions which can be reached

from the pH experiments are that there is no titration event occuring which is detectable by this method between pH 5.5 and 8 and that the dissociation constants obtained for divalent binding to the chloride binding site are valid over the same pH range for sulfate and selenate (and probably for hydrogen phosphate and hydrogen arsenate). These experiments also demonstrate a small effect of valency on hydrogen arsenate and hydrogen phosphate binding to the DNDS-sensitive transport site.

REFERENCES

1. Gunn, R.B. (1980) **Mechanisms of Intestinal Secretion** (H.J. Binder, ed.) Alan R. Liss Inc. New York, 25-43.

2. Stein, W.D. (1986) **Transport and Diffusion Across Cell Membranes**, Academic Press, New York p. 171.

3. Knauf, P.A. (1979) *Current Topics in Membranes and Transport* **12**, 249-363.

4. Passow, H. (1986) *Rev. of Physiol., Pharmacol., and Biochem.* **103**, 61-203.

5. Dalmark, M. and Wieth, J.O. (1972) *J. Physiol. (London)* **244**, 583-610.

6. Ku, C.-P., Jennings, M.L., and Passow, H. (1979) *Biochim. Biophys. Acta*, **553**, 132-141.

7. Milanick, M.A. and Gunn, R.B. (1984) *Am. J. Physiol.* **247**, C247-259.

8. Falke, J.J. and Chan, S.I. (1988) *J. Biol. Chem.* **260**, 9537-9544.

9 Gunn, R.B. (1978) **Membrane Transport Processes** (J.F. Hoffman, ed.) Raven Press, New York, 61-77.

10. Jennings, M.L. (1978) *J. Membrane Biol.* **28**, 187-198.

11. Milanick, M.A., and Gunn, R.B. (1982) *J. Gen. Physiol.*. **79**, 87-114.

12. Gunn, R.B., Dalmark, M., Tosteson, C. and Wieth, J.O. (1973) *J. Gen. Physiol.* **61**, 185-206.

13. Funder, J.F. Tosteson, C. and Wieth J.O. (1978) *J. Gen. Physiol.* **71**, 721-746.

14. Lepke, S. and Passow, H. (1977) *J. Membr. Biol.* **6**, 158-182.

15. Schnell, K.F., Gerhardt S. and Schoppe-Fredenburg, A. (1977) *J. Membr. Biol.* **30**, 319-350.

16. Wieth, J.O., Andersen, O.S., Brahm, J., Bjerrum, P.J., and Borders, C.L. (1982) *Phil. Trans. Royal Soc. London, Series B.* **299**, 383-399.

17. Werner, P.K., and Reithmeier, R.A.F. (1988) *Biochim. Biophys. Acta,* **942**, 19-32.

18. Jennings, M.L., and Andersen, M.P., (1987) *J. Biol. Chem.* **262**, 1691-1697.

19. Knauf, P.A., Tarrshis, T., Grinstein, S., and Furuya, W. (1980) **Membrane Transport in Erythrocytes** (Lassen, U.V., Using, H.H., and J.O. Wieth, eds.) Munksgard, Copenhagen.

20. Jennings, M.L., and Adams, M.F. (1981) *Biochem.* **20**, 7118-7123.

21. Matsuyama, H., Kawano Y., and Hamasaki, N., (1986) *J. Biochem.* **99**, 495-501.

22. Chiba T., Sato, Y., and Suzuki Y. (1986) *Biochim. Biophys. Acta* **858**, 107-117.

23. Bjerrum, P.J., Wieth, J.O., Borders, C.L. (1983) *J. Gen. Physiol.* **81**, 453-484.

24. Wieth, J.O., Brahm, J., and Funder J., (1980) *Ann. N.Y. Acad. Sci.* **341**, 394-418.

25. Brahm, J., (1977) *J. Gen. Physiol.* **70**, 283-306.

26. Barzilay, M., Ship, M., and Cabantchik, Z.I. (1979) *J. Membrane Biochem.* **2**, 227-281.

27. Runyon, K.R., and Gunn, R.B., (1984) *Biophys. J.* **45**, 18a.

28. Kenney, L.J., and Kaplan, J., (1988) *J. Biol. Chem.* **263**, 7954-7960.

29. Aubert, L., and Motais, R. (1975) *J. Physiol. (London)* **246**, 259-269.

30. Hajjawi, O.S., and Hider, R.C. (1987) *Mol. Cell. Biochem.* **75**, 43-49.

31. Vogelaar, N.V. (1989) *Doctoral Thesis* (California Institute of Technology).

32. Falke, J.J. (1985) *Doctoral Thesis* (California Institute of Technology).

33. Falke, J.J., Pace, R.J., and Chan, S.I. (1984) *J. Biol. Chem.* **259**, 6472-6480.

34. Falke, J.J., Kanes, K.J., and Chan, S.I. (1985) *J. Biol. Chem.* **260**, 9545-9551.

35. Jones, M.N. and Nickson, J.K. (1981) *Biochim. Biophys. Acta* **650**, 1-20.

36. Markwell, M.A., Haas, S.M., Bieber, L.L., and Tolbert, N.E. (1978) *Anal. Biochem.* **87**, 206-210.

37. Lowry, O.H., Rosebrough, N.J. Farr, A.L. and Randall, R.J. (1951) *J. Biol. Chem.* **193**, 265-275.

38. Robinson, R.A. and Stokes, R.H. (1965) **Electrolyte Solutions, Second Edition**, Butterworths, London 24-29, 457, 479, 481, 500-507.

39. Guggenheim, M.A., and Stokes, R.H. (1969) **The International Encyclopedia of Physical Chemistry and Chemical Physics Topic 15: The Equilibrium Properties of Electrolyte Solutions,Vol. 1** (R.A. Robinson, ed.) Pergamon Press, Oxford, 111.

40. Vangala, R., and Schnell, K.F., (1979) *Pflugers Archiv. Eur. J. Physiol.* **Supplement to 379**, r25 (abstract).

41. Schnell, K.F. and v. der Mosel, R., (1979) *Pflugers Archiv. Eur. J. Physiol.* **Supplement to 379**, r27 (abstract).

42. Schnell, K.F., Besl, E., and v. der Mosel, r. (1981) *J. Membr. Biol.* **61**, 173-192.

43. Gunn R.B., Milanick M., and Frolich O. (1980) *Fed. Proc.* **39**, 1715 (abstract).

44. Freir, R.K. (1978) **Aqueous Solutions, vol. 2**, Walter Gruyter, New York.

45. Berghout, A., Raida, M., Romano L., and Passow, H. (1985) *Biochim. Biophys. Acta* **815**, 281-286.

46. Labotka, R.J., and Omachi, A. (1987) *J. Biol. Chem.* **262**, 305-311.

47. Brauer, M., Spread, C.Y., Reithmeier, R.A.F., and Sykes, B.D. (1985) *J. Biol. Chem.* **260**, 11643-11650.

48a. Dalmark, M. (1975) *J. Physiol.* **250**, 39-64.

48. Dalmark M. (1976) *J. Gen. Physiol.* **67**, 223-234.

49. Brazy, P.C. and Gunn, R.B. (1976) *J. Gen. Physiol.* **68**, 583-599.

50. Schnell, K.F. (1977) *J. Membr. Biol* **37**, 99-136.

51. Conway, B.E. (1981) **Studies in Physical and Theoretical Chemistry: Ionic Hydration in Chemistry and Biophysics, Vol. 12** Elsevier, New York.

52. Nightengale E.R. (1959) *J. Chem. Phys.* **63**, 1381-1387.

53. Skoog, D.A. and West, D.M.(1976) **Analytical Chemistry, Third Edition**, Holt, Rinhart and Wilson, New York.

54. Falke J.J., and Chan, S.I. (1986) *Biochem.* **25**, 7895-7898.

Chapter III

Determination of Transmembrane Helices

INTRODUCTION

As stated in Chapter I, the main goal of this work was to determine the location of the functionally essential arginine in the transport site of the band 3 protein. ^{14}C-phenylglyoxal was chosen to modify this residue because of its propensity to label active-site arginines. (A description of this reaction and its experimental basis can be found in Chapter IV.) With the labeling procedure used, two to three arginines are labeled per band 3 monomer[1]. It was therefore necessary to show that the labeled fragment(s) contained the active-site arginine. Without proof that the protein is being labeled in only one location, a labeling would not necessarily occur at the essential arginine at the transport site. For example, without some idea of the protein topography, it would be impossible to rule out labeling at a 'loop' or some non-membrane-spanning, non-helical portion of the protein. This would presumably occur somewhere near the end of a transmembrane segment. For example, an arginine within the ion channel but near either end might be labeled. Many of the amino acids at the interface between the membrane and the surrounding solution were modeled by Chan

and Vogelaar[2], as well as by the hydropathy plots of Lodish[3], to contain high concentrations of positive charges (presumably to direct the negative ions into the channel). In addition, Jay and Cantley suggest that from either side of the membrane, band 3 can be compared to a positively charged funnel that leads into the center of the membrane where the active-site residues are located[4]. Without some idea of how the protein is folded in the membrane, it would be difficult to show convincingly that a labeled proteolytic fragment contains the essential active-site arginine.

In order to gain a better understanding of the topography of the protein in the membrane, this work focussed on determining the composition of the transmembrane segments of the band 3 protein (in other words, showing the precise number and location of N-termini of the membrane-spanning sequences). The experimental approach involved proteolysis of as much of the exposed, non-membrane-spanning parts of the membrane as possible and removal of the cytoskeletal components by stripping. The lipid-protected transmembrane sequences constituted the remaining peptides. Among the major erythrocyte membrane proteins, only two (with appreciable quantities, i.e. >200,000/erythrocyte) are known to span the lipid membrane and have functional groups exposed to both the cytoplasm and the extracellular solution: PAS-1 (glycophorin A) and band 3[5,6]. Fortunately, PAS-1 spans the membrane only once and should not provide appreciable contamination[6].

Papain was chosen to proteolyze the extra-membrane regions because it is readily available and has demonstrated broad specificity for peptide-bond hydrolysis. Falke *et al.* have shown that papain will proteolyze band 3 into a series of small peptides (with molecular weights < 8,600 daltons). These form a diffuse band on silver-stained, electrophoretic polyacrylamide gels[7]. No whole band 3 or large proteins are visible in the gel under these conditions. Furthermore, while still in the membrane, the band 3's active-site will bind chloride, as determined by ^{35}Cl NMR[7]. Papain apparently has an

active-site region of seven amino acid residues[8]. This creates a potential disadvantage in obtaining all of the transmembrane segments because not all aqueous-accessible 'loops' have more than seven amino acids which are exposed to solution. Band 3 has been modeled by Vogelaar and Chan to have several membrane-spanning regions which almost directly join each other with separations of less than seven residues[2]. Lodish has modeled at least two band 3 transmembrane helices which do not completely span the membrane[3]. (This was diagrammed in Chapter 1, Figure 1.1.)

The band 3 helices have been shown to be closely associated by protein-protein interactions in the membrane[7]. Other studies indicate that they share the following characteristics which make them difficult to separate: (1) they are amphiphilic but similar in their overall hydrophobicity; (2) they are α-helices, with the same secondary structure; (3) they are approximately the same size. Appendix I in Chapter IV describes conventional experimental methods which failed to separate these transmembrane helices. This chapter describes the modification of an experimental method to separate the transmembrane helices. The method was developed by Tomich *et al.* to separate synthetic hydrophobic peptides[9]. It is important to note that sequencing, in general, can be accomplished on only the first 10 to 25 amino acids of a peptide, unless it is extremely pure and highly concentrated. Because of the difficulty in obtaining pure, concentrated peptides and due to the extreme hydrophobic character, it proved impossible to find all of the transmembrane peptides.

Theoretically, 21 hydrophobic amino acid residues in an α-helical arrangement can traverse the lipid bilayer once[10]. Assuming 28-35 amino acids are needed to traverse the membrane and form a 'loop', then the 509 amino acid integral membrane domain can have at least 15 transmembrane helices. In this chapter, a method is described for separrating generating and separating transmembrane helices. Then the N-termini for 6 transmembrane helices in band 3 are determined.

MATERIALS AND METHODS

Materials

Chemicals: Reagents and their sources are: Beta-mercaptoethanol, sodium dodecyl sulfate (SDS), L-cysteine hydrogen chloride, n-octyl-β-D-glucopyranoside (octylglucoside) and phenylmethylsulfonylfluoride (PMSF) (Sigma Chemical Co.); morpholine, High-Performance Liquid Chromatography (HPLC) grade acetonitrile, n-propanol, and trifluoroacetic acid (TFA) (Aldrich Chemical Co.); dichloromethane, anhydrous diethyl ether, nitric acid, and acetic acid (Mallinckrodt); dimethylformamide, tetrahydrofuran, and methanol (all HPLC grade) (Burdick and Jackson); papain (*Caricca papaya)* (Calbiochem), [^{35}S]SDS (Amersham), dithiothreitol (DTT) (Schwarz/Mann Biotech). Scintillation counting was performed using 10 ml of Safety-Solve (Research Products International).

Methods

Ghost Preparation:

Recently outdated human blood (packed red cells) was a kind gift of the Los Angeles Chapter of the American Red Cross. One to two units of any blood type were mixed and ghost membranes were prepared as described previously[11,12] with modifications described elsewhere[13].

Papain Proteolysis of Ghost Membranes:

Papain's thioester active site was first activated with cysteine. The papain activating solution consisted of 250 ml of 50 mM sodium acetate pH 5.2 and 10 ml of

1.75% L-cysteine hydrogen to which 2.5 g of papain had been added. This suspension was stirred gently, then centrifuged at room temperature for 20 minutes at 11,000 rpm (19,700 x g_{max}). The pellet contained any unactivated (or excess) papain and contaminants. Two to three volumes of this papain solution were mixed with one volume of ghost membranes in SS-34 Sorvall centrifuge tubes and incubated at 37°C for 1.5 hours in a shaker bath, with vortexing every 5 to 10 minutes. The purpose of continual shaking and vortexing was to prevent aggregation of the papain-treated ghost membranes. Proteolysis was inhibited by pelleting the membranes twice at 15,000 rpm (27,000 x g_{max}) for 15 min in 5 mM Na_2HPO_4 adusted to pH 8 (henceforth called 5P8) and aspirating the supernatant.

Washing and Stripping:

All washes were performed in SS-34 Sorvall tubes at 15,000 rpm (27,000 x g_{max}) for 15 minutes. The resulting hard pellets were resuspended by pipeting and/or vortexing after aspirating off supernatant and adding the next solution.

High pH stripping of ghost membranes: Ghosts were stripped of the cytoskeletal proteins and proteolytic fragments by exposure to high pH at low ionic strength. This was accomplished by washing first in water, and then in 10 mM NaOH, and again in water. The pH was then lowered by the salt washes below.

High-salt washes of ghost membranes: High-salt washes disrupt salt bridges and ionic interactions of fragments or cytoskeletal proteins with integral membrane fragments. Ghosts were washed once in 250 mM NH_4Cl in 5P8, once in 100 mM NH_4Cl in 5P8, and lastly in 5P8 to return the conditions to normal.

Initial HPLC:

Proteolyzed, washed and stripped ghosts were solubilized by adding 1 volume of a 10% SDS (w/v) solution to 9 volumes of ghost preparation. Purification of membrane-spanning peptides was carried out using a nonionic detergent based system. This method is based on a method for the solubilization and purification of hydrophobic synthetic peptides developed by Tomich *et al.*[9]. Both mobile phase buffers (A and B) were deaerated by simultaneously sonicating and aspirating. A Vydac C_{18} Model 218TP510 semi-preparative reverse-phase column was equilibrated with buffer A (0.2% v/v TFA, 0.1% v/v morpholine, 0.1% w/v octylglucoside in 95% H_2O, 5% n-propanol). The concentration of the organic phase, buffer B (0.2% v/v TFA, 0.1% v/v morpholine, 0.1% w/v octylglucoside in 45% n-propanol, 45% acetonitrile, 10% H_2O) was increased according to the following scheme:

Time Program 1

time (min)	function	value	
0.1	total flow	0.8	ml/min
0.1	B concen.	0	%
0.1	wave length	215	nm
20	total flow	0.5	ml/min
20	B concen.	60	%
30	B concen	85	%
50	B concen	94	%
57	B concen	94	%
76	B concen	95	%
86	B concen	95	%
93	B concen	96	%
100	B concen	96	%
107	B concen	97	%
114	B concen	97	%
118	B concen	98	%
120	B concen	98	%
125	B concen	99	%
128	B concen	99	%
135	B concen	100	%
140	B concen	100	%
155	B concen	0	%
165	B concen	0	%
165	total flow	0.5	ml/min

Time Program 1 (continued)

time (min)	function	value	
170 stop	total flow	0	ml/min

One ml of the SDS solubilized membranes was injected on to the column using a 1 ml injection port. Elution of the peptides was monitored at 215 nm using a Shimadzu Model SPD-6 AV wavelengh uv-vis detector. All chromatographed sample fractions were collected at 3 minutes per tube.

Preparation of Samples for Second HPLC:

The fractions comprising a particular peak were combined from at least 7 HPLC runs. About 1 ml of 10% SDS was added to the pooled fractions. This mixture was then lyophilyzed to near dryness (from 2 to 5 ml depending on the original fraction volumn). The cloudy suspension was then dialyzed against 1.5 to 2 l of a 1 mM HCl, 0.01% SDS solution to remove the residual TFA and morpholine and all octylglucoside. This dialysis step was necessary since the octylglucoside prevented large quantities of sample (>.15 ml) from being injected on to the column. The SDS and low pH helped to keep the protein solubilized. The resulting dialysate was frequently cloudy. If this step was omitted, high back pressures developed on the column.

Second HPLC:

One ml of the above dialysate was loaded onto the column with buffers A and B as described above. However, the gradient was changed to the following:

Time Program 2

time	function	value
total flow	0.6	ml/min
B concen.	0	%
wave length	215	nm
total flow	0.8	ml/min
B concen.	0	%
B concen.	40	%
total flow	0.8	ml/min
B concen.	100	%
B concen.	100	%
B concen.	0	%
total flow	0.8	ml/min
total flow	0	ml/min
stop		

Protein Sequencing:

Samples were prepared for sequencing as they were above for the second injection onto the HPLC. However, a second dialysis was performed to ensure that the total concentration of SDS in the final sample did not exceed 0.01%. The dialysates were lyophilyzed to insure that the protein concentration was high (approximately 10μM of protein per sample) and the sample volume was small (<300 μl).

From 150 μl to 400 μl of fractions prepared as above were sequenced by automated Edman degradation on an Applied Biosystems Model 477A pulsed liquid microsequencer. The PTH derivatized amino acids were analyzed on a narrow bore HPLC (Applied Biosystems Model 120A). Most of the proteolyzed fragments were sequenced at the Sequencing Facility at the Children's Hospital of Los Angeles. The remainder were sequenced at the California Institute of Technology Microsequencing Facility.

Amino Acid Analysis:

Amino acid analysis was performed by the Caltech Microsequencing Facility.

Sequence Alignment:

Determination of the sequence position within band 3 was performed using the DNA Master program (L. E. Hood Laboratory) at the California Institute of Technology. The first pure sequences were subjected to a computer search of all proteins in the Protein Information Resource data bank (which contains over 10,000 protein sequences) using the method of Lipman and Pearson (this method does not yield a percentage; it yields a weighting factor out of 100, which is biased by conserved versus non-conserved substitutions)[14]. Because some of the less pure proteolysis fragments were not long enough to give unambiguous search ratings, they were compared only with band 3. The sub-program called *Sub-sequence Homology (between 2 sequences)* or *Similarity Comparison Between Two Sequences* was used to predict likely sequences in band 3. This was followed by a more exact alignment performed using the method of Needleman and Wunsch[15]. The experimentally determined sequence was also compared with glycophorin A (the second most abundant integral membrane protein in erythrocyte ghosts) and with papain. The comparison with glycophorin A was used to determine if the single membrane-spanning helix from that protein had been obtained. The comparison with papain was a control to determine the amount of homology with a random protein.

Interpretation of Amino Acid Analysis:

The general scheme for the amino acid analysis can be summarized as follows. The N-terminal position of the proteolyzed peptides were known. From this amino acid, different length fragments of the mouse erythrocyte band 3 sequence were input into a computer program which counted the number of each residue in a peptide. The lengths of the input peptides were varied in 5 amino acid increments from 30 to 80 residues. If there was a detectable amount of histidine, the initial amounts of amino acid in the

analysis was normalized to 1 histidine. Then this amino acid analysis (normalized to one histidine) was compared to the counts obtained above. The number of histidines was adjusted to obtain values for proline and arginine (and then leucine and valine, and the all other amino acids except those discussed below) which best fit an amino acid count for one of the different lengths of sequence. In these analyses, normalizations based on 1 histidine gave values for arginine, proline, tyrosine, isoleucine, lysine, methionine, and threonine, which were close to the values in one of the tallys for that sequence starting point. The same method was used to find the most likely length within the 5 amino acid increment.

Residues G and S were ignored in the amino acid analyses since they gave anomalously high values (possibly due to residual G and S in the dialysis tubing, pipet tips, etc.). D, E, N, and Q gave low values. D and E many have had low values due to poor extractability in the instrument[16]. W is acid-hydrolyzed. C is frequently undetectable[16]. N and Q were not present due to deamidation[16]. Using this approach, the length of the peptide was approximated.

[^{35}S]SDS HPLC Studies :

Three serial dilutions of [^{35}S]SDS in 10% cold SDS were performed to determine the amount of [^{35}S]SDS to be loaded onto each column. The non-protein SDS sample was prepared by making a 0.05% [^{35}S]SDS/10% SDS solution. Ten µl of this solution were injected onto a 25-cm octylglucoside-equilibrated C_4 Vydac analytical column. One ml fractions were collected. A 200 µl aliquot from each fraction was added to scintillation vials containing 10 ml of scintillation cocktail. Each vial was counted for 2 minutes using a Beckman LS9000 scintillation counter. The protein / SDS sample was prepared by adding 50 µl of a 0.05% [^{35}S]SDS-10% SDS solution to 450 µl of freshly prepared erythrocyte ghosts that had been stripped of nonintegral

membrane proteins as above. This solution was boiled for 5 min, and 250 µl were injected onto the C_4 column. For each, one-ml fractions were collected, 300 µl were added to 10 ml of scintillation cocktail and counted for 2 minutes.

RESULTS and DISCUSSION

[^{35}S]]SDS Chromatographic Studies:

[^{35}S]SDS was passed over the column to judge how effectively the SDS was being removed from the sample. This was important because, with other detergent-based HPLC, the SDS in the mobile phase elutes from the column with the proteins. The proteins presumably were contaminated with some lipid (demonstrated by joule heating of gels). Additionally, the proteins eluted as detergent-protein micelles containing a number of different sizes of protein per micelle. Figure 3.1 shows the elution profiles for the radiolabeled SDS using this experimental protocol. Very similar profiles were obtained with and without protein. If SDS had bound tightly to the peptides, so that mixed micelles occurred as described above, the radiolabel should have co-eluted with the proteins. The SDS repeatedly eluted at 55% B, indicating that this procedure removes the SDS, and probably the lipids with it. Mixed micelles of protein and octylglucoside were probably present, but the SDS did not stick to the proteins. The current model for the observed separations (as described in Reference 9) is that, below the critical micelle concentration, monomers of octylglucoside bind the column support and reduce the potential sites of interaction on the solid matrix. This allow peptides which would normally tightly bind the column to elute. Thus, this method is ideal for hydrophobic proteins or peptides.

Characteristics of the HPLC Profiles:

Figures 3.2 and 3.3 show the typical HPLC profile of the papain-generated peptides. This profile was completely reproducible even after 100 runs on the same column using several different preparations of papain-treated

Figure 3.1

(A) The [^{35}S]SDS elution profile was generated by passing labeled SDS, diluted into carrier SDS, over the octyl-C_4 column. The labeled detergent was injected alone or boiled (dotted line) with freshly prepared stripped erythrocyte ghosts. The flow rate was 1 ml / min and 1-ml fractions were collected. The gradient is indicated by the dashed line. (B) The ultraviolet absorbance spectrum for the SDS + protein sample was measured at 220 nm. This curve has been plotted to follow the same time scale as the curves in (A).

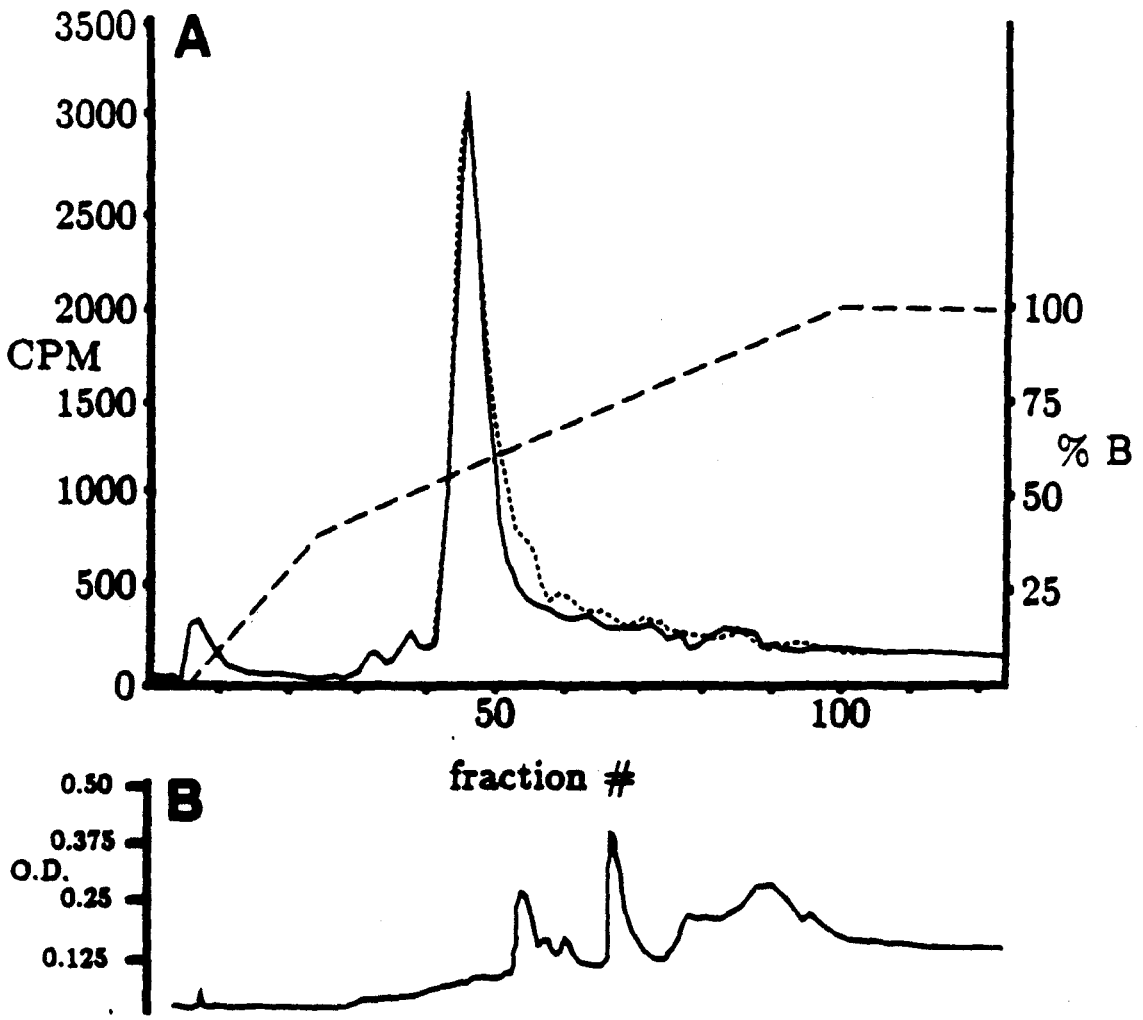
A
3500
3000
2500
2000
CPM
1500
1000
500
0
50
100
fraction #
100
75
% B
50
25
B
0.50
0.375
O.D.
0.25
0.125

Figure 3.2

This figure shows an HPLC profile for papain-proteoyzed ghosts with an early numbering scheme. Peaks II and III resulted in extremely pure, sequencable peptides. Peak I gave an identifiable sequence. This figure is included separately because fractions corresponding to peaks I, II and III were sequenced with rechromatographing first. Peaks I, IV, and V were rechromatographed without dialysis against SDS. Eventually it became impossible to rechromatograph without dialysis due to high back pressures which developed in the column. Then fractions corresponding to peaks were dialyzed and lyophilized before rechromatographing.

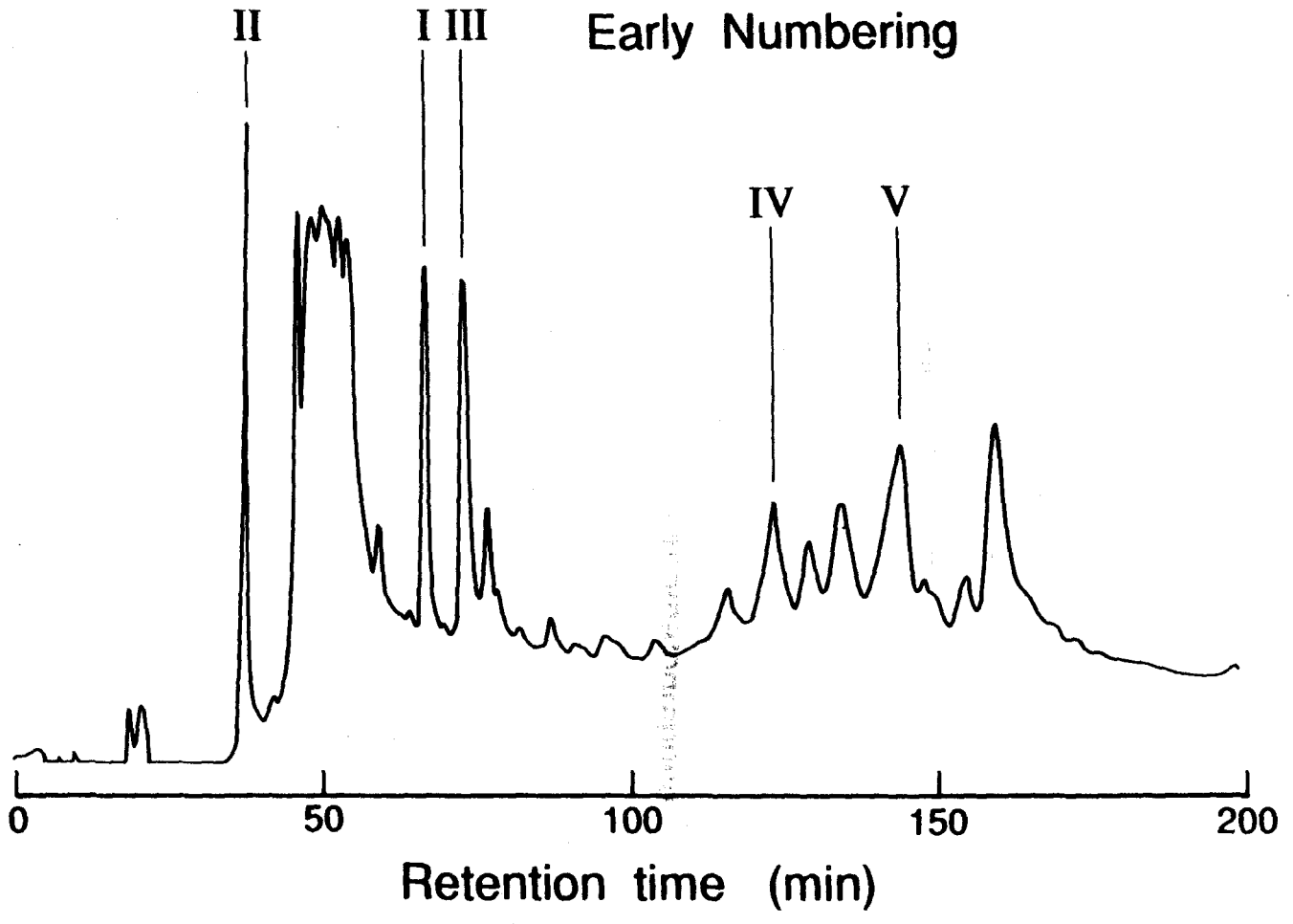
II
I III
Early Numbering
IV
V
0
50
100
150
200
Retention time (min)

Figure 3.3

Figure 3.3 shows the identification scheme used for peaks which were to be rechromatographed as described in the text. The dashed line illustrates the gradient profile which had been optimized to separate peaks. The gradient is very shallow after 89% buffer B.

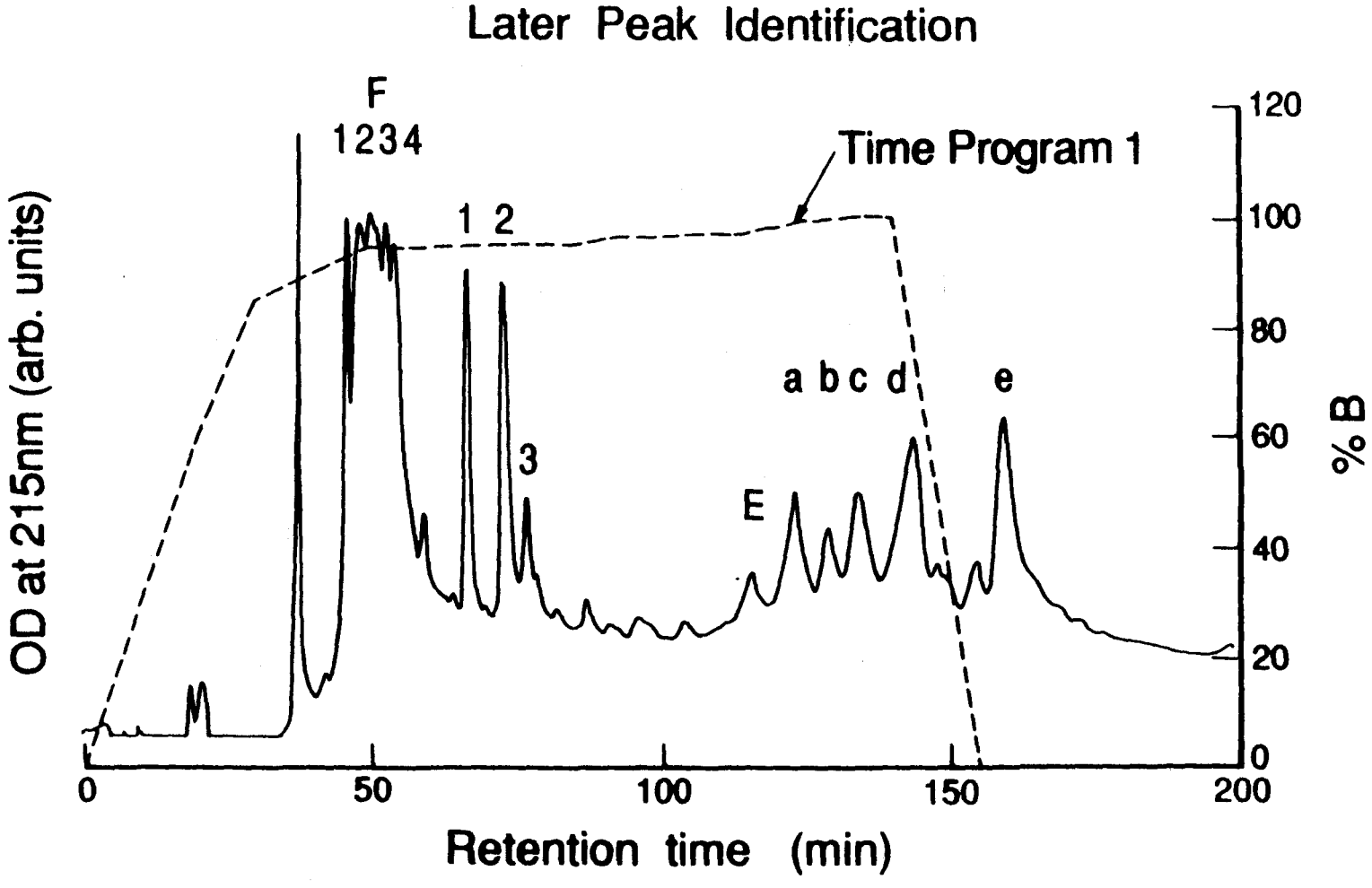
Later Peak Identification
F
1234
Time Program 1
1 2
3
E
a b c d
e
OD at 215nm (arb. units)
% B
120
100
80
60
40
20
0
0
50
100
150
200
Retention time (min)

ghosts. Figure 3.4 shows HPLC profiles obtained from rechromatographing peaks I and II in Figure 3.2. These two peaks are sharper than peaks occurring at later retention times in the HPLC profile. They both proved to be pure peptides (see sequence II in Table 2 and sequence III in Table 4 of Appendix 1). Only two major peaks resulted from rechromatographing peak I in Figure 3.2. As shown in Figure 3.4 B, pure peptide eluting at 58 minutes resulted from rechromatographing peak II. This peptide was frequently present in other HPLC profiles of rechromatographed samples. It is possible that because it is a hydrophobic peptide, it elutes efficiently from the column, in contrast to other peptides which adhere to the column and are eluted at only low yields. Conversely, it may be that the peptide from peak II is not fully eluted after one HPLC run and continues to be eluted from the column during successive runs. The peptides obtained from peaks II and III proved to be essentially homogeneous.

Some peaks in Figures 3.2 and 3.3 contained multiple peptides. These peaks were generally broad or appeared as a group of poorly resolved single sharp peaks (as in the **F** region of Figure 3.3). Figure 3.5 shows a typical profile obtained after collecting and rechromatographing a peak eluting at a late retention time. Peak **e** from Figure 3.3 was rechromatographed. (Intervening steps between chromatography included concentration by lyopholyzing and dialysis.) It is clear from this figure that many of the protein peaks obtained during the initial HPLC runs were aggregates of peptides. They contained multiple peptides which co-eluted. Figure 3.5 shows the general numbering scheme for rechromatographed peptides. Table 1a shows which of the peptides in Figure 3.2 were sequenced. Table 1b demonstrates that sequencing was attempted on most of the peptides purified by two dialyses and two HPLC steps. It is clear from Table 1b that peaks obtained at different retention times in the initial HPLC contained peptides which eluted at the same retention time after the second set of purification steps. The peptides eluting at a particular retention time in the second

Figure 3.4

This figure demonstrates the purity of peptides (eluting as sharp peaks at high yield) and the reproducibility of detergent saturated reverse-phase HPLC. (A) shows the profile obtained when peak I was rechromatographed. (B) shows peak II rechromatographed. Retention times are written to the left of the peaks.

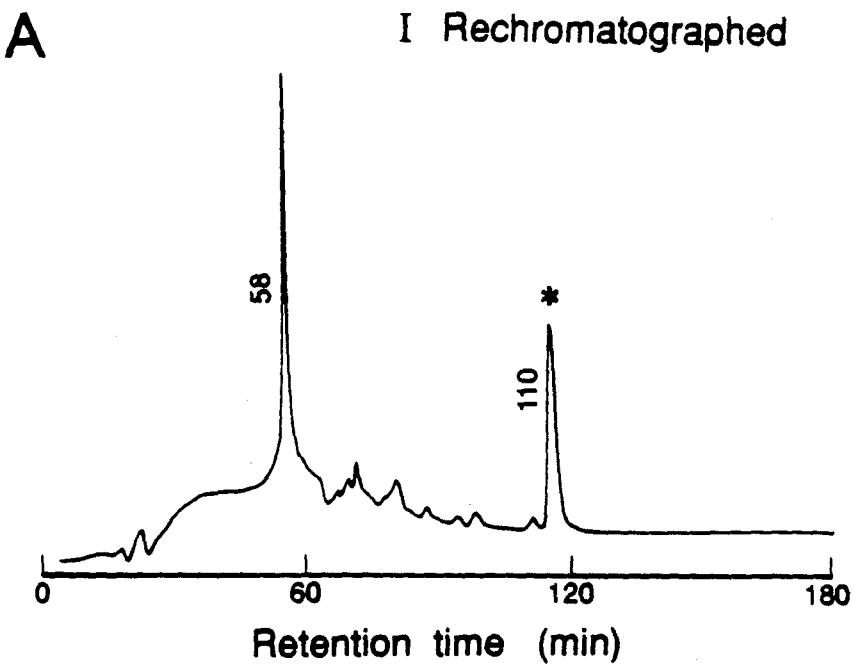
A
I Rechromatographed
58
110
*
0
60
120
180
Retention time (min)

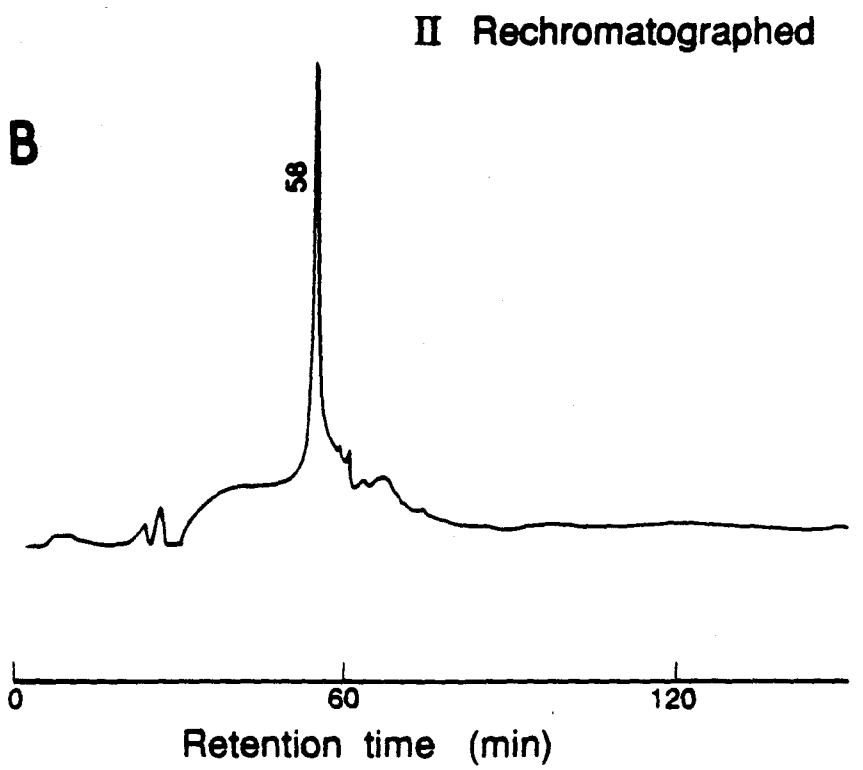
II Rechromatographed
B
58
0
60
120
Retention time (min)

Figure 3.5

This figure shows a typical HPLC profile obtained after collecting and rechromatographing a peak that occurred late in the initial HPLC profile. In this case, **e** was rechromatographed. It shows that many peptides co-eluted under peak **e** in the first HPLC run. However, this figure demonstrates that it is possible to rechromatograph and obtain high yields. The peaks are labeled by the numbers in parentheses which will be used to identify them. Retention times are indicated on the left side of each peak. The gradient from Time Program 2 is shown with the dashed line.

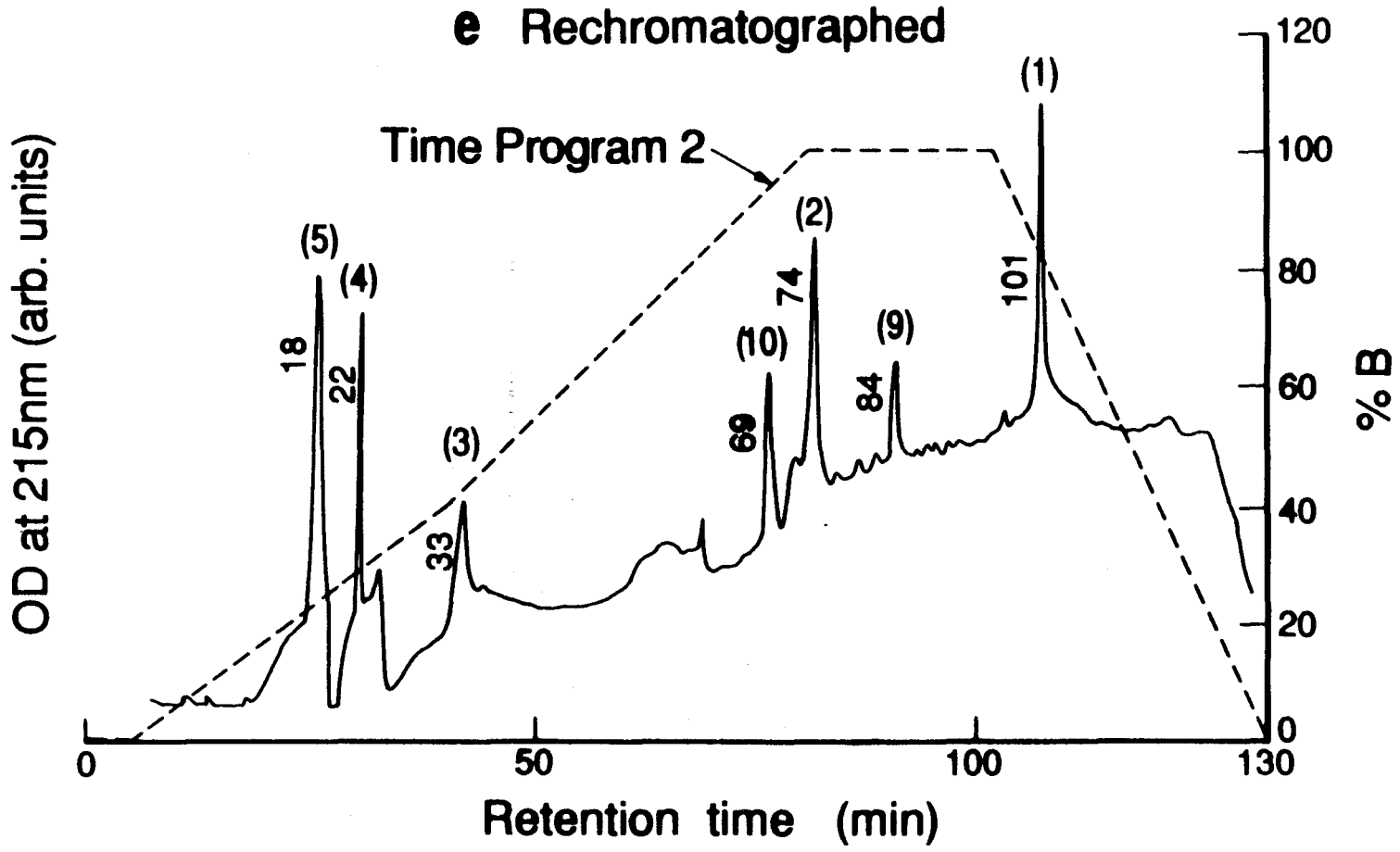
e Rechromatographed
Time Program 2
OD at 215nm (arb. units)
% B
Retention time (min)
0
50
100
130
0
20
40
60
80
100
120
(1)
(2)
(3)
(4)
(5)
(9)
(10)
18
22
33
68
74
84
101

Tables 1a and 1b

The following tables list the major HPLC peaks shown in Figures 3.3 and 3.4. Beside the parent peak identifications (a,b,c,1,2, etc.) are a list of the major peaks obtained after rechromatograping. In some cases, the same rechromatographed peaks were obtained for two or more parent peaks. Therefore, peaks were combined for parent peaks 2 and 3 and then for a and e. This gives final peak names like **ae2**, **ae9** and **2,3(5)**. Their exact sequences are shown in Tables 1-8 of Appendix 1.

Table 1a

major peaks								
peak	retention times		76	81	90	94	110	
(min)		-78	-84	-91	-95			
I	sequenced directly						I	
II	sequenced directly							
III	sequenced directly							
IV				IVa*	IVb*			
V			Vb*			Va*		

Table 1b

major peaks												
peak	retention				67	71	76p	81	90	94	97	115
time (min)	18	22	33	-69	-74	-78	-84	-91	-95	-100	-118	
a		a4		a10*	a2		a9*			a1*		
b				b10								
c		c4	c3	c10	c2					c1		
d									d1*	d2*	d3*	
e	e5	e4	e3	e10*	e2		e9*			e1*		
already cleanly sequenced												
2(5)*	2(1)*	2(2)*		2(4)*			2(3)					
3(5)*	3(1)*	3(2)*		3(4)*			3(3)					
F1	F1*											
F2		F2(4)		F2(1)								
F4	F4(1)*	F4(2)		F4(3)			F4(4)*					

* represents peaks that were sequenced.

HPLC step were sequenced. It was found that they contained the same peptides even if they eluted at different retention times (under different peaks) in the initial HPLC profile. a1 and e1 were combined to yield **ae1**. **ae1** eluted at the same retention time as **d2** in the second HPLC step (see Table 1b). Both peptides proved to be concentrated and pure enough to give an unequivocal sequence. They began at MEB3 residue 511 and contained about 77 amino acids as determined by amino acid analysis. Thus, by performing the second set of purification steps, it was usually possible to obtain pure and concentrated peptides for sequencing purposes. However, sometimes even after dialysis and another HPLC step, some of the peaks contained more than one peptide. In these cases, although sequencing was attempted, unequivocal sequences were not obtained.

Sequences obtained:

Figure 3.6 compares the purest human band 3 proteolytic product obtained by HPLC with the mouse sequence for that fragment. This peptide had not previously been sequenced for human band 3. This sequence demonstrates that it is possible to obtain pure, sequenceable peptides using the methods presented. For example, using a window of 30 amino acids and a filter of 1amino acid, 7133 protein sequences in the Protein Information Resource data bank were searched using the method of Lipman and Pearson[14]. The comparison with murine band 3 gave a match of 97 (because the method does not yield a percentage; it yields a weighting factor out of 100 which is biased by conserved versus non-conserved substitutions). The next highest value achieved was 81-- for a probable secY protein. A window of 30 amino acids instead of 42 (the length of the sequence) was chosen because any insertions or deletions can cause the computer to miss sequence homologies. It is still obvious that band 3 (and

Figure 3.6

Peak III was generated this previously undetermined human band 3 sequence. Forty-two amino acids were sequenced indicating the high purity and concentration of the sample.

Residue Number (mouse)	509	510	511	512	513	514	515	516	517	518	519
Mouse Sequence	**R**	**A**	**W**	**I**	**G**	**F**	**W**	**L**	**I**	**L**	**L**
Sequence III	**S**	**V**	**W**	**I**	**G**	**F**	**W**	**L**	**I**	**L**	**L**

Residue Number (mouse)	520	521	522	523	524	525	526	527	528	529	530
Mouse Sequence	**V**	**M**	**L**	**V**	**V**	**A**	**F**	**E**	**G**	**S**	**F**
Sequence III	**V**	**V**	**L**	**V**	**V**	**A**	**F**	**E**	**G**	**S**	**F**

Residue Number (mouse)	531	532	533	534	535	536	537	538	539	540	541
Mouse Sequence	**L**	**V**	**Q**	**Y**	**I**	**S**	**N**	**Y**	**T**	**Q**	**E**
Sequence III	**L**	**V**	**R**	**F**	**I**	**S**	**N**	**Y**	**T**	**Q**	**E**

Residue Number (mouse)	542	543	544	545	546	547	548	549	550
Mouse Sequence	**I**	**F**	**S**	**F**	**L**	**I**	**S**	**L**	**I**
Sequence III	**I**	**F**	**S**	**F**	**L**	**I**	**V**	**L**	**I**

not glycophorin A or some other erythrocyte membrane-spanning protein) is the protein from which this sequence was derived.

The purity of this sequence further shows that papain will generate proteolytic fragments with discrete cleavage points. There is a precedent for this. Papain-generated peptides with discrete extracellular cleavage sites beginning at residues corresponding to 586[17] and 650[18] in the MEB3 sequence have been isolated. But it was possible that papain, with its broad specificity, would yield families of peptides which had been proteolyzed within a few amino acids of each other. These sometimes proved difficult to separate and sequence. In fact, at least two of the peptides in the **F** region in Figure 3.3 had closely spaced N-termini, delineating VC-13 and demonstrating that this broad peak may consist of aggregates of related peptides. In addition, of all the predicted transmembrane peptides, the helix VC-1, corresponding to the first part of sequence III, has the highest average hydrophobicity (as defined by Kyte and Doolittle[19]). VC-5 and VC-6, and VC-11 have the highest hydrophobic moments (as defined by Eisenberg[20]). VC-4 is modeled to be separated from VC-5 with a loop of 1 amino acid. A loop of this small size is probably not accessible to papain cleavage. A starting point corresponding to the edge of VC-11 was found for two sequences. Thus, this method is able to separate the most hydrophobic peptides in band 3, as defined by average hydrophobicity and by hydrophobic moment.

Appendix 1 shows much of the sequence data obtained for papain cleavage fragments; it tabulates the raw data for the sequences and the amino acid analyses. The starting points of each sequence are shown in Figure 3.7. Except for helices 1 and 2, the starting points of the papain-generated proteolytic fragments lie within 5 amino acids of the transmembrane helix starting points modeled by Vogelaar and Chan (designated as VC# in Figure 3.7). Because many labeling and proteoylsis experiments

Figure 3.7

Figure 3.7 shows the results of sequencing different HPLC separated peptides (blue) and their amino acid anlaysis (red). The N-termini of sequencable peptides are designated according to the identification of their parent peak (shown in Figure 3.2 or 3.3) followed by their identification in the rechromatographed HPLC profile (shown in Figure 3.5) The lengths of several pure peptides were obtained from amino acid analysis. These are labeled accordingly.

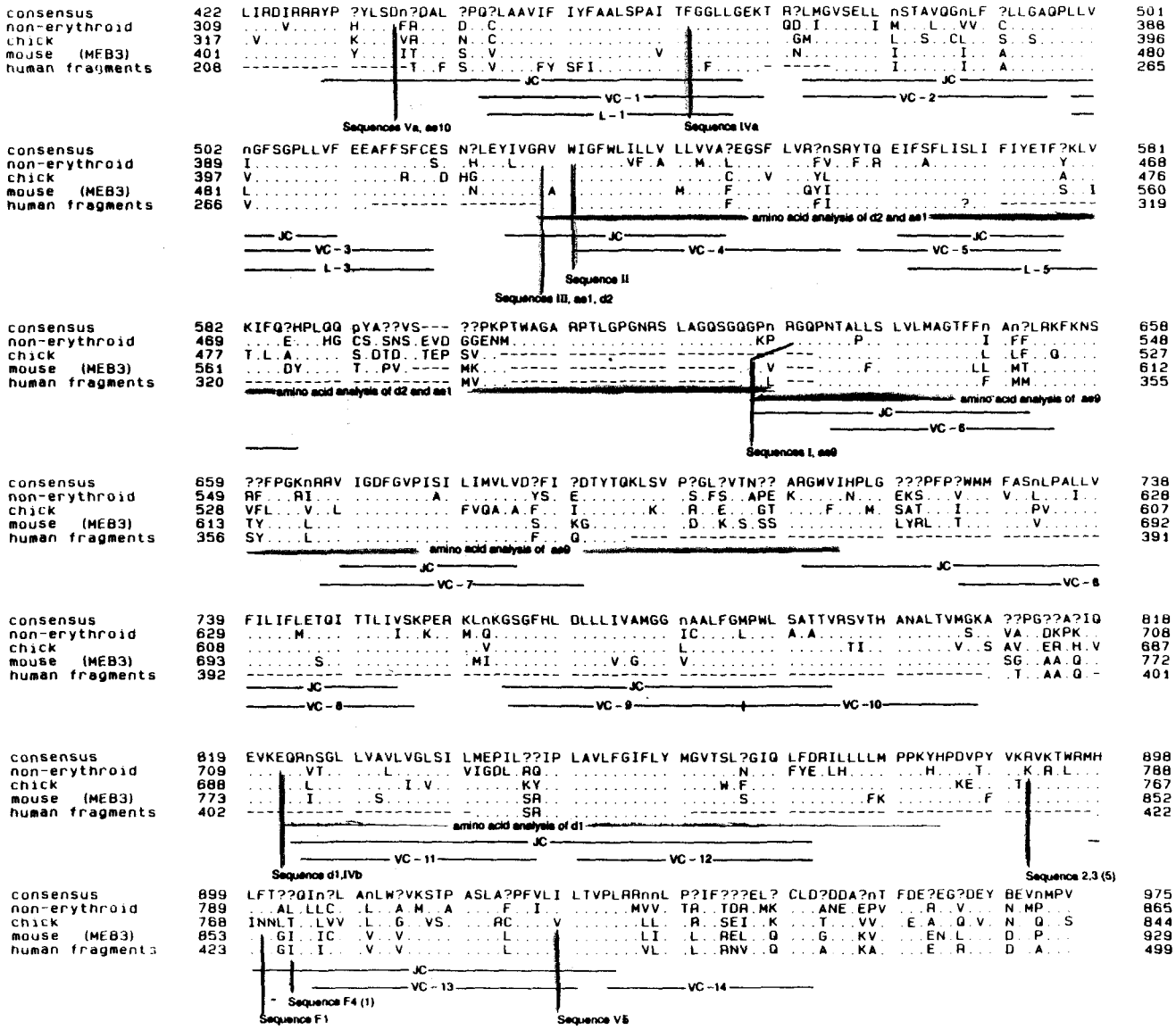
consensus 422 LIRDIRRRYP ?YLSDn?DAL ?PQ?LAAVIF IYFAALSPAI TFGGLLGEKT R?LMGVSELL nSTAVQGnLF ?LLGAQPLLV 501
non-erythroid 309 ....V..... H...FR... D..C..... .... QD.I.....I M...L..VV. C..... 388
chick 317 .V..... K...VR... N..C..... .... .GM..... L..S..CL.. S..S..... 396
mouse (MEB3) 401 ..... Y...IT... S..V..... .....V .... .N..... I.....I.. A..... 480
human fragments 208 ---------- -----T..F S..V...FY SFI..... .....F..... ----------..... I.....I.. A..... 265
JC
JC
VC - 1
VC - 2
L - 1
Sequences Va, as10
Sequence IVa
consensus 502 nGFSGPLLVF EEAFFSFCES N?LEYIVGAV WIGFWLILLV LLVVA?EGSF LVA?nSAYTQ EIFSFLISLI FIYETF?KLV 581
non-erythroid 389 I..... .....S..H...L..... .....VF.A ..M..L..... ...FV..F.A ...A..... .....Y... 468
chick 397 V..... .....R...D HG..... ....C...V ...YL..... .....A... 476
mouse (MEB3) 481 L..... ..... .N..... .....A ....M....F..... ...QYI..... .....S..I 560
human fragments 266 V..... ..---------- ---------- ....F..... ...FI.....?..... ---------- 319
amino acid analysis of d2 and as1
JC
JC
JC
VC - 3
VC - 4
VC - 5
L - 3
L - 5
Sequence II
Sequences III, as1, d2
consensus 582 KIFQ?HPLQQ pYA??VS--- ??PKPTWAGA APTLGPGNAS LAGQSGQGPn RGQPNTALLS LVLMAGTFFn An?LAKFKNS 658
non-erythroid 469 ....E...HG CS.SNS.EVD GGENM..... ....KP.....P..... .....I..FF..... 548
chick 477 T.L.A..... S.DTD..TEP SV..------ ---------- ---------- ---------- ---.....L..LF..Q.... 527
mouse (MEB3) 561 ....DY..... T..PV.----- MK...------ ---------- ------..V ---.....F.....LL..MT..... 612
human fragments 320 ---------- ---------- MV..------ ---------- ------..L ---.....F.....F..MM..... 355
amino acid analysis of d2 and as1
amino acid analysis of as9
JC
VC - 6
Sequences I, as9
consensus 659 ??FPGKnRRV IGDFGVPISI LIMVLVD?FI ?DTYTQKLSV P?GL?VTN?? ARGWVIHPLG ???PFP?WMM FASnLPALLV 738
non-erythroid 549 RF..RI..... .....A..... .....YS.E..... .....S.FS..APE K.....N... EKS...V... V..L...I.. 628
chick 528 VFL...V..L ..... FVQA.A.F.. I.....K. .R..E...GT ....F...M. SAT...I... ...PV..... 607
mouse (MEB3) 613 TY...L..... .....S..KG ....D..K.S.SS ....LYRL..T..... ...V..... 692
human fragments 356 SY...L..... .....F..Q. ..---- ---------- ---------- ---------- ---------- 391
amino acid analysis of as9
JC
JC
VC - 7
VC - 8
consensus 739 FILIFLETQI TTLIVSKPER KLnKGSGFHL DLLLIVAMGG nAALFGMPWL SAITVRSVTH ANALTVMGKA ??PG??A?IQ 818
non-erythroid 629 .....M..... ...I..K... M.Q..... ....IC....L.... A.A..... .....S.. VA..DKPK.. 708
chick 608 ....V..... ....L..... .....TI..... .....V..S AV..ER.H.V 687
mouse (MEB3) 693 .....S..... ..... .MI..... .....V.G... V..... .... SG..AA.Q.. 772
human fragments 392 ---------- ---------- ---------- ---------- ---------- ---------- ---------- ---------- T..AA.Q.- 401
JC
JC
VC - 8
VC - 9
VC - 10
consensus 819 EVKEQRnSGL LVAVLVGLSI LMEPIL??IP LAVLFGIFLY MGVTSL?GIQ LFDRILLLLM PPKYHPDVPY VKAVKTWRMH 898
non-erythroid 709 .....VT..... ...L..... VIGDL.RQ..... ....N... FYE.LH..... ...H...T.. .K.R.L... 788
chick 688 .....L..... ...I.V..... .....KY..... ....W.F..... ....KE... T..... 767
mouse (MEB3) 773 .....I.....S..... ....SR..... ....S..... .....FK..... .....F..... 852
human fragments 402 ---------- ---------- ---------- .....SR..... .... ---------- ---------- ---------- 422
amino acid analysis of d1
JC
VC - 11
VC - 12
Sequence d1,IVb
Sequence 2,3 (5)
consensus 899 LFT??QIn?L AnLW?VKSTP ASLA?PFVLI LTVPLRRnnL P?IF???EL? CLD?DDA?nT FDE?EG?DEY BEVnMPV 975
non-erythroid 789 ...AL.LLC. .L..A.M..A ....F..I. ....MVV. TR..TDR.MK ...ANE.EPV ...R..V... N.MP..... 865
chick 788 INNLT..LVV .L..G..VS. ....RC...V ....LL. .R..SEI..K ...T..VV.. .E.A..Q.V. N..Q..S 844
mouse (MEB3) 853 ...GI..IC. .V..V..... ....L..... ....LI. .L..REL..Q ...G...KV. ...EN.L... D..P..... 929
human fragments 423 ...GI..I.. .V..V..... ....L..... ....VL. .L..RNV..Q ...A...KA. ...E..R... D..A..... 499
JC
VC - 13
VC - 14
Sequence F4 (1)
Sequence F1
Sequence V5

have been performed on red blood cells (where the label may react preferentially from the external solution while a protease cannot diffuse across the membrane) there is a great deal of information on the sidedness of these sites[4,21-26]. Therefore, to obtain as many proteolytic cleavage points as possible, it was reasonable to perform proteolysis experiments on ghosts, where the protease has equal access to band 3 from both sides of the membrane. Proteolysis boundaries which constrain models of band 3's folding in the membrane are summarized in Chapter 1 (Figure 1.2). Vogelaar and Chan positioned their first transmembrane helix at residue 422 on the basis of its hydrophobic moment[2]. However, because papain cleaves at MEB3 residue 415 and pepsin (a protease with relatively broad specificity for hydrophobic and aromatic residues[8]) cleaves at MEB3 residue 413[22], it seems likely that this is near the N-terminus of the first transmembrane helix. Because of uncertainty in some of the less pure sequences (those with contamination such that the proteolytic fragment yielded less than 60% homology to the mouse band 3 sequence), starting boundaries marked by only one sequence designation are not considered definite. They are only suggested as possible proteolytic fragment starting points. We did not obtain any sequences in the region of VC-9 or VC-10. While VC-9 is a hydrophobic peptide, VC-10 is a relatively hydrophilic peptide[2], and it is possible that it eluted in the beginning of the HPLC run where the the baseline was low and peptides were not collected. Alternatively, VC-9's hydrophobicity may have caused it to adhere to the column so that it was eluted very slowly.

Amino Acid Analyis:

Amino acid analyses were performed on some of the sequences to obtain an estimate for the length of several papain proteolytic products. An additional benefit was that two of these analyses demonstrated that peptides eluting at a particular retention time after the second HPLC purification were the same length (in addition to beginning at the

same amino acid). These two fragments, **d2** and **ae1**, were obtained from peaks which eluted at different times in the initial HPLC and eluted at the same retention time during rechromatography (after lyophilyzing and dialyzing). Four of the peptides which gave pure sequences were subjected to amino acid analysis. Amino acid analyses were not performed on sequences which were not pure because any contamination from other peptides prevents accurate estimates of the number of each type of residue and, therefore, the length of the peptide. Figure 3.7 shows the position and length of the peptides subjected to amino acid analysis. The actual amino acid analysis data are arranged in Tables 9-12 of Appendix 1.

CONCLUSION

By using the method of detergent saturation of a reverse-phase column developed by Tomich *et al.*[9], and with the modifications described in this chapter, it proved possible to identify the starting points membrane-bound sequences of integral membrane proteins. We obtained two new sequences which were pure enough to define the sequence for that fragment of human band 3, including one of the two helices having the highest average hydrophobicity (as found in a plot of hydrophobicity versus hydrophobic moment[2]). The human band 3 DNA is presently being cloned[22], and purification of protein to obtain the exact human sequences was not of primary importance to this study. We have found the N-termini for 6 putative transmembrane sequences. If the assumption that papain will cleave band 3 at points very near the edged of the membrane surface is correct, we have provided the starting points for two transmembrane helices as an initial aid for band 3 modelling. Later acquisitions of other helix starting points have shown that the Vogelaar and Chan model was basically correct in predicting the transmembrane helices. Therefore, modelling transmembrane helices on the basis of hydrophobic moment analysis of Eisenberg[20] agrees very well with these experimental observations.

Very sharp, well-resolved peaks were sequenced with no further treatments to yield pure peptides. One sharp peak resulted in a pure fragment with a sequence which was not previously known for human band 3. Another led to a proteolytic fragment previously isolated by Jennings *et al.* after treatment with papain. Broader peaks generally occurred at later retention times. These peaks were dialyzed twice and rechromatographed to obtain sequencable peptides since each gave rise to a number of peaks in the second chromatography step. Amino acid analyses were performed on

four of these peptides. Peptides from two different initial HPLC peaks which eluted at the same retention time after rechromatographing proved to have the same initial sequence and the same number of amino acids. This indicates that, in some cases, protein-detergent micelles containing a variety of peptides coeluted during the initial HPLC run, while pure peptide eluted in others. Presumably, under optimal HPLC conditions in a system with fewer peptides, all could be resolved. Using the methods developed in this chapter, it is possible eventually to separate peptides even if they are not completely resolved in the first HPLC step, since after dialysis and rechromatography, most peaks contained pure peptide.

All proteins were initially solubilized in SDS to prevent protein aggregation. Experiments using [^{35}S]SDS demonstrated that the SDS was eluted from the column at 55% B whether or not protein was present, signifying that it could be removed from the protein during this procedure. Detergent saturated reverse-phase HPLC is effective in separating hydrophobic peptides of the approximately the same size. It appears to coat the column's stationary phase, allowing these peptides to elute. The best separation of these peptides was obtained with a very shallow gradient.

We have been able to isolate two sequences (**Va** and **ae10**), which might correspond to the edge of the first (or N-terminal membrane-spanning) helix, VC-1. We have obtained 4 sequences (**II, III, ae1**, and **d2**) which defined the edge of VC-4, and two sequences (**I** and **ae9**) which defined the edge of VC-6. We have also found two sequences (**d1** and **Vb**) which correspond to the edge of VC-11. Sequences **F1** and **F4(1)** delineate the N-terminus of VC-13. Amino acid analysis of **d2** and **ae1** suggest that these peptides are over 70 amino acids amino acids in length and contain modeled segments VC-4 and VC-5. Amino acid analysis of **ae9** suggests that this peptide is over 80 amino acids long, and contains segments corresponding to VC-6 and VC-7. Amino acid analysis of **d1** suggests that this peptide is over 60 amino acids

long and that it contains VC-11 and VC-12. The edge of helix 1 has been reassigned on the basis of this data. Also the sixth and thirteenth helices may lie closer to the edges of predicted helices from other models (see Figure 3.7) than the Vogelaar-Chan model. However, the deviation between the model and our experimental results for the start of helices 6 and 13 is still less than 5 amino acids from the beginning of the papain-generated helices.

These experiments have demonstrated that most of the transmembrane helices are obtained and then isolated to sufficient purity and concentration for sequencing and/or amino acid analysis. In addition, these results showed that papain proteolyzes near the edges of many of the modeled band 3 transmembrane helices which are joined by large 'loops'. This method can be used to obtain topographical information if crystallographic evidence is not available to describe the folding of a protein in the membrane. (Of all intrinsic membrane proteins, only the reaction centers of *Rhodopseudomonas viridis* and *Rhodobacter sphaeroides* have high-resolution x-ray crystallographic structures; a low-resolution structure is available for bacteriorhodopsin; and crystals of the nicotinic acetylcholine receptor have been investigated by electron diffraction[2].) It can also be used to obtain hydrophobic peptides in sufficient quality and purity to sequence.

REFERENCES:

1. Zaki, L., (1984) *FEBS Lett.* **189**, 234-240.
2. Vogelaar, N.S. (1989) *Doctoral Thesis*, California Institute of Technology.
3. Lodish, H.F. (1988) *The Harvey Lectures* **Series 82**, 19-46.
4. Jay, D., and Cantley, L., (1986) *Ann. Rev. Biochem.* **55**, 511-538.
5. Gunn, R.B. (1979) **Mechanisms of Intestinal Secretion** Alan R. Liss New York 25-43.
6. Marchesi, V.V., Furthmayr, H., Tomita, M. (1976) *Annu. Rev. Biochem.* **45**, 667-698.
7. Falke, J. J., Kanes, K.J. and Chan, S.I. (1985) *J. Biol. Chem.* **260**, 13294-13303.
8. Walsh, C., (1979) **Enzyme Reaction Mechanisms** S.H. Freeman and Co. San Francisco.
9. Tomich, J.M., Carson, L.W., Kanes, K.J., Emerling, M.R., and Richards, J.H. (1988) *Anal. Biochem.* **174**, 197-203.
10. Eisenburg, D. (1984) *Ann. Rev. Biochem.* **53**, 595-623.
11. Steck, T.L. (1974) **Methods in Membrane Biology** (E.D. Korn, ed.) Plenum, New York 245-381.
12. Fairbanks, G., Steck, T.J., and Walach, D.F.H. (1971) *Biochem.* **10**, 2606-2616.
13. Falke, J.J., Pace, R.J. and Chan, S.I. (1984) *J. Biol. Chem.* **259**, 6472-6480.
14. Lipman, D.J., and Pearson, W.R. (1985) *Science* **227** 1435-1441.
15. Needleman, S.B., and Wunsch, C.D. (1970) *J. Mol. Biol.* **48** 443-453.
16. D. B.Teplow (personal communication).

17. Jennings, M.L. , Adams-Lackey, M., and Denney, G.H. (1984) *J. Biol. Chem.* **259**, 4652-4660.

18. Drickamer, L.K. (1981) *J. Biol Chem.* **251**, 51115-51123.

19. Kyte, J., and Doolittle, R.F. (1982) *J. Mol. Biol.* **157**, 105-132.

20. Eisenberg, D., Swartz, E., Komaromy, M. and Wall, R. (1984) *J. Mol. Biol.* **179**, 125-142.

21. Grinstein, S., Ship, S. and Rothstein A. (1978) *Biochim. Biophys. Acta* **507**, 294-304.

22. Mawby, W.J. and Findlay J.B.C. (1983) *Biochem. J.* **205**, 465-475.

23. Brock, C.J., and Tanner, M.J.A. (1986) *Biochem. J.* **235**, 899-901.

24. Brock, C.J., Tanner, M.J.A., and Kempf, C. (1983) *Biochem. J.* **213**, 577-586.

25. Jennings, M.L., and Passow, H. (1979) *Biochim. Biophys. Acta* **554**, 498-519.

26. Rudloff, V., Lepke, S., and Passow, H. (1983) *FEBS Lett.* **163**, 14-21.

27. R.B. Gunn (personal communication).

Appendix 1 to Chapter III

Appendix 1 gives tables containing the raw data for the peptide sequences and amino acid analyses of different papain-generated *in situ* proteolytic products.

Tables 1-8

Tables 1 through 8 show the amino acid sequences obtained for various HPLC fractions. Under the sequence name(s) are listed the residue numbers from the N-terminus, then the first choice(s) for that amino acid, the second choice(s), the actual murine (house mouse) residues to which these correspond, and, if known, the human sequence.

Table 1

sequences I, ae9

residue number	1	2	3	4	5	6	7	8
first choice(I)	G	E	F	P	N	T	A	L
second choice (I)	SHM	V F	L	G I	I W	A W	M L	V M
first choice (ae9)	?	?	L	P	G	F	A	G
second choice (ae9)				F	N D	R W		
residue number (mouse)	583	584	585	586	587	588	589	590
actual mouse sequence	G	P	V	P	N	T	A	L
known human sequence	G	P	L	P	N	T	A	L

Table 1 (continued)

residue number	9	10	11	12	13	14	15	16
first choice (I)	LA	L	V	G	G I	A		
second choice (I)	AFV	SI	IG					
first choice (ae9)	F	?	L	V	L	M	A	F
second choice (ae9)	L		W	T W		T A	V L	W(IK)T
residue number (mouse)	591	592	593	594	595	596	597	598
actual mouse sequence	L	S	L	V	M	A	G	T
known human sequence	F	S	L	V	M	A	G	T

Table 2

sequence II

residue number	1	2	3	4	5	6	7	8
first choice	?	F	I	G	F	L	L	I
second choice		VSA	P	P		MA	MV	FV
residue number (mouse)	510	511	512	513	514	515	516	517
actual mouse sequence	W	F	I	G	F	W	L	I

no previously known human sequence

residue number	9	10	11	12	13	14	15	16
first choice	L	L	V	V	P	A	V	A
second choice	AI		W	G	LG	VG	A	
residue number	518	519	520	521	522	523	524	525
actual mouse sequence	L	L	V	M	L	V	V	A

no previously known human sequence

Table 2 (continued)

residue number	17	18
first choice	F	E
second choice		
residue number (mouse)	526	527
actual mouse sequence	F	E

Table 3

sequence Vb

residue number	1	2	3	4	5	6	7	8
first choice	R S	V	L	T	P	T	P	?
second choice	P A	P I		I	N L	D A	F I	
residue number (mouse)	879	880	881	882	883	884	885	886
actual mouse sequence	F	V	L	I	L	T	V	P
known human sequence	F	V	L	I	L	T	V	P

residue number	9	10	11
first choice	L	T	V
second choice	DFP		N L
residue number (mouse)	887	888	889
actual mouse sequence	L	R	R
known human sequence	L	R	R

Table 4

sequences III, ae1, d2

residue number	1	2	3	4	5	6	7	8
first choice (III)	S	V	W	I	G	F	W	L
second choice (III)	TGR	FPQ	FLK	PTM	N A	TLA	MEA	V T
first choice (ae1)	?	V	F	(IK)*	F	F	L	L
second choice (ae1)			L	P	N			
first choice (d2)	?	V	?	I	G	F	W	L
second choice (d2)			F L K N		F	V	L I M	M
residue number (mouse)	509	510	511	512	513	514	515	516
actual mouse sequence	R	A	W	I	G	F	W	L

no previously known human sequence

Table 4 (continued)

residue number	9	10	11	12	13	14	15	16
first choice (III)	I	L	L	V	V	L	V	V
second choice (III)	G	S A	Q V		A I	M	A	G K
first choice (ae1)	V	A	L	V	V	M	V	V
second choice (ae1)		L	V				A D	W
first choice (d2)	I	L	L	V	V	L	V	V
second choice (d2)	G V		V Q	W		G	A F	
residue number (mouse)	517	518	519	520	521	522	523	524
actual mouse sequence	I	L	L	V	M	L	V	V

no previously known human sequence

Table 4 (continued)

residue number	17	18	19	20	21	22	23	24
first choice (III)	A	F	E	G	S	F	L	V
second choice (III)	T F					M	M	
first choice (ae1)	W	F	W?	W	R	F	L	
second choice (ae1)	I	L			AGV			
first choice (d2)	A	I	E	G				
second choice (d2)	I	L						
residue number (mouse)	525	526	527	528	529	530	531	532
actual mouse sequence	A	F	E	G	S	F	L	V

no previously known human sequence

Table 4 (continued)

residue number	25	26	27	28	29	30	31	32
first choice (III)	R	F	I	S	N	Y	T	Q
second choice (III)		K Y		K	R			
residue number (mouse)	533	534	535	536	537	538	539	540
actual mouse sequence	Q	Y	I	S	N	Y	T	Q

no previously known human sequence

residue number	33	34	35	36	37	38	39	40
first choice (III)	E	I	F	S	F	L	I	V
second choice (III)			G					
residue number (mouse)	541	542	543	544	545	546	547	548
actual mouse sequence	E	I	F	S	F	L	I	S

no previously known human sequence

Table 4 (continued)

residue number	41	42
first choice (III)	L	I
second choice (III)		
residue number (mouse)	549	550
actual mouse sequence	L	I

no previously known human sequence

Table 5

sequence IVa

residue number	1	2	3	4	5	6	7	8
first choice	S	L I F	G	G	L	V	I	E
second choice		V Q	Q N		W		L A	V
residue number (mouse)	441	442	443	444	445	446	447	448
actual mouse sequence	T	F	G	G	L	L	G	E
known human sequence	T	F	G	F	L	L	G	E

residue number	9	10	11	12	13	14	15	16
first choice	Y	Q	?	F	N	L	K	L
second choice	R	E		L	K	Q		
residue number (mouse)	449	450	451	452	453	454	455	456
actual mouse sequence	K	T	R	N	L	M	G	V
known human sequence	K							V

Table 5 (continued)

residue number	17	18	19
first choice	S	Y	L
second choice	L		
residue number (mouse)	457	458	459
actual mouse sequence	T	A	V
known human sequence	T	A	V

Table 6

sequence d1

residue number	1	2	3	4	5	6	7	8
first choice	GAY	V	W L	P	M	V	L	L
second choice	PMV	Q	N R	T D	WNQ		R	M D
residue number (mouse)	776	777	778	779	780	781	782	783
actual mouse sequence	E	Q	R	I	S	G	L	L

no previously known human sequence

residue number	9	10	11	12	13	14	15	16
first choice	V	A	V	L	V	G	A	S
second choice	W G	(I,K)*	D	G A	V	Y	(I,K)*D	G M
residue number (mouse)	784	785	786	787	788	789	790	791
actual mouse sequence	V	S	V	L	V	G	L	S

no previously known human sequence

*I and K cannot be resolved.

Table 6 (continued)

residue number	17	18	19
first choice	P	D	H
second choice	HYW	WST	
residue number (mouse)	792	793	794
actual mouse sequence	I	L	M
known human sequence			M

* I and K cannot be resolved.

Table 7

sequence 2,3(5)

residue number	1	2	3	4	5	6	7	8
first choice	?	W	P	G	W	F	(KL)*	H
second choice			S Q	F W	N(KL)	N V	G A	
residue number (mouse)	845	846	847	848	849	850	851	852
actual mouse sequence	R	V	K	T	W	R	M	H
human sequence								H
residue number	9	10	11	12	13	14	15	16
first choice	(KL)	W	T	G	I	V	(KL)	T
second choice	T D	S	G N		N		G	W
residue number (mouse)	853	854	855	856	857	858	859	860
actual mouse sequence	L	F	T	G	I	Q	I	I
human sequence	L	F	T	G	I	Q	I	I

* L and K cannot be resolved.

Table 7 (continued)

residue number	17	18	19	20
first choice	S	(KL)	A	D
second choice	AQ	GE	N(KL)	
residue number (mouse)	861	862	863	865
actual mouse sequence	C#	L	A	V
human sequence	C	L	A	

* L and K cannot be resolved.

\# C is not detectable on this amino acid sequencer.

Table 8

sequences F1, and F4(1)

residue number (F1)	1	2	3	4	5	6	7	8
first choice (F1)	?	TE	?	PE	NF	Y	I	(KL)*
second choice (F1)			F			HYV	A	V
residue number (F4(1))				1	2	3	4	5
first choice (F4(1))				?	QP	(KL)	I	N
second choice (F(41))					VF	FI	P	F
residue number (mouse)	854	855	856	857	858	859	860	861
actual mouse sequence	F	T	G	I	Q	I	I	C#
human sequence	F	T	G	I	Q	I	I	C

residue number (F1)	9	10	11	12	13	14	15	16
first choice (F1)	(KL)	?	I	F	W	Y	N	?
second choice (F1)	Y				R	DHA	QW	
residue number (F4(1))	6	7	8	9	10	11	12	13
first choice (F4(1))	A	MI	V	VA	ID	V	V	(KL)
second choice (F4(1))	V	A	(KL)	P	FW	(KL)		I
residue number (mouse)	862	863	864	865	866	867	868	869
actual mouse sequence	L	A	V	L	W	V	V	K
human sequence	L	A	V	L	W	V	V	K

* L and K cannot be resolved.

\# C is not detectable on this amino acid sequencer.

Table 8

sequences F1, and F4(1) (continued)

residue number (F1)	17	18	19	20				
first choice (F1)	F	I	P N	Y H				
second choice (F1)	I	(KL)*	Q W	W A				
residue number (F4(1))	14	15	16	17	18	19	20	21
first choice (F4(1))	P	A	G	W A	S F	F	F V	(KL)
second choice (F(41))	I F	(KL)	A P	P I	W I	Y H	A P	H Y
residue number (mouse)	870	871	872	873	874	875	876	877
actual mouse sequence	S	T	P	A	S	L	A	L
human sequence	S	T	P	A	S	L	A	L

residue number (F4(1))	22	23	24
first choice (F4(1))	P	G P	M V
second choice (F4(1))	I V	M V	I G
residue number (mouse)	878	879	880
actual mouse sequence	P	F	V

* L and K cannot be resolved

Tables 9-12

The following tables give the amino acid analyses for several of the more pure proteolytic fragments. The purpose of these analyses is to determine the length of each of the fragments. In this manner, the carboxy-terminus of the fragment is approximated. Thus, both papain cleavage points are obtained from one sequence. **ae9** and **d2** have the same N-terminus as determined by sequencing. They were both amino acid analyzed to find if they had the same length. They eluted at the same retention time during rechromatography step, but originated from different peaks in the initial HPLC step.

Table 9

amino acids	D&N[1]	E&Q[2]	S	G	H	R	T	A	P	Y	V	M	C	I	L	F	K	tot
amino acid analysis for sequence																		
d2	2	3	16	8.9	0.8	2	4	5.9	4.3	1.2	5.2	0.9	0.1	5.9	9.4	5	1.2	
amino acid analysis for the corresponding																		
sequence in mice	1	9	5	3	0	2	3	3	5	5	7	2	0	9	9	8	4	77
amino acid analysis for the corresponding sequence																		
in chickens	2	8	7	2	1	3	5	3	3	4	9	0	1	7	12	5	2	76
amino acid analysis for the known portions of the corresponding sequence in																		
humans	0	4	4	3	0	3	1	1	2	1	6	2	0	6	8	6	1	51

[1,2] N and Q are not present due to deamidation.

Notes:

W is acid hydrolyzed and has a value of 0 in the amino acid analysis. There are two W's in both mouse and chicken fragments in a length of 77 amino acids.

The values for S and G are anomalously high. Reasons are discussed in the Materials and Methods section of this chapter.

Table 10

amino acids	D&N[1]	E&Q[2]	S	G	H	R	T	A	P	Y	V	M	C	I	L	F	K	tot
amino acid analysis for sequence																		
ae 1	3.1	8.2	13.5	10	0.7	3.3	4.8	6.1	4	1.3	6.2	1.7	0	7.1	10.7	9	2.7	
amino acid analysis for the corresponding																		
sequence in mice	1	9	5	3	0	2	3	3	5	5	7	2	0	9	9	8	4	77
amino acid analysis for the corresponding sequence																		
in chickens	2	8	7	2	1	3	5	3	3	4	9	0	1	7	12	5	2	76
amino acid analysis for the known portions of the corresponding sequence in																		
humans	0	4	4	3	0	3	1	1	3	1	6	2	0	6	8	6	1	41

[1,2] N and Q are not present due to deamidation.

Notes:

W is acid hydrolyzed and has a value of 0 in the amino acid analysis. There are two W's in both mouse and chicken fragments in a length of 77 amino acids.

The values for S and G are anomalously high. Reasons are discussed in the Materials and Methods section of this chapter.

Table 11

amino acids	D&N[1]	E&Q[2]	S	G	H	R	T	A	P	Y	V	M	W	I	L	F	K	tot
amino acid analysis for sequence																		
ae9	5	6	12.4	12	1.1	3	5	6.7	4	1.4	4.9	1.9		4.5	8.6	24	2.9	
amino acid analysis for the corresponding																		
sequence in mice	6	1	8	8	1	4	6	4	5	2	8	3	1	6	11	6	6	86
amino acid analysis for the corresponding sequence																		
in chickens	4	6	4	7	1	5	6	6	4	1	6	1	1	6	12	10	4	84
amino acid analysis for the known portions of the corresponding sequence in																		
humans	5	2	4	5	0	3	4	3	4	2	5	4	0	5	9	8	3	66

[1,2] N and Q are not present due to deamidation.

Notes:

W is acid hydrolyzed and has a value of 0 in the amino acid analysis.
There is no designation for C unless it is present in the sequence or the amino acid analysis.
There is an absorbing species which coelutes with F causing extremely high values.
The values for S and G are anomalously high. Reasons are discussed in the Materials and Methods section of this chapter.

Table 12

amino acids	D&N[1]	E&Q[2]	S	G	H	R	T	A	P	Y	V	M	W	I	L	F	K	tot
amino acid analysis for sequence																		
d1	4.9	5.9	11.3	10	0.8	3.5	4	7.2	4	1.6	6.6	1.7		6.2	11.5	18	2.4	
amino acid analysis for the corresponding																		
sequence in mice	1	4	6	5	1	3	1	1	4	2	5	2	0	7	14	4	2	62
amino acid analysis for the corresponding sequence																		
in chickens	1	4	2	5	1	2	1	2	4	3	4	3	1	7	16	4	2	62
amino acid analysis for the known portions of the corres ponding sequence in																		
humans	0	1	1	1	0	1	0	1	2	1	1	2	0	3	4	2	0	20

[1,2] N and Q are not present due to deamidation.

Notes:

W is acid hydrolyzed and has a value of 0 in the amino acid analysis.
There is no designation for C unless it is present in the sequence or the amino acid analysis.
There is an absorbing species which coelutes with F causing extremely high values.
The values for S and G are anomalously high. Reasons are discussed in the Materials and Methods section of this chapter.

Chapter IV

Location of Band 3's Active-Site Arginine

INTRODUCTION

Much of what is known about structure/function relationships in band 3 is derived from chemical modification studies. The general approach followed by this laboratory and others, is to modify band 3 and examine the functional consequences of that modification. The ease of modification as well as the ability to label selectively on either side of the membrane (as cells, vesicles or ghosts) make this a desirable system to study. Following covalent modifications, the approximate location of a phenylglyoxal-modified arginine in the band 3 protein has been determined to be in the 35,000 dalton fragment resulting from extensive treatment with extracellular chymotrypsin[1,2].

The extracellular pH dependence of monovalent anion exchange indicates that an arginine residue is of central importance in the catalysis of anion transport[3,4]. ^{35}Cl NMR studies have shown that phenylglyoxal (PG) and 1,2-cyclohexanedione (CHD),

two arginine-specific reagents, will inhibit chloride binding to the active site of band 3, implicating arginine as the important residue in anion transport[5]. Transport experiments (as distinct from the aforementioned studies of binding to band 3's active site) using chemical modification by PG and CHD also give support to arginine as an amino acid essential for transport[1,6]. Wieth *et al.* showed that inhibition of band 3 anion transport with PG is a second order process. By varying the pH and anionic composition of the reaction medium, the kinetics of transport inactivation were consistent with the assumption that phenylglyoxal reacts with functionally essential arginine residues[7,8]. The experiments of Funder *et al.*[9], and Brahm[10] on the effect of pH and temperature on chloride exchange flux showed that monovalent anion transport is independent of pH in the range of pH 7.2 to at least 11.0 at 0°C and that the pK_a of the transporting group decreases at least by 2 pH units with a temperature increase to 38°C, suggesting a group with a very high ionization enthalpy (thought to be the guanidino group of an arginine residue).

The role of arginine (a positively charged and mobile side chain) in band 3 has been been modeled by Vogelaar and Chan to form a complex with the transported anion so that the uncharged complex is able to cross a wide hydrophobic layer in the middle of the anion transport channel[11]. ^{35}Cl NMR experiments have shown that an arginine must provide the essential positive charge in the inward- or outward-facing conformation of the transport site or in both.[12] The specificity of phenylgloxal modification appears to be sensitive to the 'inward-facing' or 'outward-facing' sides of the protein[13]. This fact and differences in asymmetry of modification by a number of other band 3 transport inhibitors[13] from the two sides of the membrane have led other workers to propose more complicated mechanisms for anion transport than one in which a single arginine side-chain is responsible for monovalent anion transport. In the Vogelaar and Chan model, however, a single essential arginine is responsible for the

transport of monovalent anions[11]. This is consistent with experimental evidence if the accessibility of the arginine differs from either side of the membrane. The situation changes with divalents (see Chapter II of this thesis). However, it is likely that there are lysines and arginines within the transport channel (especially near the ends) to facilitate diffusion of the negatively charged species down into the middle of the channel[14].

In studies of other proteins (such as creatine kinase, hexokinase, and alcohol dehydrogenase), PG and CHD were able to modify selectively the active site arginine of a number of proteins under certain conditions[16,17,18], especially arginine residues that are involved in the anion recognizing sites of enzymes[19]. It is believed that these reagents react with the uncharged (deprotonated) arginine side chain, selecting for arginine residues in relatively hydrophobic environments where its pK_a is decreased[7,19]. PG and CHD react with proteins in a pH-dependent fashion, with increased reactivity at higher pH's. PG typically reacts with arginyl residues with a 2:1 stoichiometry[16], probably as shown in Figure 4.1. The binding is a pseudo-first order reaction, with the rate limited by the first reaction step[8].

When labeling with [^{14}C]phenylglyoxal (^{14}C-PG) is carried out under conditions in which only about one amino acid residue is modified per copy of the protein, the label is on the COOH-terminal third of the protein in the membrane-spanning region of the protein[1]. PG labeling from the intracellular compartment leads to more labeling with less specificity. The most effective method of preventing intracellular phenylglyoxylation is to establish a pH gradient across the membrane[8]. This selective modification of the extracellularly exposed arginines was achieved when ghosts with a neutral or acidic intracellular pH were reacted with PG in an alkaline medium[1]. Although PG permeates the membrane rapidly ($t_{1/2}$ = 40 msec[20]), it is less likely to covalently react with arginines under acid conditions. Thus, it would react

Figure 4.1

This figure shows possible reactions of phenylglyoxal with arginine. The phenylglyoxal : arginine stoichiometry in the covalent reaction is 2 : 1. However, the structure of the resulting adduct is not known. The first step (formation of a 1:1 complex) and rate-limiting and reversible.

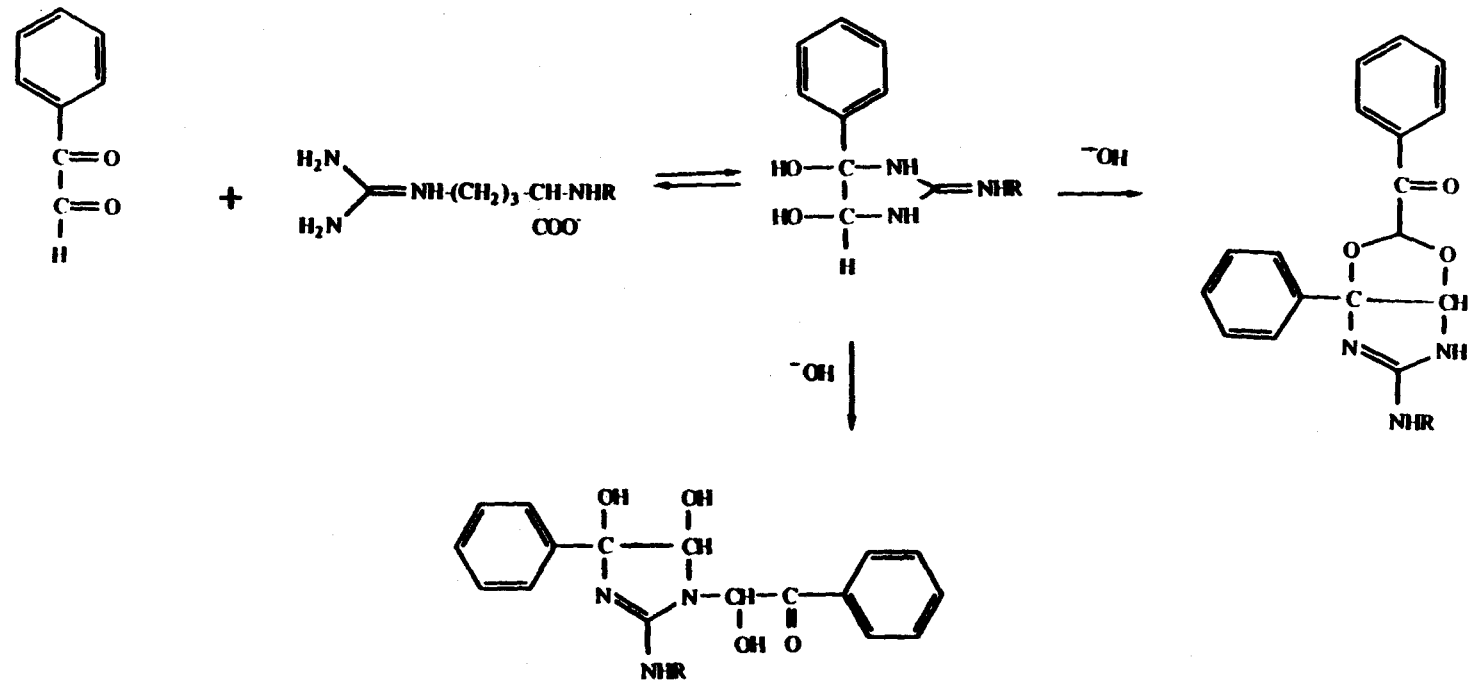

Possible
Reactions of Phenylglyoxal with Arginine

preferentially with the arginines exposed to alkaline external solution. When phenylglyoxalation was performed in the absence of chloride, maximal inhibition of anion transport in ghosts was obtained by the binding of about 2 million PG molecules per ghost. Since most of the reaction occurred in band 3[8], this corresponds to one modified arginine per reacted band 3[1].

Because the conditions of transport-site labeling used by Bjerrum *et al.*[1] proved difficult to reproduce on a large scale, and because the PG derivatives p-hydroxyphenylglyoxal and p-nitrophenylglyoxal proved labile under HPLC conditions (See Appendix to this chapter), we used the PG labeling method of Zaki[21]. Under the conditions employed by Zaki, only two proteins are labeled, band 3 and spectrin, the major cytoskeletal component[21]. Membranes then were subjected to low ionic strength and high pH stripping and washing to eliminate the cytoskeletal components (including spectrin) leaving only transmembrane proteins. Under the conditions, two to three arginines are labeled per band 3 monomer[21]. We employed this less specific labeling method in order to obtain large quantities of labeled band 3 to perform chromatography. With the information obtained about the structure of band 3 in the membrane, and with topographical constraints imposed by proteolytic and labeling experiments from this laboratory and others, it would be possible to distinguish the active-site residue from other arginines.

The location of the reactive arginine has been hypothesized by this laboratory based on hydrophobic moment analysis and energy minimizaion of protein-protein interactions in band 3. Vogelaar and Chan postulate that the active-arginine lies at R748 (in the MEB3 sequence) or possibly at R888[11]. The position of these residues is shown in Figure 4.2. Jay and Cantley have predicted that the functionally essential arginines might be located at MEB3 residues R675, R748 or R800[14]. These residues are highlighted in Figure 4.2. Using the Zaki method for labeling, we demonstrate that it is possible to expose the labeled membranes to relatively harsh (in the sense of low

pH, which is not conducive to retaining labels) conditions in proteloysis and HPLC and still retain the phenylglyoxal label. Furthermore, the utility of different HPLC stationary phases (using the peptide separation method of Tomich *et al*[22]) was investigated. The appendix to this chapter lists conventional techniques which failed to separate the papain-generated transmembrane helices of band 3. In this chapter, the location of the essential arginine is experimentally restricted from the 14 modeled transmembrane helices to about 6 helices. The number can be further restricted because some helices do not contain an arginine, or even a lysine (a residue which can be modified to a small extent by α-dicarbonyls[17]). Another restriction is due to the the principle that an important acive-site residue will be conserved. Based on the Vogelaar and Chan model for band 3 folding in the membrane and on proteolytic data from Chapter III, the exact location of the essential arginine is predicted.

Figure 4.2

The membrane-spanning C-terminal 520 amino acids of band 3 are shown in this figure. The arginines suggested as possible active-site arginines in Reference 14 are labeled as blue vertical lines. The arginine residues which are likely active-site candidates as suggested by Vogelaar and Chan in Reference 11 are boxed in red.

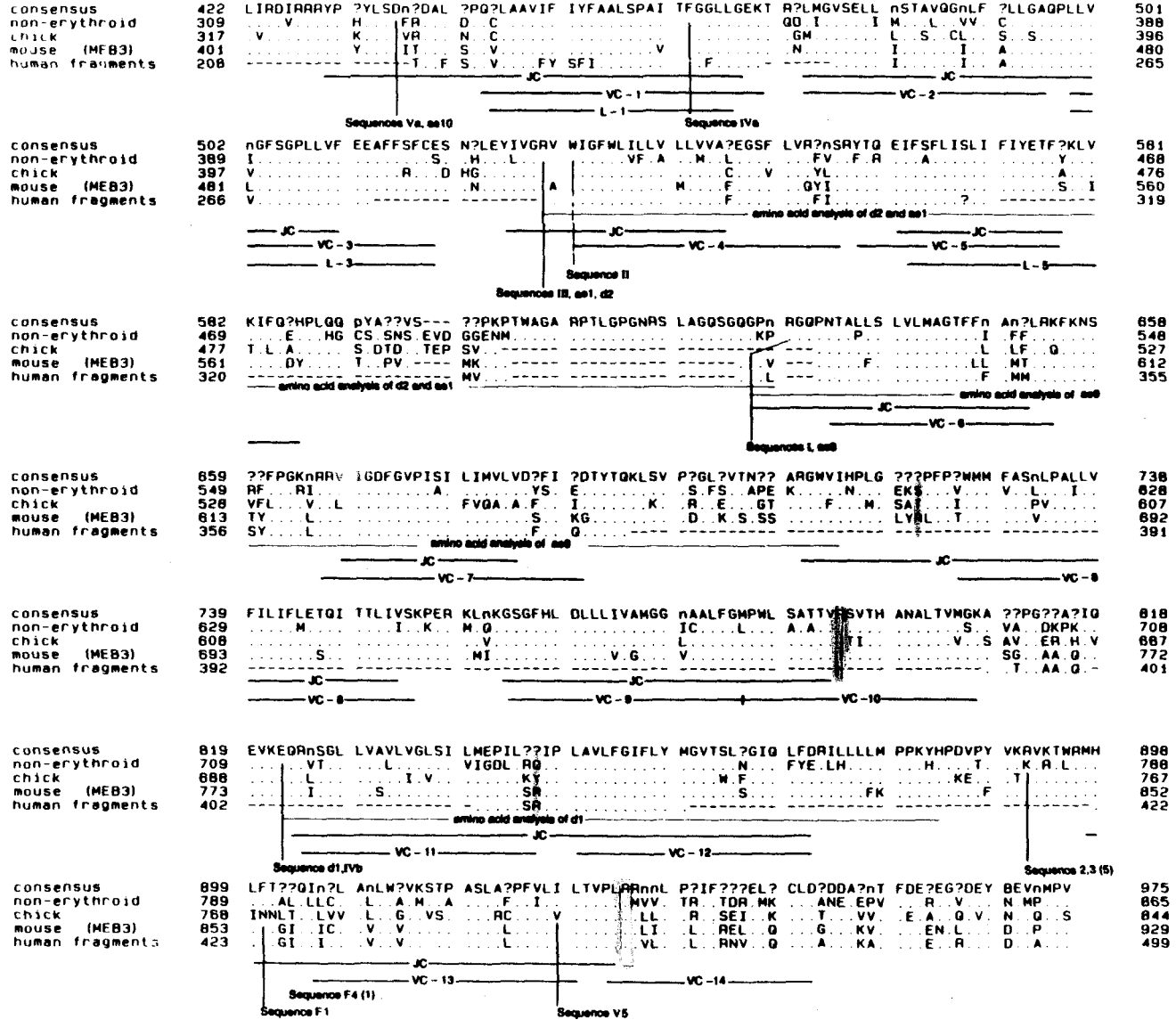
consensus 422 LIRDIRRRYP ?YLSDn?DAL ?PQ?LAAVIF IYFAALSPAI TFGGLLGEKT R?LMGVSELL nSTAVQGnLF ?LLGAQPLLV 501
non-erythroid 309 H FR D C QD I I M L VV C 388
chick 317 K VR N C GM L S CL S S 396
mouse (MEB3) 401 Y IT S V V N I I A 480
human fragments 208 T F S V FY SFI F I I A 265
JC
VC - 1
L - 1
VC - 2
Sequences Va, aa10
Sequence IVa
consensus 502 nGFSGPLLVF EEAFFSFCES N?LEYIVGRV WIGFWLILLV LLVVA?EGSF LVR?nSRYTQ EIFSFLISLI FIYETF?KLV 581
non-erythroid 389 I S H L VF A M L FV F R A Y 468
chick 397 V R D HG C V YL A 476
mouse (MEB3) 481 L N A M F QYI S I 560
human fragments 266 V F FI ? 319
amino acid analysis of d2 and aa1
JC
VC - 3
L - 3
VC - 4
VC - 5
L - 5
Sequence II
Sequences III, aa1, d2
consensus 582 KIFQ?HPLQQ pYA??VS--- ??PKPTWAGA RPTLGPGNRS LAGQSGQGPn RGQPNTALLS LVLMAGTFFn An?LAKFKNS 658
non-erythroid 469 E HG CS SNS EVD GGENM KP P I FF 548
chick 477 T L A S DTD TEP SV L LF Q 527
mouse (MEB3) 561 DY T PV MK V F LL MT 612
human fragments 320 MV L F MM 355
amino acid analysis of d2 and aa1
amino acid analysis of aa9
JC
VC - 6
Sequences I, aa9
consensus 659 ??FPGKnRRV IGDFGVPISI LIMVLVD?FI ?DTYTQKLSV P?GL?VTN?? ARGWVIHPLG ???PFP?WMM FASnLPALLV 738
non-erythroid 549 RF RI A YS E S FS APE K N EKS V V L I 628
chick 528 VFL V L FVQA A F I K R E GT F M SAI I PV 607
mouse (MEB3) 613 TY L S KG D K S SS LYAL T V 692
human fragments 356 SY L F Q 391
amino acid analysis of aa9
JC
JC
VC - 7
VC - 8
consensus 739 FILIFLETQI TTLIVSKPER KLnKGSGFHL DLLLIVAMGG nAALFGMPWL SATTVISVTH ANALTVMGKA ??PG??A?IQ 818
non-erythroid 629 M I K M Q IC L A A S VA DKPK 708
chick 608 V L I V S AV ER H V 687
mouse (MEB3) 693 S MI V G V SG AA Q 772
human fragments 392 T AA Q 401
JC
JC
VC - 8
VC - 9
VC - 10
consensus 819 EVKEQRnSGL LVAVLVGLSI LMEPIL??IP LAVLFGIFLY MGVTSL?GIQ LFDRILLLLM PPKYHPDVPY VKRVKTWRMH 898
non-erythroid 709 VT L VIGDL RQ N FYE LH H T K R L 788
chick 688 L I V KY W F KE T 767
mouse (MEB3) 773 I S SR S FK F 852
human fragments 402 SR 422
amino acid analysis of d1
JC
VC - 11
VC - 12
Sequence d1,IVb
Sequence 2,3 (5)
consensus 899 LFT??QIn?L AnLW?VKSTP ASLA?PFVLI LTVPLRRnnL P?IF???EL? CLD?DDA?nT FDE?EG?DEY BEVnMPV 975
non-erythroid 789 AL LLC L A M A F I MVV TR TDR MK ANE EPV R V N MP 865
chick 788 INNLT LVV L G VS RC V LL R SEI K T VV E A Q V N Q S 844
mouse (MEB3) 853 GI IC V V L LI L REL Q G KV EN L D P 929
human fragments 423 GI I V V L VL L RNV Q A KA E R D A 499
JC
VC - 13
VC - 14
Sequence F4 (1)
Sequence F1
Sequence V5

MATERIALS AND METHODS

Materials

Reagents and their sources are: [7-^{14}C]phenylglyoxal (^{14}C-PG), (Amersham); N-2-hydroxyethyl piperazine N'-2-ethane sulfonic acid (HEPES), (Research Oraganics); Bovine serum albumin (BSA), gluconic acid (sodium salt), phenylmethylsulfonyl fluoride (PMSF), sodium dodecyl sulfate (SDS), n-octyl-β-D-glucopyranoside (octylglucoside) (Sigma); n-octyl-β-D-glucopyranoside (octylglucoside) (Boeringer-Mannheim); trifluoroacetic acid (TFA), HPLC grade 1-propanol and acetonitrile, morpholine, phenylglyoxal monohydrate (PG) (Aldrich); papain (Calbiochem); Safety-Solve™ (Research Products International); 4,4'-dinirostilbene-2,2'-disulfonic acid (DNDS) (Pfatz and Bauer) was recrystallized as described previously[22]. Outdated packed human red cells were the kind gift of the Los Angeles American Red Cross.

Methods

Membrane Preparation:

Leaky red cell membranes (ghosts) were prepared as described previously[23].

Covalent Modification of Ghost Membranes by ^{14}C-PG:

Ghosts were modified with ^{14}C-PG in two steps. First, 10 ml of labeling buffer containing 250 μCi of ^{14}C-PG were added to 16 ml of membranes. The labeling buffer contained 200 mM sucrose, 25 mM gluconate, 25 mM citrate, 5 mM HEPES, and 1 mM sodium sulfate as described by Zaki[20]. The resulting suspension was incubated at 37°C for 1 hour. Ten ml of 16 mM nonradioactive PG was added to each tube, and the resulting suspension was centrifuged at 15,000 rpm (27,000 x g_{max}) for 7 minutes. The supernatant was removed and the membranes were incubated with 16 mM

nonradioactive PG for 30 minutes. The radiolabeled ghosts were then washed twice with 0.5% bovine serum albumin in 5 mM NaH_2PO_4 buffer, pH 8 (henceforth called 5P8). The purpose of this step was to adsorb any free label onto the BSA and therefore remove it from solution.

Proteolysis of Ghost Membranes:

Packed ghost membranes were resuspended in 50 mM sodium acetate buffer, 4 mM in L-cysteine-HCl and containing 10 mg / ml papain. The ratio of ghost membranes to papain solution was at least 1:2 by volume. The resulting suspension was incubated with shaking at 37°C for one hour. Additional vortexing was done every 5 minutes to prevent excessive aggregation of the membranes. The papain was removed and inhibited by washing twice in 5P8 containing 10 mg / ml PMSF.

Stripping of Nonintegral Proteins:

Membranes were stripped of non-integral membrane-associated proteins through exposure to high pH at low ionic strength followed by treatment with concentrated salt solutions. Membranes were washed once in distilled water, once in 10 mM NaOH, and again in distilled water. Finally, they were washed in 250 mM ammonium chloride in 5P8, and 100 mM ammonium chloride in 5P8, and in salt-free 5P8.

Separation of Protein Fragments by High-Performance Liquid Chromatography:

Membrane suspensions were solubilized by adding 1 volume of a 10% w/v solution of SDS to 9 volumes of the membrane pellet. Proteins and peptides were separated with either a 25-cm Vydac C_4 214TP54 analytical reverse-phase HPLC column or on a Vydac C_{18} 218TP510 semi-preparative reverse-phase HPLC column. Buffer A for the C_4 column consisted of 0.2% v/v TFA, 0.1% v/v morpholine, and 0.1% octylglucoside in distilled water. Buffer B for this column consisted of 0.2% v/v TFA,

0.1% v/v morpholine, and 0.1% octylglucoside in 2:2:1 acetonitrile : 1-propanol : water. Buffer A for the C_{18} column consisted of 0.2% v/v TFA, 0.1% v/v morpholine, and 0.1% octylglucoside in 95% distilled water, 5% 1-propanol. Buffer B for this column consisted of 0.2% v/v TFA, 0.1% v/v morpholine, and 0.1% octylglucoside in 4.5:4.5:1 acetonitrile:1-propanol:water. Initially the buffer B used on the C_{18} column had the same 2:2:1 composition, but it was found that better resolution was obtained with the 4.5:4.5:1 mix. The column temperature was maintained at 55°C. For the C_4 column, the concentration of buffer B was increased according to Time Program 2 in Chapter III of this thesis. For the C_{18} column, the gradient is described in Chapter III of this thesis by Time Program 1. Because the C_4 column is an analytical HPLC column, the greatest amount of SDS-solubilized membrane suspension that could be injected into the port for a single HPLC run was two 100 µl injections (or 200 µl). Elution of the peptides is monitored at 215 nm using a Shimadzu SPD-6AV variable-wavelenghth ultaviolet-visible detector.

Scintillation Counting:

Fractions were collected at the indicated time intervals for HPLC runs with ^{14}C-PG labeled ghosts, stripped ghosts and proteolyzed, stripped ghosts. Anywhere from 100 µl to 1 ml from each fraction was added to scintillation vials containing 10 ml of scintillation cocktail Each vial was counted for at least 2 min using a Beckman LS9000 scintillation counter.

SDS-Polyacrylamide Gel Elecrophoresis and Silver Staining:

A description of the methods used in the low-molecular weight gel system needed in identification of HPLC peaks is described in the Appendix of this chapter.

RESULTS

^{14}C-PG Labeled Whole Ghost Membranes.

Using an octylglucoside-saturated C_{18} column, proteins in 1 ml of a suspension of ^{14}C-PG labeled whole ghosts were separated. The resulting profile is shown in Figure 4.3(A). Fractions obtained at 3 minutes intervals were scintillation counted. A plot of the radioactivity from 1 ml of each fraction is represented in Figure 4.3(B). The large peak at about 40 minutes (45% B) represents mainly labeled free label as determined by SDS polyacrylamide gel electrophoresis (data not shown). The broad feeature at 40 minutes in Figure 4.3(A) is characteristic of band 3 although it was not seen in the gel lane.

^{14}C-PG Labeled, Stripped Ghost Membranes:

Using an octylglucoside-saturated C_4 columm, ^{14}C-PG labeled stripped and washed ghost proteins were separated. The resulting profile is shown in Figure 4.4(A). 300 µl of each fraction (obtained at 1 minutes intervals) were scintillation counted. A plot of the radioactivity obtained is represented in Figure 4.4(B). Except for significant counts obtained near 10 minutes (containing free label), the major radioactive peak is centered at 35 minutes. This peak contains about 1/7 of the radioactivity of the labeled whole ghost membranes (if the smaller volume of sample scintillation counted is taken into account) and elutes at a retention time typical of band 3. This peak does not contain any residual radioactivity from previous samples. Thus, the stripping procedure tends to wash away much of the label. However, it is clear that protein retains some label.

^{14}C-PG Labeled Papain-Proteolyzed Stripped Ghost Membranes:

Using an octylglucoside-saturated C_{18} column, peptides in 1 ml of ^{14}C-PG labeled, papain-treated, stripped and washed membranes were separated. Figure 4.5(A) shows

Figure 4.3

Figure (A) shows the HPLC absorbance profile for preparation of ^{14}C-PG labeled whole, leaky ghosts. Figure (B) shows the scintillation profile for the fractions in (A). 1 ml from each fraction was scintillation counted. An octylglucoside-saturated C_{18} column was used to obtain the separation.

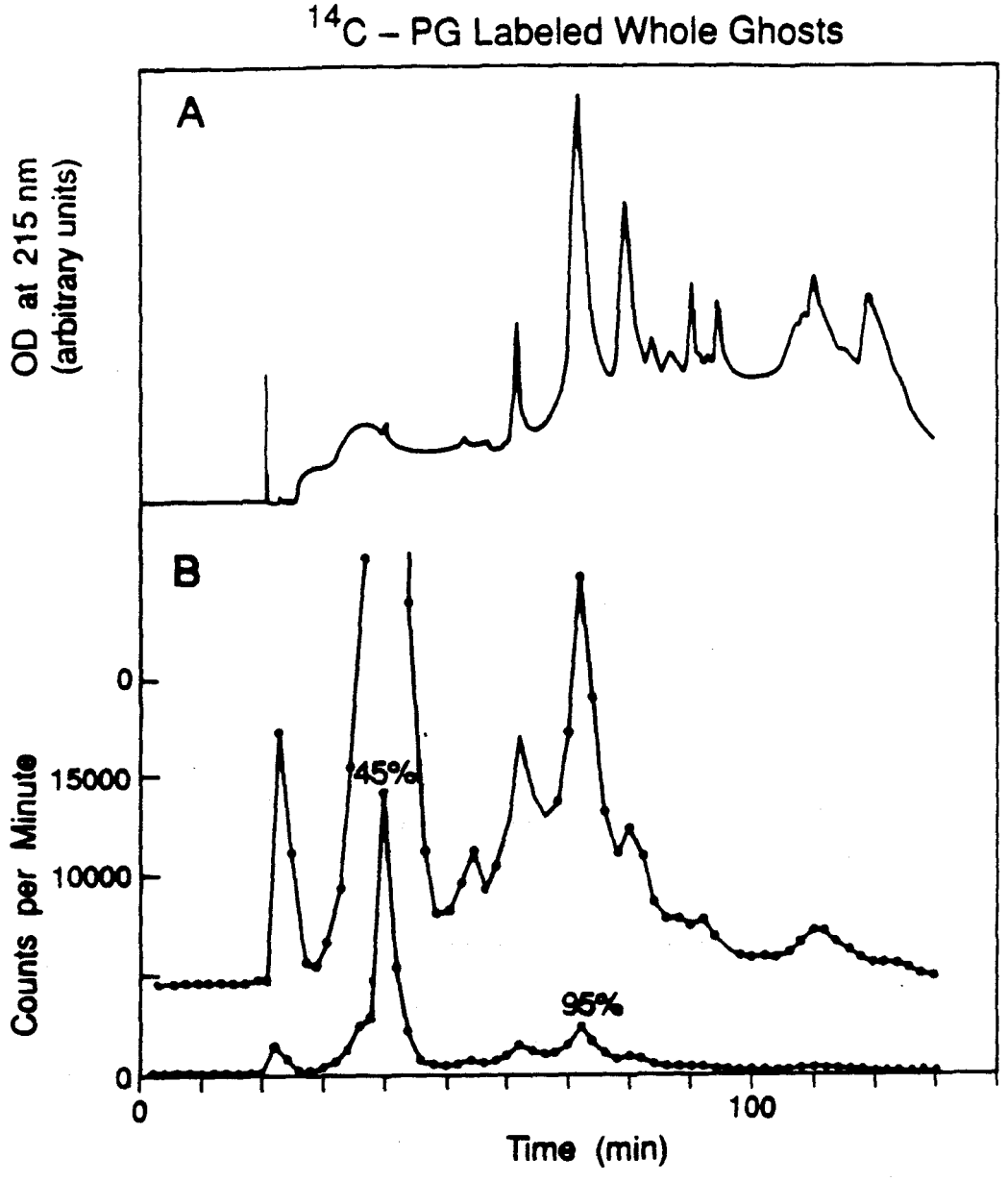
^{14}C – PG Labeled Whole Ghosts
A
OD at 215 nm
(arbitrary units)
B
Counts per Minute
0
15000
10000
0
45%
95%
0
100
Time (min)

Figure 4.4

Figure (A) shows the HPLC absorbance profile for a separation of ^{14}C-PG labeled stripped, leaky, ghost membranes. Figure (B) shows the scintillation profile obtained of 300 µl from each fraction collected in (A). An octylglucoside-saturated C_4 column was used to obtain the separation. Much of the label appears to have been lost during the stripping and washing procedures. A C_4 column was used for this separation.

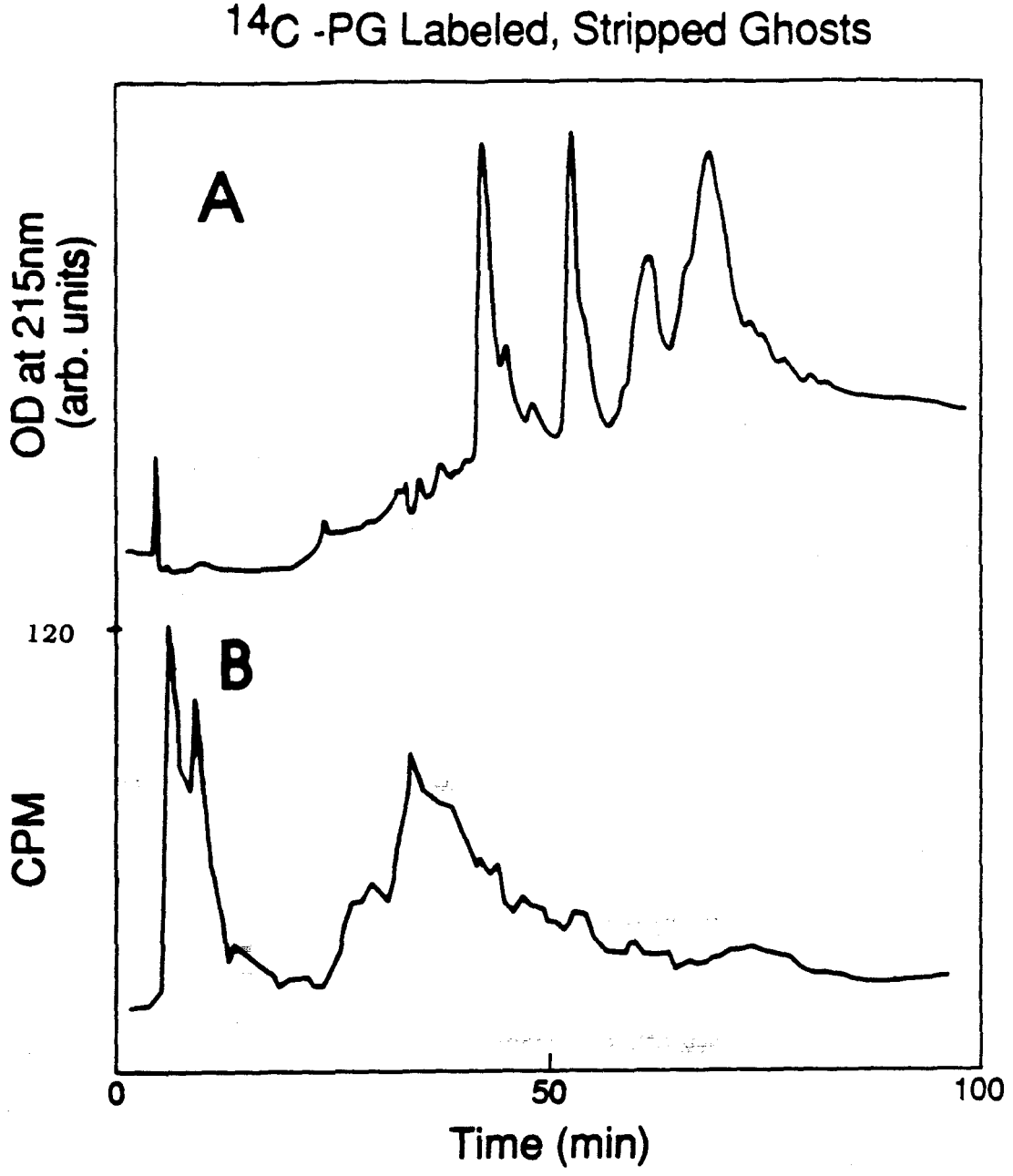
^{14}C -PG Labeled, Stripped Ghosts
A
OD at 215nm (arb. units)
120
B
CPM
0
50
100
Time (min)

Figure 4.5

Figure (A) shows the absorbance profile for the ^{14}C-PG labeled, papain-treated ghost membranes. It is similar to the profiles seen in Chapter III, except that long-term freezing at -20° C causes some aggregation of protein so that its peaks are not as clearly resolved. The scintillation profile in Figure (B) demonstrates that some of the label is retained by peptides even with the harsh conditions of HPLC. The peak labeled 95% B (95% organic buffer) may result from residual protein in the sample shown in Figure 4.4. The peak eluting at 91%B is discussed in the text. It has been very well characterized, and there is very little probability that it contains the active-site arginine. However, since by the labeling method used two to three residues are modified[21], it is possible that this peak represents the second modification and not the active site modification. Furthermore, this peak's intensity was not entirely reproducible.

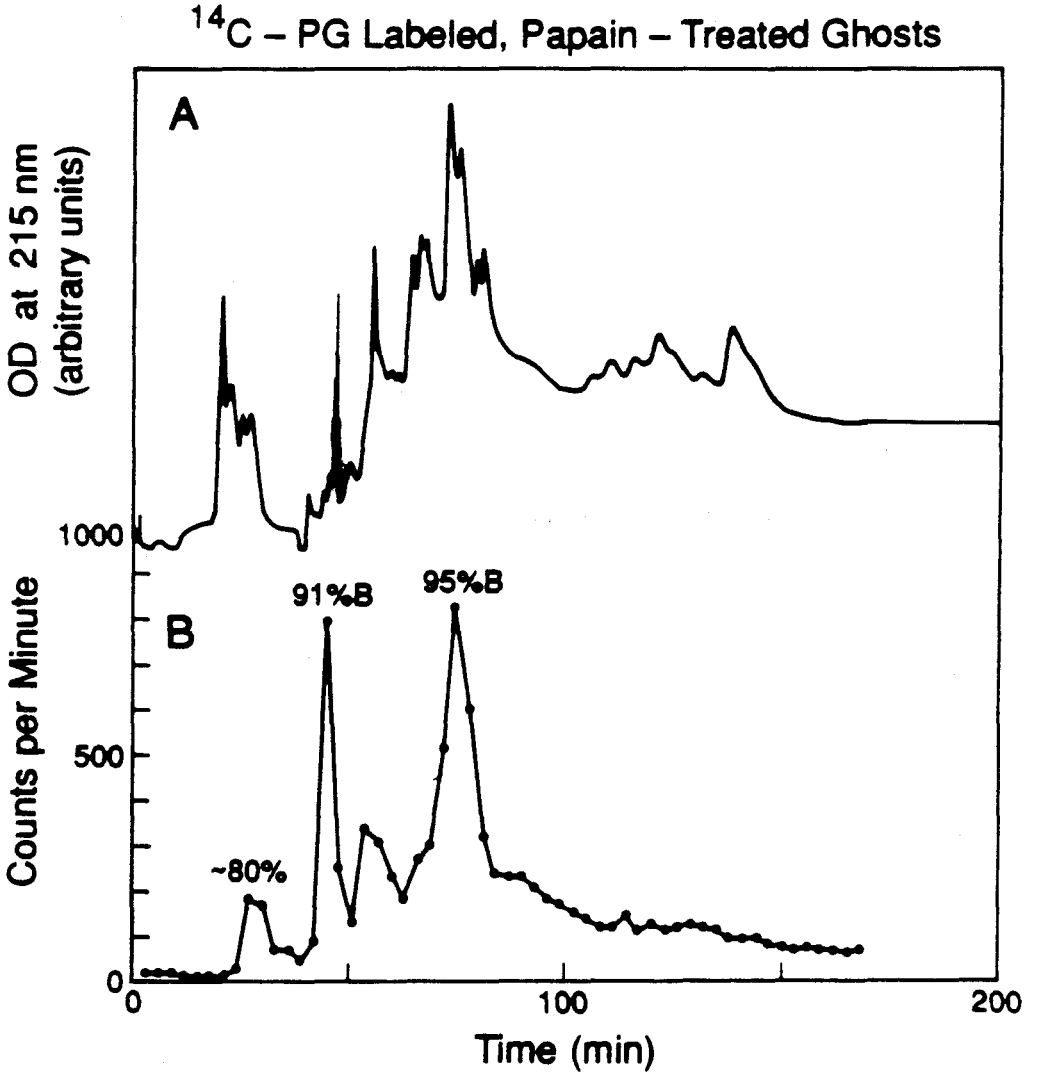
^{14}C – PG Labeled, Papain – Treated Ghosts
A
OD at 215 nm (arbitrary units)
1000
B
91%B
95%B
~80%
Counts per Minute
500
0
0
100
200
Time (min)

the absorbance profile for this sample. Figure 4.5(B) illustrates its scintillation profile. Fractions were collected at 3 minute intervals. The presence of label was detected by scintillation counting 1 ml of each fraction. This sample had been frozen, and the resolution is not as complete as it is in normal HPLC profiles. The maximum number of counts per minute was 1000, or 1/15 of the maximum in the profile for labeled whole ghosts. The absorbance and scintillation profiles for a blank run are shown in Figure 4.6. With nothing injected onto the column, peaks in the scintillation profile are present. These represent residual protein and label from the previous HPLC of labeled whole ghosts. Combined protein or label from the previous sample and from the current sample may have resulted in significant counts for the papain-proteolyzed ghost preparation at 95% B. Once again, the maximum number of counts obtained was about 1/15 of the maximum for the whole ghosts. Although the largest peak elutes at different percentages of the organic phase, B, the profiles for papain-treated membranes and whole ghost membranes have very similar features. This peak could also represent a labeled proteolytic fragment. In this case, its position is typical of the peaks in the **F** region of the HPLC absorbance profile. In particular, it is in the **F1** region. The N-terminus of the **F1** peptide begins before the modeled transmembrane helix VC-13. **F1** probably contains VC-13 and VC-14. (They are modeled to be separated by only two amino acids.) The broad nature of **F** is probably due to multiple cleavage sites (two distinct but closely spaced N-termini were found for two sequenced peptides from **F**. However, the peptides in **F** were not very pure and are probably contaminated peptides from other parts of the protein. The sharp nature of the peak in the scintillation implies that it does not contain one of the peptides cleaved near the putative N-terminus for VC-13.

Figure 4.6

Figure (A) shows the HPLC absorbance in a blank run (nothing injected) following the sample injected in Figure 4.4. An octylglucoside-saturated C_{18} column was used to obtain the separation. Clearly protein elutes at 73%B. This protein contains label as is demonstrated in Figure (B). The identity of the protein eluting at 73% is unknown. This peak gives support to the argument that some peptides are retained by the column and are eluted only at low yields for any particular HPLC run.

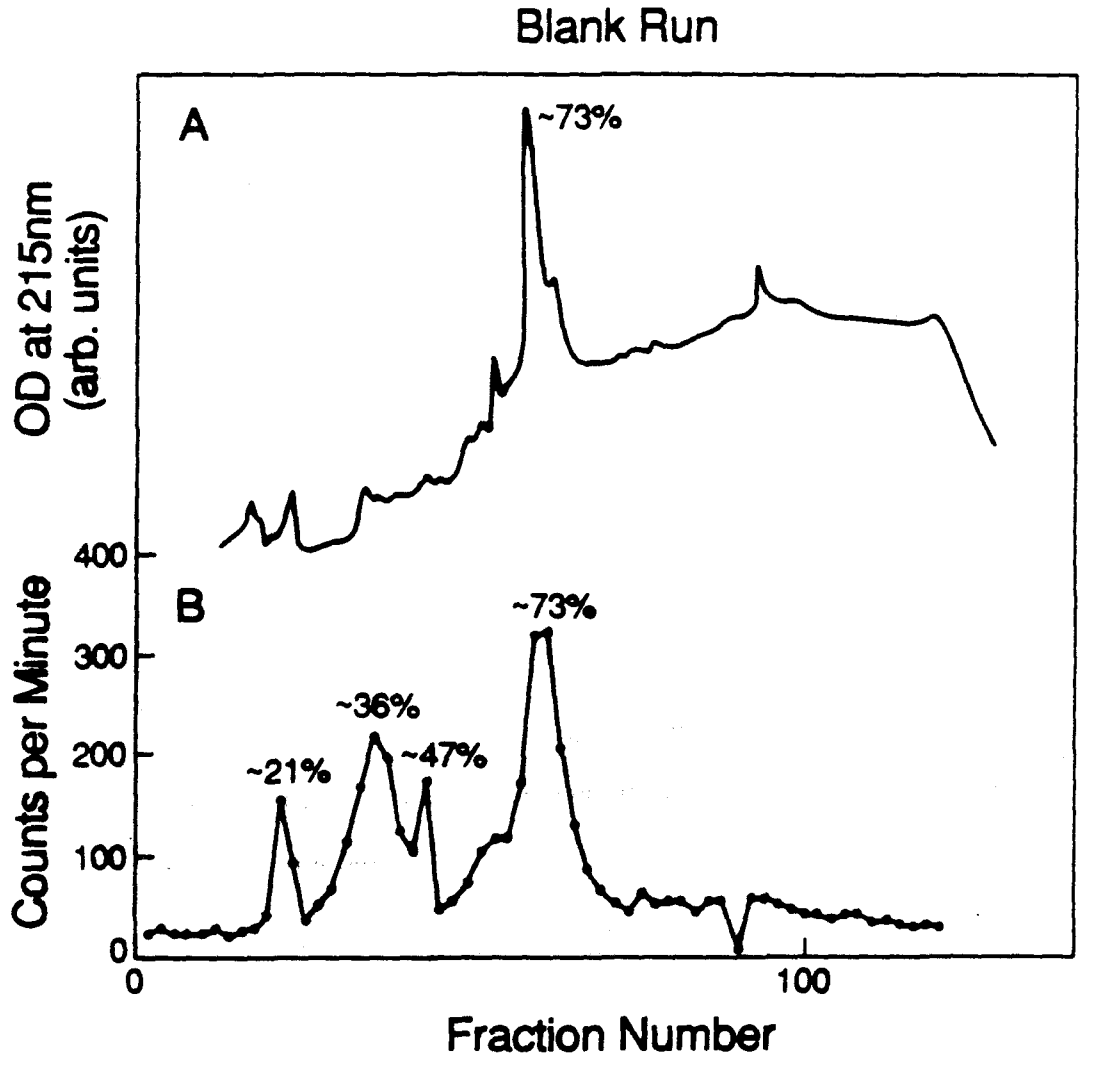
Blank Run
A
~73%
OD at 215nm
(arb. units)
400
B
~73%
300
~36%
~47%
~21%
200
100
0
Counts per Minute
0
100
Fraction Number

The peak at 91%B corresponds to the location of sequence III in Figure 4.2. This sequence was extremely pure and was sequenced to 42 amino acids. It begins at mouse erythrocyte band 3 amino acid number 509. Two proteolysis fragments starting at the same point have been amino acid analyzed and contain over 80 amino acids (as seen in Figure 4.2). The human peptide contains arginines corresponding to positions MEB3 523, 527 and 530. None of them is modeled by Lodish[25] or Voglaar and Chan to lie buried in a transmembrane helix. R523 and R530 are not conserved among all four sequences. There is one lysine (which can also react with α-dicarbonyls[17]) conserved among all four sequences at MEB3 K558 (and another nonconserved lysine at K561). Neither is modeled by Vogelaar and Chan to lie within a transmembrane helix, although Lodish places both at the edge of L-5[25]. Thus, sequence III may be labeled, but probably it does not contain the active-site arginine. Zaki has evidence for two to three modifications which may implicate this modifiction as the second label. Unfortunately, the peak was not entirely reproducible in intensity of scintillation counts.

The inability to obtain sequencable amounts of modeled helices VC-3, VC-7, VC-8, VC-9 and/or VC-10, and possibly VC-14 could have several causes. Fragments containing these helices either aggregate and coelute at low concentrations with other peptides, or they may be retained on the column. Another possibility is that a family of proteolytic fragments with closely spaced N-termini were eluted with poor resolution over a broad range.

Scintillation profiles in Figure 4.7 for papain-treated membrane proteins which were separated on an octylglucoside C_4 column showed promising results. In spite of the fact that only 180 µl of papain-treated, labeled membranes were injected onto an analytical column, the counts per minute reached 800. Unfortunately, gels showed that

the peak containing the most radioactivity was contamininated by several peptides of molecular weights < 9500[24]. It is clear from the broad peaks of the chromatograph

Figure 4.7

The HPLC absorbance profile for a papain-treated ghost preparation is shown in Figure (A). This profile was generated using a C_4 column before conditions for optimal separation of these peptides were established and before the procedure for papain proteolysis had been optimized. Thus, the broad and weakly radiolabeled peak occurring between 25 and 40 minutes in Figure (B) actually represents whole band 3 as demonstrated by SDS-polyacrylamide gel electrophoresis. Autoradiography of the gel lanes containing the peak at 86 minutes shows a band at low molecular weights (< 8000 daltons). Silver-stained gels showed contamination by several low molecular weight species.

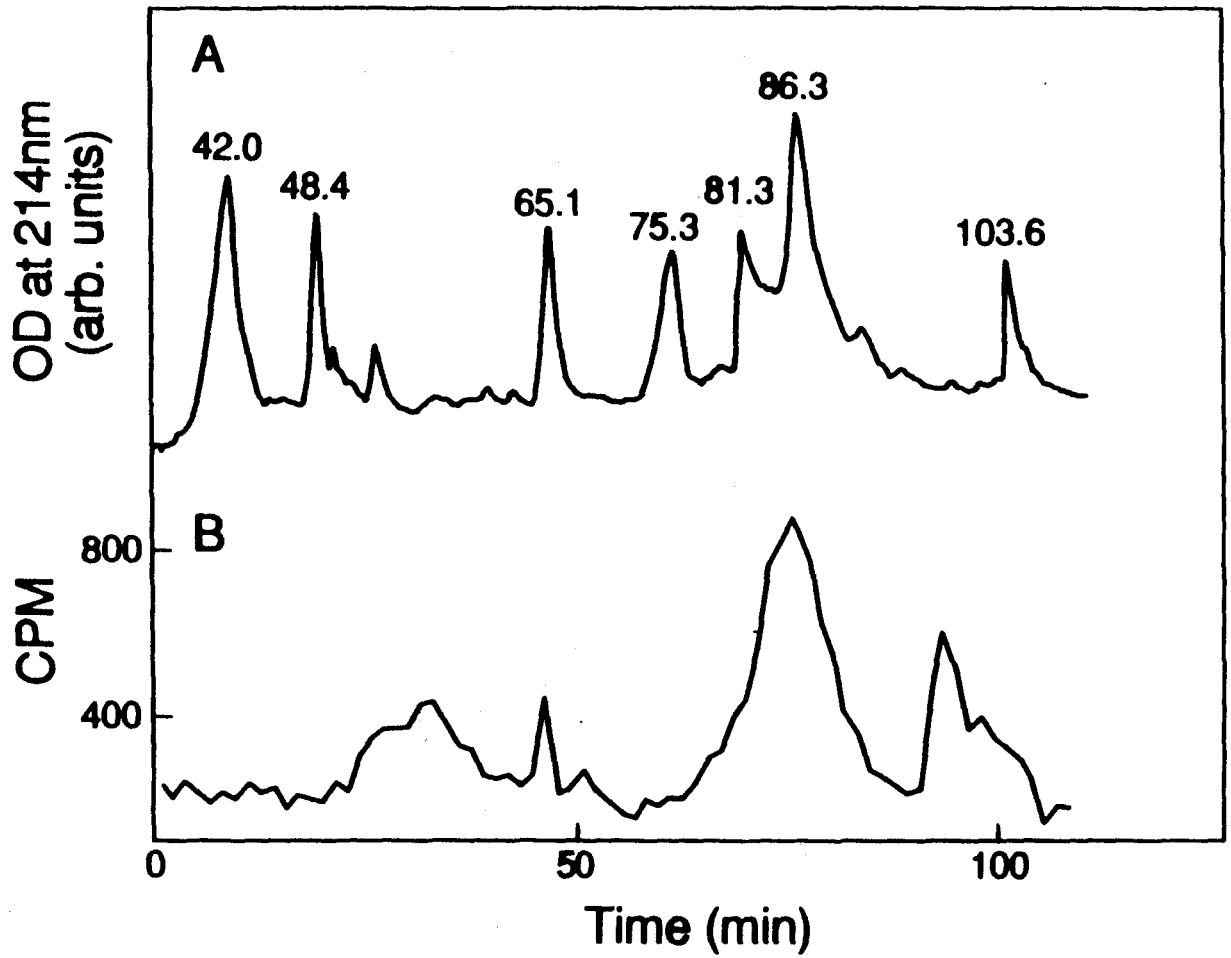
A
42.0
48.4
65.1
75.3
81.3
86.3
103.6
OD at 214nm (arb. units)
B
800
400
CPM
0
50
100
Time (min)

in Figure 4.7(A) that there was substantial aggregation of peptides.

CONCLUSION

After difficulties in separating band 3 papain-generated peptides with an octyglucoside C_4 column (as seen in Figure 4.7) and by conventional methods (as described in Appendix I of this chapter) we attempted the separation using an octylglucoside-saturated C_{18} column. It was predicted that the longer hydrophobic chains on the stationary support would provide more surface for interaction with the octylglucoside and hydrophobic transmembrane helices of band 3. The fact that the C_{18} column yielded a number of sharp, intense peaks representing very hydrophobic peptides indicates that the prediction is justified. However, the C_{18} column is probably not suitable for separating all peptides, as we have demonstrated. While the detergent C_{18} column efficiently separates many whole red blood cell proteins and transmembrane peptides, it retains some peptides or elutes them over a broad range of organic phase concentrations.

Studies in this chapter, aimed at determining the active-site arginine, demonstrate that there are probably two main fragments with labeled arginines. This is based on the fact that there are two main peaks in the scintillation profile of labeled, proteolyzed, stripped and washed ghost membranes. The identity of one is known. It corresponds to a fragment which defines the edge of VC-4 (and VC-5). The identity of the other is not known. It is tempting to assign it to a fragment whose N-terminus lies on the edge of VC-13 (and is attached to VC-14). However, this fragment is known to have a number of closely spaced cleavage points and has been found in several fragments

eluting in the first 90 minutes of Time Program 1. The peak in the scintillation profile appears to be too narrow to include all of the VC-13/VC-14 peptides.

Figure 4.2 shows the helices modeled by Vogelaar and Chan in band 3. In Chapter III, we found sequences which may define the N-terminus of helix 1. One sequence was obtained for a peptide which corresponds to the edge of helix 2. Modeled helices VC-4 and VC-5 are probably connected by so few amino acids that they cannot be separated. We obtained four sequences which defined the N-terminus of helix VC-4. VC-6 has been sequenced by this laboratory and is probably connected to VC-7 by so few amino acids such that it cannot be proteolyzed into a separate fragments (see Figure 4.2 and the amino acid analysis of **ae9** in Chapter III). Sequences for modeled helices VC-8, VC-9 and VC-10 were not obtained. Two sequences were found to define the edge of helix 11. Helices VC-11 and VC-12 are probably contained in the same proteolytic fragment which has been amino acid analyzed and contains about 62 amino acids in a papain-generated peptide. A peptide of 62 amino acids is easily long enough to contain the two helices and a 'loop' to separate them. At least two sequences in the broad F region of Figure 3.3 define the start of helix 13. There is some controversy about the position of helix 14. According to Vogelaar and Chan, it is separated from helix 13 by only a few amino acids[11]. A distinct peptide corresponding to helix 14 was never isolated. Of the helices modeled by Vogelaar and Chan, only helices 4, 5, 6, 10, 13 and 14 contain either lysines or arginines within their borders. (Within the bounds defined by papain proteolytic data, helix 2 could also contain a nonconserved arginine). Helices 10 and 14 are significantly hydrophilic and are presumed to be the best candidates to contain the essential arginine[11]. However, the position of helix 13 in the HPLC is known has been obtained from proteolytic data and is probably connected to helix 14. Its position does not correspond to any significant amounts of radiolabel. We have also shown the probable location of the second arginine labeled by the Zaki

method. If the models predicting the transmembrane helices are all wrong, it is possible that this is in fact the essential arginine. We have shown that it is possible to covalently and stably label amino acids by the Zaki method.

Therefore, we can predict the location of the essential arginine on the basis of the two types of restrictions. The experiments restricting the location of the essential arginine to several helices were: 1) scintillation studies, which demonstrated that the label could covalently and stably label the protein but was never detected bound to a reasonable, sequencable peptide, and 2) the proteolytic studies presented in Chapter III. The second major type of restriction is more theoretical and involves assumptions about conservation, the environment of the active site, and models of how the protein folds in the membrane. Combining these approaches, we have restricted the position of the active site arginine to 6 helices (helices 3, 7, 8, 9 and 10, and possibly 14). The requirement for an arginine near the middle of the anion channel makes helix 10 the most likely candidate to contain the essential arginine (R748).

References

1. Bjerrum, P.J., Wieth, J.O., and Borders, C.L. Jr. (1983) *J. Gen. Physiol.* **81**, 453-484.

2. Brahm, J. (1988) **Cell Physiology of Blood,** Rockefeller Univ. Press, New York, 141-150.

3. Wieth, J.O., and Bjerrum, P.J. (1982) *J. Gen. Physiol.* **79**, 253-282.

4. Falke, J.J. (1985) *Doctoral Thesis,* California Institute of Technology.

5. Falke, J.J., and Chan S.I. (1984) *Biophys. J.* **45**, 91-92.

6. Zaki, L. (1981) *Biochem. Biophys. Res. Commun.* **99**, 243-251.

7. Wieth, J.O., Bjerrum, P.J. and Borders, C.L. Jr. (1982) *J. Gen. Physiol.* **79**, 283-312.

8. Bjerrum P.J. (1983) **Structure and Function of Membrane Proteins** (E. Quagliariello and F. Palmieri, eds.) Elsevier Science Pub. New York, 107-115.

9. Funder, J. and Wieth, J.O. (1976) *J. Physiol.* **262**, 679-698.

10. Brahm, J. (1977) *J. Gen. Physiol.* **70**, 283-306.

11. Vogelaar, N.S. (1989) *Doctoral Thesis* California Institute of Technology.

12. Falke, J.J., and Chan, S.I. (1984) *J. Biol. Chem.* **259**, 6481-6491.

13 Knauf, P.A. (1979) *Current Topics in Membranes and Transport* **12**, 249-363.

14. Jay, D., and Cantley, L. (1986) *Ann. Rev. Biochem.* **55**, 511-538.

15. Riordan, J.F., McElvany, K.D. and Borders, C.L. Jr. (1987)*Science* **195**, 884-885.

16. Takahashi K. (1986) *J. Biol. Chem.* **243**, 6171-6179.

17. Dietl, T., and Tschesche, H. (1976) *Hoppe-Seylers Z. Physiol. Chem.* **357**, 657-665.

18. Patthey, L. and Thesz, J. (1980) *Eur. J. Biochem.* **105**, 387-393.

19. Cheung, S.T. and Fonda, M.L. (1979) *Biochem. Biophys. Res. Commun.* **90**, 940-947.

20. Wieth, J.O., Bjerrum, P.J. , Brahm, J., and Andersen, O.S. (1982) *Tokai J. Clin. Exp. Med.,* **Supplement to Vol. 7**, 91-101.

21. Zaki, L. (1984) *FEBS Lett.* **189**, 234-240.

22. Tomich, J.M., Carson, L.W., Kanes, K.J., Vogelaar, N.S., Emerling, M.R., and Richards, J.H. (1988) *Anal. Biochem.* **174**, 197-203.

23. Falke, J.J., Pace, R.J., and Chan, S.I. (1984) *J. Biol. Chem.* **259**, 6472-6480.

24. Kanes K.J., Vogelaar, N.S. and Chan, S.I. (1986) **Membrane Proteins, Proc. Membr. Protein. Symp., Meeting Date 1986.** (S.C. Goheen, ed.) 343-352.

25. Lodish, H.F. (1986) *The Harvey Lectures* **Series 82**, 19-46.

Appendix 1 to Chapter IV

Conventional Approaches for Isolation of the Transmembrane Peptides and Approaches for Isolation of the Peptide Containing the Active Site

As was mentioned in Chapter I, the goal of this thesis was to isolate and determine the sequence of the transmembrane helix containing the essential arginine in the active site of the band 3 protein. The obvious problem was to obtain a separation of the transmembrane fragments. Papain was used to generate the transmembrane helices, as described in Chapters III and IV. However, we found it impossible to isolate sequencable amounts of pure, papain-generated, hydrophobic peptides using conventional techniques. These early attempts and the related experiments are summarized below.

Although we attempted to separate the peptides by many different conventional methods, the initial attempts were using HPLC (High Performance Liquid Chromatography). Tempst *et al.* were successful in obtaining separations of a large membrane-spanning glycoprotein and its trypsinized products using a two-step reverse-

phase HPLC method[1]. They also separated cyanogen bromide (CNBr) generated polypeptide fragments of this protein using a size-exclusion HPLC step and a reverse-phase HPLC step.

Using reverse-phase HPLC and size-exclusion HPLC and following protocols similar to those of Tempst *et al.*, we were unable to obtain papain-generated, membrane-spanning peptides from red blood cell ghosts. Conventional reverse phase HPLC was attempted using a C_{18} analytical Vydac reverse-phase column. However, the chromatographs contained only a few broad peaks under some conditions while under other conditions the peaks were small and sharp but not reproducible. Reverse-phase HPLC was then attempted using a C_4 analytical Vydac column. Because the peaks seemed so broad and had so little absorbance, we thought perhaps the papain was not proteolyzing effectively. Therefore, we performed a papain incubation time course experiment. The difference in profiles between a 1 hour incubation and a 1.5 hour incubation was negligible, indicating that the papain was proteolyzing completely within the first hour. This was confirmed by SDS polyacrylamide gel electrophoresis of different HPLC fractions. Although some of the gel lanes showed no visible protein, others showed contamination by multiple, low molecular weight proteolytic species. The small number of broad peaks in the chromatographs probably indicated that many different peptides were co-eluting. Thus, we were unable to obtain reproducible reverse-phase chromatographs or chromatographs with significant separations. It appeared that the membrane proteins adhered to either the guard column or the reverse-phase HPLC column using conventional mobile phases, so this method was abandoned.

---

[1] Tempst, P., Woo, D.D.-L., Teplow, D.B., Aebersold, R., Hood, L.E., and Kent, S.B.H. (1986) *J. Chromatography* **359**, 403-412.

We believe that Tempst *et al.* were successful in isolating the proteolytic products of a large transmembrane glycoprotein because CNBr permeates the membrane and can cleave the protein at methionines within the membrane as well as in the 'loops'. (For example, Ross *et al.* have cleaved in the middle of the single, membrane-spanning portion of glycophorin A using CNBr[2].) CNBr generated randomly spaced cleavages, resulting in peptides which were not completely hydrophobic and thus more easily separated.

When attempting to separate papain treated integral membrane proteins on standard, discontinuous 10% and 12% sodium dodecyl sulfate-polyacrylamide gels by electrophoresis (SDS-PAGE) (see the Materials and Methods section of this Appendix), the presence of large amounts of membrane lipid caused Joule heating. This resulted in smaller, more mobile peptides running as a very frayed edge at the dye front. In the past, we have been successful in separating the papain-treated ghost membrane peptides by polyacrylamide gel electrophoresis[3,4]. However, fraying near the dye front has frequently been evident in our gels. In order to obtain large enough quantities of peptide to sequence, it was important that we use a method with good reproducibility and large yields. As a result of the heating phenomenon, it was often difficult to separate and visualize the low molecular weight peptides.

Therefore, we established a dialysis protocol to eliminate lipids from the membrane suspension before loading sample onto the gels. Fraying was still somewhat evident.

---

2 Ross, A.H., Radhakrishnan, R., Robson, R.J., and Khoraba, H.G. (1982) *J. Biol. Chem.* **257**, 4152-4161.

3 Falke, J.J., Kanes, K.J., and Chan, S.I. (1985) *J. Biol. Chem.* **260**, 13294-13303.

4 Kanes, K.J., Vogelaar, N.J., and Chan, S.I. (1987) **Membrane Proteins, Proc. Membr. Protein Symp., Meeting Date, 1986** (S.C. Goheen, ed.), 343-352.

We concluded that our dialysis procedures had little effect on the the excessive heating for the more mobile peptides, because the dialysis was performed against high concentrations of urea--which adds to excessive heating. Additionally, some of the protein is lost in dialysis since the protein stained poorly in dialyzed samples. Attempting to perform HPLC after dialysis of these samples resulted in a precipitate. This precipitate was evident when trifluoroacetic acid was added to the sample containing urea.

In an effort to isolate the fragment containing the active site arginine without using radiolabel, we tried to label the active site with substituted phenylglyoxal (PG) analogues. These analogues contained substituents on the phenyl group so that they had absorbance maxima at wavelengths that could be monitored conveniently. Para-hydroxyphenylglyoxal (p-OH PG) was synthesized by the method of Fodor and Kovacs[5]. According to several sources, the α-dicarbonyls 1,2-cyclohexanedione and PG can be made more specific for arginines in anion recognition sites of proteins if the reaction is carried out in the presence of borate[6 7]. However, when applying the procedure to phenylglyoxal analogues (para-hydroxyphenylglyoxal and para-nitrophenylglyoxal) they would not label irreversibly under conditions when borate was present. After the reaction, the presence of unbound PG derivative was evident in stripping wash supernatants when monitored by uv-vis spectrophotometry. There were also large amounts of free label in the void volume of HPLC chromatographs when

---

[5] Fodor, G., and Kovacs (1949) *J. Am. Chem. Soc.* **71**, 1045-1048.

[6] Dietl, T., and Tschesche, H. (1976) *Hoppe-Seyler's Z. Physiol. Chem.* **357**, 657-665.

[7] Patthy, L., and Smith, E.L. (1975) *J. Biol. Chem.* **250**, 557-564.

labeled ghosts proteins were monitored at 340 nm (for p-OH PG) or 450 nm (for para-nitophenylglyoxal).

Next, we used the method of Zaki to label band 3 in ghost membranes with p-OH PG[8]. This method seemed to stabilize p-OH PG labeling of the protein as shown by ^{35}Cl NMR. Although it has been determined that PG modifies the band 3 transport site, it was not known if p-OH PG reacts with the active site. For this reason, it was necessary to characterize the modification of band 3 with this reagent. This was accomplished using the ^{35}Cl NMR assay developed in this laboratory[9 10]. Data comparing transport site linebroadening of unmodified membranes and membranes modified by p-OH PG showed that p-OH PG is interfering with the chloride binding to the transport site, indicating that the transport site is modified. The extent of modification was estimated by the decrease in transport site linebroadening. More than 80% of the transport site appeared to have been modified[3]. However, as discussed below, this label proved to be too unstable for detection of the active site. The PG analogues labelling band 3 were not stable to acid hydrolysis. Reverse-phase columns are intolerant of pH's above 7, a condition which favors loss of label. Furthermore, neither the products nor the stoichiometry of reaction of these analogues with arginine is known.

We also used para-nitrophenylglyoxal (p-NO_3 PG) to label ghosts which we then proteolyzed with papain. HPLC was performed on a variety of samples at p-NO_3 PG's absorbance maximum (450 nm) using a Spherogel™-TSK SW 2000 column for size-exclusion chromatography. This column was used becaause it tolerates higher pHs

---

8 Zaki, L. (1984) *FEBS Lett.* **169**, 234-242.

9 Falke, J.J., Pace, R.J. and Chan, S.I. (1984) *J. Biol. Chem.* **259**, 6481-6491.

10 Falke, J.J. (1985) *Doctoral Thesis* California Institute of Technology.

than reverse phase columns. Under neutral pH conditions of this column, detection of the bound label should have been possible. We had hoped that the bound label would have a shift in its absorbance maximum. This did not occur. In addition, Tempst *et al.* successfully used a similar size-exclusion column as the second step of their protein purification. None of the retention times of peaks visible at 220 nm corresponded exactly with peaks monitored at 450 nm. Therefore the labeling with p-NO_3 PG was not pursued. We chromatographed p-OH PG labeled papain-treated ghosts on a TSK column and obtained results which were reproducible but had only a few poorly resolved peaks.

In order to determine if the peaks obtained by HPLC on a TSK column contained pure protein, we collected protein fractions from peaks and electrophoresed them on SDS polyacrylamide gel. We then stained the gels by a very sensitive silver staining method. In some lanes we saw no protein, indicating that there was not enough protein to visualize by this method. In one lane we saw several bands of very light intensity, including one diffuse band of molecular weight 95,000 daltons which we assumed was band 3. However, we concluded that the TSK was not purifying the proteins. Instead, it was chromatographing detergent-protein micelles which contained a variety of protein species.

The biggest disadvantage to these conventional HPLC techniques was that few peaks were present on the chromatographs. According to the information obtained by SDS polyacrylamide gel electrophoresis, they contained a large number of peptides. Therefore, we did not continue with size-exclusion chromatography.

Because the HPLC chromatographs for peptides labeled by both analogues were not entirely reproducible and because of the disadvantages described above, approaches to labeling band 3 using p-OH PG and p-NO_3 PG were not pursued.

In order to obtain large quantitiies of pure protein, we then attempted to separate the proteins by electroeluting excised strips containing protein from SDS polyacrylamide preparatory gels. We then used HPLC to determine the amount of protein recovered. The protein recovery and resolution on the preparatory were very poor, so we did not pursue this method.

Using the method of Tomich *et al.*[11], we obtained reproducible HPLC chromatographs of papain-generated membrane protein fragments. We then separated peptides in the fractions collected for different chromatographed peaks by linear gels and later gradient gels. We obtained a few different peptides under different peaks, but the recovery was good, and the peaks were generally of similar sizes. This would be expected if the peptides are eluted by the mechanisms described in Chapter III. Electrophoretically transferring (electroblotting) these SDS polyacrylamide gradient mini-gels onto p-phenylene diisothiocyanate-(DITC) treated filter blots was attempted in order to isolate the proteins for sequencing. The electroblots were stained with a variety of reagents. A gold stain yielded the best results. Unfortunately, while the molecular weight standards were visible, protein from the papain preparation was not. In retrospect, either the composition of the peptides (hydrophobic, with small net charge) or their relatively small size reduced the efficiency of the electroblotting procedure and the ability to stain efficiently.

We attempted to optimize the membrane solubilization conditions in order to obtain the best resolution possible in the HPLC chromatographs using the method of Tomich *et al.*[11] A variety of different protein denaturing reagents were used. These include the use of other detergents such as octylglucoside and SDS, formic acid, urea, and

---

[11] Tomich, J.M., Carson, L.W., Kanes, K.J., Vogelaar, N.J., Emerling, M.R., and Richards, J.H. (1988) *Anal. Biochem.* **174**, 197-203.

trifluoroacetic acid. The best resolution in the chromatographs obtained for papain-generated transmembrane fragments was found using SDS. We also found that it is not necessary to boil samples in SDS before injection. There is sometimes more aggregation, demonstrated by poorer resolution in the chromatograph, after the samples are boiled. The separation of peaks and their retention times in the chromatograph is dependent upon the temperature at which the HPLC column is kept. Low temperatures lead to many fewer peaks and poor resolution. Maintaining the column at high temperatures does not seem to damage the column since the profiles of papain-generated peptides was constant for over 150 runs.

Iso-electric focusing was attempted using a vertical mini-gel format according to the method described by Aebersold *et al.*[12] . While the method seemed to show some promise in separating the proteins, it proved difficult to electroblot from the focused gel.

In summary, we attempted to separate both unlabeled and labeled whole membrane proteins and proteolyzed ghost fragments by a variety of methods. We labeled ghosts with two different PG analogues but were unable to label the protein or its proteolysis fragments irreversibly. Furthermore, using a variety of conventional protein separation techniques, we were unable to obtain large recoveries of peptides. In addition, these methods were labor-intensive, time consuming, and never yielded pure peptide.

---

[12] Aebersold, R.H., Pipes, G., Hood, L.E., and Kent, S.B.H.(submitted manuscript)

MATERIALS AND METHODS

Materials.

Reagents and their sources are: p-nitrophenylglyoxal monohydrate (Pierce Chem. Co); morpholine, trifluoroacetic acid (TFA) (Aldrich); 1-propanol, acetonitrile (CH_3CN) (all HPLC grade) (Aldrich); dithiothreitol (DTT) ICN; Molecular weight standards, BRL; phenylglyoxal, Aldrich; papain, Calbiochem.

Methods

Membrane Preparation:

Leaky red cell membranes (ghosts) were prepared as described previously[13].

SDS-Polyacrylamide Gel Electrophoresis and Silver Staining:

The gel system for low-molecular weight peptides used the discontinuous buffer system of Laemmli[14]. The stacking gel contained 9.6% acrylamide and 0.048% bisacrylamide. The separatory gel contained 16% acrylamide, 0.5% bisacrylamide, 21.6% urea, and 13.3% glycerol (v/v). The stacking and separatory solutions were filtered and copolymerized[15]. These low molecular weight gels were silver-stained as described previously[16], except that gels were first fixed in 10% trichloroacetic acid and

---

13 Falke, J.J., Pace, and Chan, S.I. (1984) *J. Biol. Chem.* **259**, 6472-6480.

14 Laemmli, U.K. (1970) *Nature* **227**, 680-685.

15 Merle, P., and Kadenbach, B. (1980) *Eur. J. Biochem.* **105**, 499-507.

16 Oakley, B.R., Kirsch, D.R., and Morris, R. (1980) *Anal. Biochem.* **105** 361-363.

40% methanol for > 4 hr. All solutions before the staining solution and after the reducing solution contained 40% methanol to prevent gel swelling. Photographs and negatives were made using a Polaroid land camera and Type 55 Polaroid film. Molecular weight standards included the following proteins: phosphorylase b (94 kDa), carbonic anhydrase (30 kDa), soybean trypsin inhibitor (20.1 kDa), lactalbumin (14.4 kDa), aprotinin (6.5 kDa), and insulin A (2.3 kDa).

Dialysis Removal of Lipids:

A solution of 100 mM sodium dihydrogen phosphate was pH adjusted to 7.8 to 8.0, and DTT was added to a concentration 1 mM. Enough of this solution was added to double the volume of the ghosts. The resulting mixture was allowed to stand for 5 minutes. The following were added to denature: Enough urea was added until a final concentration of 6 M was reached, SDS was added until it comprised 2% of the final volume, and iodoacetimide was added to give 15 mM final concentration. This clarified mixture was dialyzed against 100 volumes of 4 M urea and 1% SDS. The SDS was added to prevent protein precipitation.

Conventional C-18 Reverse-Phase HPLC:

The mobile phase was composed of an aqueous buffer A (0.1% TFA in water) and an organic buffer B (0.1% TFA in 10% water 90% CH_3CN). The following gradient was used:

time (min)	function	value
0.01	T.flow	1 ml/min
0.01	B conc.	28
0.01	wavelength	220
5	B conc.	44
63	B conc.	100
73	B conc.	100
78	B conc.	28
88	B conc.	28
90	stop	

end

Para-hydroxyphenylglyoxal Labeling Membrane Proteins in Borate:

A solution of 200 mM borate was pH adjusted to 8 with sulfuric acid and solid p-hydroxyphenylglyoxal (p-OH PG) was added to make a final concentration of 50 mM. one volume of this solution was added to one volume of ghosts. This suspension was incubated at 37 degrees for 1 hour with shaking. The mixture was washed twice in 5P8 by centrifugation for 15 minutes each at 15K rpm (27,000 x g_{max}) to pellet the membranes in order to wash away excess p-OH PG. Then enough fresh p-OH PG solution to equal the membrane pellet was added, and the procedure was repeated.

Para-hydroxyphenylglyoxal Labeling of Ghost Membranes in Zaki Buffer:

Ghosts were modified with p-OH PG by diluting one part ghosts with one part labeling buffer. The labeling buffer contained 200 mM sucrose, 25 mM gluconate, 25 mM citrate, 5 mM HEPES, and 1 mM sodium sulfate and as the same as that used by Zaki[8]. The final concentration of p-OH PG was about 4 mM.

NMR Sample Preparation:

Packed membranes were diluted by half using 5 mM NaH_2PO_4 at pH 8 (henceforth referred to as 5P8). A volume of this membrane suspension was then mixed with an equal volume of ammonium chloride solution to give a final ionic strengh of 0.4 M and a pH of 8.0. The ammonium chloride concentration varied from 0.025 to 0.40 M and sodium citrate was used to adjust the ionic strength. The solution also contained 20% deuterium oxide to provide an NMR lock signal. Finally, the samples were sonicated for 6 minutes using a probe microtip sonicator at 50% duty to ensure chloride access to both sides of the membrane. In order to determine the linebroadening associated with the transport site two 2.0 ml aliquots of membranes were added to each of two NMR

tubes, one containing 50µl of 40 mM DNDS, the other containing 40 µl of distilled water.

NMR Spectroscopy:

^{35}Cl NMR spectra were taken at 25°C on a Varian XL200 spectrometer at the ^{35}Cl resonance frequency of 19.6 MHz. To ensure temperature equilibration, 200 dummy scans were routinely taken before data acquisition.

NMR Data Analysis:

Linebroadening for each sample was determined by subtracting the half-height linewidth for chloride in the absence of membranes from the half-height linewidth of the sample. To normalize the linebroadening to the amount of protein (and therefore band 3) present, protein concentrations were determined by the modified Lowry protein assay[17].

Size Exclusion HPLC:

The column used for these experiments was a Spherogel™-TSK SW 2000 size exclusion HPLC column. The buffer was 50 mM Na_2HPO_4 with 1% SDS at pH 7. The runs were performed under isocratic conditions at room temperature. The flow rate was maintained at 1 ml/min.

SDS Polyacrylamide Gradient Gel Electrophoresis:

---

17 Markwell, M.A., Haas, S.M., Bieber, L.L., and Tolbert, N.E. (1978) *Anal. Biochem.* **87**, 206-210.

Linear gradient gels were prepared as described in the Bio-Rad Model 395 gradient instruction manual. The acrylamide concentration was varied from 9% to 16%. The method is briefly described in Reference 12.

Electroelution Procedure:

Eight 15 cm x 1 cm gel tubes were cleaned in 1:1 saturated KOH in ethanol/H_2O and rinsed. They were inserted into the gel tank. 30 ml of the separatory gel solution was prepared, poured to the 4 cm line and overlayed with water. Meanwhile protein containing gel strips excised from the preparatory gel were soaked in 5 ml of 1 x Laemmli stack gel with 20 µl of 1% in ethanol bromphenol blue. The excised strips were chopped into 1-3 cm pieces and loaded into the gel tank tubes, allowing 1 cm between the top of the tank and gel pieces. An agarose solution containing 116.6 ml of water, 3 g of agarose, and 50 ml of a stack gel solution was warmed in a water bath to liquify. It was then poured to nearly the top of gel slices. Bubbles were ejected and removed. The agarose/stack gel was allowed to polymerize for 10 minutes. This step was repeated with more of the same solution. The purpose of splitting this part of the procedure into two steps was to prevent the gel slices from floating to the top. Running buffer was poured into the upper and lower tank and bubbles were dislodged from the bottom of each tube. The tube gels were run at 50 mA, with positive on top. When the top dye front neared the top of the gel, 1 cm of the 30% glycerol in 1 x Laemmli stack gel solution was layered on the top of the gel and the diffuse dye collecting in the glycerol phase was collected. This step was repeated for the lower dye front.

Electroblotting Procedure:

Papain-generated proteoytic fragments separated on gradient gels prepared as above were electroblotted onto activated glass filter paper by the method outlined by

Aebersold *et al.*[18,19] . A variety of dyes were used to stain the electroblot. These include a sulfhydryl stain, a 'coumarin' stain whose principal reagent is 7-diethylamino-3-((4'-iodoaceylamino)phenyl)-4 methylcoumarin, a gold dye called AuroDye® (Janssen product number 30.703.51) and a Biorad Colloidal Gold protein detection assay (catalog number 170-6517).

---

[18] Aebersold, R.H., Teplow, D.B. Hood, L.E. and Kent, S.B.H. (1986) *J. Biol. Chem.* **261**, 4229-4238.

[19] Aebersold, R.H., Teplow, D.B., Hood, L.E. and Kent, S.B.H. (1985) **Modern Methods in Protein Chemistry** (J.J. L'Italien, ed.) Plenum Press, New York.

Table 1

Table 1 shows the techniques attempted for isolation of band 3 transmembrane peptides and the limitations of each.

Method	Description	Limitations
Reverse Phase HPLC (organic and aqueous phases)	C_4 column	Poor recovery of peptides. Broad, poorly resolved peaks contained multiple peptides as seen by SDS-PAGE.
	C_{18} column	Loss of protein, as demonstrated by peaks with little absorbtion at 215 nm.
Size Exclusion HPLC	Spherogel™-TSK 2000-SW	Few peaks (2 major and 3 minor).
Gels	Linear, 10% acrylamide	Poor resolution at low molecular weights.
	Gradient, 9-16% acrylamide	Poor resolution.
Electroelution	Excised protein from linear preparatory gels	Poor recovery.
Electroblotting	using a variety of stains from the above gradient gels	Poor recovery and/or detection.